

Jaqueline Stecanela Mandelli

**INKJET PRINTING OF FLEXIBLE ORGANIC ELECTRODES
FOR TISSUE ENGINEERING APPLICATIONS**

Dissertação submetida ao Programa de Pós-Graduação em Ciência e Engenharia de Materiais da Universidade Federal de Santa Catarina para a obtenção do Grau de Mestre em Engenharia de Materiais.
Orientador: Prof. Dr. Carlos R. Rambo
Co-orientador: Dr.^a Janice Koepp

Florianópolis
2012

Ficha de identificação da obra elaborada pelo autor,
através do Programa de Geração Automática da Biblioteca Universitária da UFSC.

Mandelli, Jaqueline Stecanela
INKJET PRINTING OF FLEXIBLE ORGANIC ELECTRODES FOR
TISSUE ENGINEERING APPLICATIONS [dissertação] / Jaqueline
Stecanela Mandelli ; orientador, Carlos Renato Rambo ;
co-orientadora, Janice Koepp. - Florianópolis, SC, 2012.
139 p. ; 21cm

Dissertação (mestrado) - Universidade Federal de Santa
Catarina, Centro Tecnológico. Programa de Pós-Graduação em
Ciência e Engenharia de Materiais.

Inclui referências

1. Ciência e Engenharia de Materiais. 2. Inkjet
Printing. 3. Organic electronics. 4. Flexible electrodes.
5. Tissue Engineering. I. Renato Rambo, Carlos . II.
Koepp, Janice. III. Universidade Federal de Santa
Catarina. Programa de Pós-Graduação em Ciência e Engenharia
de Materiais. IV. Título.

Jaqueline Stecanela Mandelli

**INKJET PRINTING OF FLEXIBLE ORGANIC ELECTRODES
FOR TISSUE ENGINEERING APPLICATIONS**

Esta Dissertação foi julgada adequada para obtenção do Título de Mestre e aprovada em sua forma final pelo Programa de Pós-Graduação em Ciência e Engenharia de Materiais.

Florianópolis, 13 de dezembro de 2012.

Prof. Dr. Antônio Pedro Novaes de Oliveira
Coordenador do Curso

Prof. Dr. Carlos Renato Rambo
Orientador
Universidade Federal de Santa Catarina

Dr.^a Janice Koepp
Co-Orientadora
Universidade Federal de Santa Catarina

Banca Examinadora:

Prof. Dr. Guilherme M. O. Barra
Universidade Federal de Santa Catarina

Dr.^a Janaína Accordi Junkes
Universidade Federal de Santa Catarina

Prof. Dr. Luismar Marques Porto
Universidade Federal de Santa Catarina

*À minha mãe,
Ivone Stecanela Mandelli,
por todos esses anos de amor e
dedicação.*

AGRADECIMENTOS

Ao *Prof. Carlos Renato Rambo* por orientar-me dentro da Universidade Federal de Santa Catarina, pelo suporte, por todas as palavras de apoio e valiosa amizade durante a elaboração deste trabalho.

À *Dr.^a Janice Koepp* pela co-orientação durante este trabalho, por toda ajuda e por oferecer a oportunidade de participar de seu projeto de pesquisa.

Ao *Dr. Giles A. Rae*, pelas palavras sempre positivas e também pelo entusiasmo e curiosidade pelo trabalho desenvolvido.

Aos amigos, por todo carinho, amor e compreensão que tornam meus dias mais felizes.

À minha nova família, *Natalia Bruns* e *Tobias*, por todo o suporte e amor incondicional.

Aos meus pais *João Batista Mandelli* e *Ivone Stecanela Mandelli*, por serem as pessoas mais importantes da minha vida, por todo o amor dedicado durante todos estes anos e, principalmente, por terem formado a pessoa que sou hoje.

I thank to all *members of BEL group*, for friendship and great moments, to *CMP* for technical support and use of its facilities, and especially to *Sébastien Sanaur* for all the help and contribution in this work, and *George Malliaras* for his enthusiasm in research and total assistance.

"The significant problems we face cannot be solved at the same level of thinking we were at when we created them."

- Albert Einstein (1879-1955)

RESUMO

A tecnologia de impressão por jato de tinta vem demonstrando ser capaz de imprimir todos os materiais necessários para a fabricação de circuitos integrados, apresentando baixos custos de fabricação quando comparada às técnicas convencionais utilizadas com silício. Com o advento da eletrônica orgânica, uma ampla gama de materiais tornou-se disponível e a fabricação de dispositivos com propriedades únicas com a interface biológica é agora possível. Um exemplo importante é a utilização de eletrodos metálicos revestidos com polímeros condutores implantados no sistema nervoso central, proporcionando estimulação elétrica aos neurônios. Este trabalho relata a fabricação de dispositivos orgânicos biocompatíveis por meio da tecnologia de impressão por jato de tinta, utilizando-se uma nova combinação de materiais. Os dispositivos foram fabricados sobre um substrato de Parileno C (PaC), um polímero flexível e biocompatível. As linhas condutoras foram impressas utilizando-se uma tinta de nanopartículas de prata, enquanto os sítios ativos foram impressos usando-se uma tinta de poli (3,4-etilenodioxitiofeno)/poliestireno sulfonado (PEDOT: PSS). Para isolar o dispositivo final foi utilizada uma tinta de poliimida para imprimir uma espessa película sobre o dispositivo, deixando pequenas janelas abertas sobre os sítios ativos de PEDOT:PSS. Caracterização elétrica do dispositivo final e avaliação de sua interface com a biologia (testes de cultura de células) foram realizadas. Os resultados mostram que um dispositivo biocompatível e de baixo custo pode ser produzido por escrita direta sem quaisquer técnicas de *pre-patterning* ou de auto-alinhamento, utilizando-se tintas orgânicas.

Palavras-chave: Impressão por jato de tinta. Eletrônica orgânica. Eletrodos flexíveis. Engenharia de Tecidos.

ABSTRACT

Inkjet printing has been demonstrated to be able to print all materials required for integrated circuits at low costs when compared to conventional silicon processing. With the advent of organic electronics, a wide range of materials became available and the fabrication of devices with unique properties for interfacing with biology is now possible. One important example is the use of conducting polymer coatings on metal electrodes that are implanted in the central nervous system, which provides electrical stimulation of neurons. This work reports on the fabrication of biocompatible organic devices by means of inkjet printing with a novel combination of materials. The devices were fabricated on Parylene C (PaC), a biocompatible, flexible polymer substrate. The contact tracks were printed using a silver nanoparticle ink, while the active sites were inkjet printed using a poly (3,4-ethylenedioxythiophene)/polystyrene sulfonate (PEDOT:PSS) solution. To insulate the final device, a polyimide ink was used to print a thick film, leaving small opened windows upon the active sites. Electrical characterization of the final device and evaluation of its interface with biology (cells culture assays) were performed. The results show that inexpensive and biocompatible devices can be produced by direct writing without any pre-patterning or self-alignment techniques using organic inks.

Keywords: Inkjet Printing. Organic electronics. Flexible electrodes. Tissue Engineering.

LIST OF FIGURES

Figure 1: The basic configuration of a piezoelectric printhead (Magdassi S., 2010).....	7
Figure 2: A schematic representation of the mechanism that occurs during the drop drying process after deposition with inkjet printing (Lim J. A. et al., 2008).	8
Figure 3: A schematic representation of the convective and Marangoni flows during the drop drying process (Lim J. A. et al., 2008).....	10
Figure 4: Optical microscopy and polarized images of inkjet-printed TIPS pentacene droplets using chlorobenzene as the major solvent mixed with 25% of the minor solvent, a) chlorobenzene, b) hexane, c) o-dichlorobenzene, and d) dodecane (scale bar represents 50 μm) (Lim J. A. et al., 2008).....	11
Figure 5: Representation of interfacial tensions during a wetting phenomenon at an ideal substrate with an angle θ . (www.attension.com/surface-free-energy, accessed October 02, 2012).	13
Figure 6: Structures of common materials for organic and printed electronics. The semiconductors a) Rubrene; b) pentacene; c) polythiophene P3HT; d) TIPSpentacene; e) PCBM; f) NTDI; g) PTCDI and the conductor h) PEDOT:PSS (OE-A Roadmap White Paper, 2011).	22
Figure 7: Charge carrier mobility of semiconductors for organic and printed electronics applications. The values refer to materials that are available in commercial quantities and to devices that are manufactured in high throughput processes. The values for amorphous silicon (a-Si) and polycrystalline silicon (poly-Si) are given for comparison (OE-A Roadmap White Paper, 2011).	24
Figure 8: Chemical structure of PEDOT (bottom) and of its dopant PSS (top) (Barret M. 2007).....	25
Figure 9: Different applications where PEDOT can be applied (Nilsson D., 2005).....	26
Figure 10: Past and predicted future progress in conductivity of PEDOT-PSS. (OE-A Roadmap White Paper, 2011).....	27

Figure 11: Chemical structure of Parylene C (www.scscoatings.com , accessed August 20, 2011).....	31
Figure 12: Dimatix Materials Printer, Model 2800. Fujifilm Dimatix, Inc., USA.	35
Figure 13: Waveform editor on Dimatix Control Panel.....	39
Figure 14: Pattern used to perform the parameters optimization.	40
Figure 15: Design of the final device.....	41
Figure 16: Patterns of each step of printing for silver nanoparticle ink, PEDOT:PSS ink and polyimide ink, respectively.....	42
Figure 17: (a) Optimized waveform for PEDOT:PSS IJ 1005 ink. (b) Image of a PEDOT:PSS IJ 1005 jet, with a velocity of approximately 5m/s*.....	49
Figure 18: (a) Modified Waveform for PEDOT:PSS IJ 1005 ink. (b) Image of a PEDOT:PSS IJ 1005 jet using the waveform showed in (a); velocity reduced to approximately 2 m/s.	50
Figure 19: Printing with (a) 25 μm , (b) 20 μm , (c) 17 μm , (d) 15 μm and (e) 14 μm of Drop Spacing (Left: horizontal lines; middle: vertical lines and left: single dots). Scale bar: 500 μm	50
Figure 20: Printing with (a) 14 μm and (b) 13 μm of Drop Spacing (Left: horizontal lines; middle: vertical lines and left: single dots). Scale bar: 500 μm	52
Figure 21: Printing with (a) 40°C, (b) 45°C, (c) 50°C, (d) 55°C and (e) 60°C of temperature. (Left: horizontal lines; middle: vertical lines and left: single dots). Scale bar: 500 μm	52
Figure 22: Printing with (a) 13 μm and (b) 12 μm of Drop Spacing. (Left: horizontal lines; middle: vertical lines and left: single dots). Scale bar: 500 μm	54
Figure 23: Printing with (a) 20 μm , (b) 30 μm and (c) 40 μm of Drop Spacing. (Left: horizontal lines; middle: vertical lines and left: lines of different thicknesses). Scale bar: 1 mm.	55
Figure 24: Printing with (a) 35°C and (b) 40°C of temperature. (Left: horizontal lines; middle: vertical lines and left: lines of different thicknesses). Scale bar: 1 mm.	56

Figure 25: Printing with 35 μm of Drop Spacing. (Left: horizontal lines; middle: vertical lines and left: lines of different thicknesses). Scale bar: 1 mm.	56
Figure 26: Printing with (a) 35 μm and (b) 38 μm of Drop Spacing. (Left: horizontal lines; middle: vertical lines and left: lines of different thicknesses). Scale bar: 1 mm.	57
Figure 27: Printing with (a) 38 μm (2 layers), (b) 35 μm , (c) 33 and (d) 38 μm of Drop Spacing. (Left: horizontal lines; middle: vertical lines and left: lines of different thicknesses). Scale bar: 1 mm.....	58
Figure 28: Optimized waveform for Silver Nanoparticle U5603 ink (on the left) and image of Silver Nanoparticle ink U5603 jet, with a velocity of approximately 4 m/s (on the right).....	60
Figure 29: Printing with (a) 100 μm , (b) 50 μm and (c) 45 μm of Drop Spacing. (Left: horizontal lines; middle: vertical lines and left: lines of different thicknesses). Scale bar: 1 mm.....	61
Figure 30: Printing with (a) 40 μm , (b) 35 μm , (c) 30 μm and (d) 25 μm of Drop Spacing. (Left: horizontal lines; middle: vertical lines and left: lines of different thicknesses). Scale bar: 1 mm.....	62
Figure 31: Single dots of Silver Nanoparticle ink. Scale bar : 500 μm .	63
Figure 32: Horizontal line with 2 pixels of width. On the left, drop spacing of 35 μm , in the middle, drop spacing of 30 μm and on the right, drop spacing of 25 μm . Scale bar: 500 μm	63
Figure 33: On the left, horizontal lines (same thickness) and on the right, horizontal lines with different thicknesses. Drop Spacing 23 μm . Scale bar: 500 μm	64
Figure 34: Optimized waveform for Polyimide ink PI 63002 (on the left) and image of Polyimide PI 6302 ink jet, with a velocity of approximately 4 m/s (on the right).	64
Figure 35: Printed square of Polyimide ink, using a drop spacing of (a) 35 μm and (b) 25 μm . Magnification of 5X (on the left) and 10X (on the right). Scale bar: 500 μm	65
Figure 36: Polyimide printed square with drop spacing of 23 μm . (a) 1 layer, (b) 2 layers and (c) 3 layers. Magnification of 5X (on the left) and 10X (on the right). Scale bar: 500 μm	66

Figure 37: Photograph of a full-size printed device, showing a size of approximately 4 cm (including the polyimide printing, which is not visible in this photo). Scale in centimeters.....	67
Figure 38: Optical microscopy image of the device using a magnification of 50X when silver tracks were printed first (on the left) and when PEDOT rectangles were printed first (on the right). This magnification shows clearly the contact between silver and PEDOT in each way of printing. Scale bar: 100 μm	68
Figure 39: Optical microscopy image of final device where the silver tracks were printed before the PEDOT:PSS rectangles (without polyimide printing). (a) First lines of the device and (b) last lines of the device. Scale bar: 1 mm.	69
Figure 40: Optical microscopy image of complete device shown in Figure 39 after polyimide printing. Silver tracks were printed before the PEDOT:PSS rectangles. (a) First lines of the device and (b) last lines of the device. Scale bar: 1 mm	70
Figure 41: Optical microscopy image of final device where the PEDOT:PSS were printed before the silver tracks (without the polyimide printing). (a) First lines of the device and (b) last lines of the device. Scale bar: 1 mm	71
Figure 42: Optical microscopy image of complete device shown in Figure 41 after polyimide printing. The PEDOT:PSS rectangles were printed first. (a) First lines and (b) last lines of the device. Scale bar: 1 mm.	72
Figure 43: Optical microscopy image of external edges of silver tracks and the open window of polyimide on top of it. Scale bar: 1mm.	73
Figure 44: Contact angles between PaC and ethylene glycol 40% (on the left), Diiodomethane (in the middle) and deionized water (on the right).....	73
Figure 45: Contact angle between PaC and Silver Nanoparticle Ink U5603 (on the left) and between PaC and Silver Organometallic Ink TEC-IJ-010 (on the right).	74
Figure 46: Contact angle between PaC and PEDOT:PSS Orgacon IJ 1005 (on the left) and between PaC and PEDOT:PSS HC Starck (on the right).....	75

Figure 47: Contact angle between PaC and Polyimide PI 6302-002 (on the left) and between PaC and UV ink UVM 001 (on the right).	75
Figure 48: Contact angle between treated PaC and U5603 ink (on the left), contact angle between treated PaC and PEDOT:PSS Orgacon IJ 1005 (in the middle) and contact angle between treated PaC and PI 6302-002 (on the right).	76
Figure 49: Contact angle between Kapton and PEDOT:PSS IJ 1005 (on the left) and between Kapton and PEDOT:PSS HC Starck.....	76
Figure 50: 3D profiles obtained for PEDOT:PSS printing without plasma treatment (on the left) and with oxygen plasma treatment (on the right).	80
Figure 51: Profile of polyimide printed sample obtained from the mechanical profilometer.....	80
Figure 52: SEM images to different annealing conditions: (a) 60 minutes at 200°C, (b) 10 minutes at 200°C and (c) 30 minutes at 150°C. Scale bar: 200 nm.	82
Figure 53: Quantitative analysis of B16F10 cell viability, cultivated on top of surface's device, as a function of time of culture through MTS assay.	87
Figure 54: Qualitative image of cell culture upon Polyimide ink through Live/Dead assay.	88
Figure 55: Live/Dead images of cells culture upon polyimide ink at Device S (on the left) and Device P (on the right).	89
Figure 56: Live/Dead images of cells culture upon PEDOT:PSS ink at Device S (on the left) and Device P (on the right).	89
Figure 57: Nyquist plot comparing both devices. Device S is represented by the red curve and Device P is represented by the blue curve.	107
Figure 58: Bode plot for both devices. Device S is represented by the red curve and Device P is represented by the blue curve.	108
Figure 59: Nyquist (on the left) and Bode plot (on the right) showing the stability of (a) Device P and (b) Device S.	109
Figure 60: Nyquist (on the left) and Bode plot (on the right) for Device P. Right line is represented by the blue curve and left line is represented by the red line.	109

Figure 61: Nyquist (on the left) and Bode plot (on the right) for Device S. Right line (bigger width) is represented by the blue curve and left line is represented by the red line.....	110
Figure 62: Graphic of surface energy obtained from the Wu's method, measured with the goniometer.	111
Figure 63: Transponder chip and printed RFID tag.	113
Figure 64: Printed RFID as electronic product code and printed sensor for measuring electrical activity of the heart (ECG).....	113

LIST OF TABLES

Table 1: Organic Electronics Association Roadmap for organic and printed electronics, with forecast for the market entry in large volumes (general availability) for the different applications.	18
Table 2: Main properties of Parylene C.....	33
Table 3: Substrate temperatures and Drop Spacing values used for parameters adjustments of PEDOT:PSS ink.	59
Table 4: Contact angle between PaC and all the tested inks.....	77
Table 5: Thickness values for silver lines.....	77
Table 6: Silver lines profile obtained from the mechanical and optical profilometers.	78
Table 7: Thickness average values obtained for PEDOT: PSS printed with and without plasma treatment.	79
Table 8: Electrical Resistivity and Conductivity for Silver and PEDOT:PSS samples.	81
Table 9: Images of the Caco-2 cells growth on printed polyimide after 3 and 12 days of cells culture.	84
Table 10: Images of the PC-12 cells growth on printed polyimide after 4 days of cells culture.....	86

LIST OF ABBREVIATIONS

3D: Three-dimensional
AML-12: (alpha mouse liver 12) cells
B16F10: mouse melanoma cells
C57BL/6: common inbred strain of laboratory mice
Caco-2: continuous line of heterogeneous human epithelial colorectal adenocarcinoma cells
CF₄: Tetrafluoromethane
CMP: Centre Microelectronique de Provence
CNS: central nervous system
CVD: chemical vapor deposition
DMEM: Dulbecco's modified Eagle's medium (for cell culture)
DOD: Drop-on-Demand
ECG: electrical activity of the heart
ECoG: electrocorticography
EDM: Diethylene Glycol Methyl Ethyl Ether
EL: electroluminescent
FBS: Foetal Bovine Serum
ISS: Integrated Smart Systems
ITO: indium tin oxide
LEC: Light-emitting capacitor
LED: light-emitting diode
MTS: (3-(4,5-dimethylthiazol-2-yl)-5-(3-carboxymethoxyphenyl)-2-(4-sulfophenyl)-2H-tetrazolium)
NIH3T3: mouse embryonic fibroblast cells
NTDI: N,N'-bis(1,2-dimethylpropyl)-1,4,5,8-naphthalenetetracarboxylic diimide
OE-A: Organic Electronics Association
OLED: organic light-emitting diode
OPV: organic photovoltaic cells
OTFT: organic thin film transistors
P3HT: poly(3-hexylthiophene-2,5-diyl)
PaC: Parylene C (poly-(chloro-*p*-xylylene))
PC: polycarbonate
PC-12: cell line derived from a pheochromocytoma of the rat adrenal medulla
PCBM: phenyl-C61-butyric acid methyl ester
PCE: power conversion efficiencies
PEDOT: (3,4-ethylenedioxythiophene)
PEDOT: PSS: (3,4-ethylenedioxythiophene)/polystyrene sulfonate

PEEK: polyetheretherketone
PEN: poly(ethylene 2,6-naphthalate)
PES: polyethersulfone
PET: poly (ethylene terephthalate)
PHBV: poly (3-hydroxybutyrate-co-valerate)
PI: polyimide
PTCDI : N,N'-Dioctyl-3,4,9,10-perylenedicarboximide
PTFE: Polytetrafluoroethylene
PVDF: Poly (vinylidene fluoride)
RFID: radio frequency identification
RIE: Reactive-Ion Etching
RPMI: Roswell Park Memorial Institute medium (for cell culture)
SEM: Scanning Electron Microscopy
TIPS: Triisopropylsilylethyny

SUMARY

1. INTRODUCTION.....	1
1.1 OBJECTIVES	2
1.1.1 General Objective	2
1.1.2 Specific Objectives	2
2. STATE OF THE ART	5
2.1 INKJET PRINTING TECHNOLOGY	5
2.2 SUBSTRATE AND INK INTERACTIONS	11
2.2.1 Substrate Printability	12
2.2.2 Physical-chemical properties of ink.....	12
2.2.3 Wetting Phenomenon.....	13
2.3 ORGANIC AND PRINTED ELECTRONICS	15
2.4 THE ADVENT OF ORGANIC ELECTRONICS WITH THE BIOLOGICAL INTERFACE.....	19
2.5 SPECIFIC MATERIALS	21
2.5.1 Conducting Polymer – PEDOT:PSS	25
2.5.2 Conducting Metal – Silver ink	28
2.5.3 Insulating Polymer - Polyimide	29
2.5.4 Substrate – Parylene C	30
2.6 OXYGEN PLASMA TREATMENT.....	32
3. MATERIALS AND METHODS	33
3.1 MATERIALS	33
3.1.1 Parylene C	33
3.1.2 Silver Nanoparticle Ink	33
3.1.3 PEDOT:PSS ink.....	34
3.1.4 Polyimide Ink	34
3.1.5 Printer Dimatix DMP 2800	34
3.2 METHODS	35
3.2.1 Oxygen Plasma Treatment.....	38
3.2.2 Evaluation of printing parameters	38
3.2.3 Printing the Final Device.....	41
3.3 CHARACTERIZATION	44
3.3.1 Determination of Surface Energy and Contact Angles... 44	44
3.3.2 Optical Microscopy	44
3.3.3 Mechanical and Optical Profilometer	45
3.3.4 Electrical Resistivity	45
3.3.5 Scanning Electron Microscopy (SEM).....	45
3.3.6 Cell culture assays.....	45
4. RESULTS AND DISCUSSION	49
4.1 PEDOT:PSS PARAMETERS EVALUATION	49

4.2 SILVER NANOPARTICLE PARAMETERS EVALUATION.....	59
4.3 POLYIMIDE INK PARAMETERS OPTIMIZATION.....	64
4.4 FINAL DEVICE.....	67
4.5 SURFACE ENERGY OF PARYLENE.....	73
4.6 CONTACT ANGLE BETWEEN PAC AND INKS.....	74
4.7 THICKNESS.....	77
4.8 SHEET RESISTANCE.....	81
4.9 CELL CULTURE ASSAYS.....	83
4.10 MTS ASSAY.....	87
4.11 LIVE/DEAD ASSAY FOR CELL VIABILITY.....	88
5. CONCLUSIONS.....	91
BIBLIOGRAPHY.....	93
APPENDIX A - ELECTROCHEMICAL IMPEDANCE SPECTROSCOPY.....	107
APPENDIX B - GRAPHIC OF WU'S METHOD.....	111
APPENDIX C - EXAMPLES OF ORGANIC FLEXIBLE DEVICES.....	113

1. INTRODUCTION

Inorganic semiconductors such as silicon, germanium and gallium arsenide have been widely used in microelectronic industry for more than four decades. However, solution processable semiconductors and metals are replacing quickly the traditional inorganic materials due to their several advantages, highlighting low density, excellent mechanical flexibility, ease of manufacturing and control of their electrical, optical and magnetic properties.

With the advent of organic electronics, the use of a wide range of materials with unique properties for interfacing with biology has become possible. This class of materials, called “synthetic metals”, is becoming a promising substitute for metals in biomedical devices. One important example is the use of conducting polymer coatings on metal electrodes that are implanted in the central nervous system, which provides electrical stimulation of neurons. Likewise, biomedical devices as artificial sensors and implantable biosensors, and components for the improvement of probes for neural stimulation are examples already demonstrated in several studies which highlight the advantages that these materials bring to the interface with biology, including its “soft” nature which offers better mechanical compatibility with flexible substrates and tissues when compared to traditional electronic materials, enabling the development of implantable devices that best suit to non-planar shape of human organs.

Associated with this fact, a new technology used to manufacture microelectronic devices has been coming out to be promising: inkjet printing. This technology combines advantageous features such as low temperature process, direct writing, reduced material wastage, low cost and quick process when compared to conventional microfabrication techniques such as, for example, photolithography (classical microfabrication technologies demand access to very expensive equipment, as mask aligners and reactive ion beam etching; and processes, as gold deposition for example, in addition to clean room infrastructure). For these reasons, this technology is already been applied to the fabrication of OLEDs (organic light-emitting diode), organic solar cells, organic thin film transistors (OTFT), radio frequency identification (RFID), among others.

Two different classes of conductive materials (inks) are promising: one based on conducting polymers and the other based on metals. Printing with these inks provides to the device high conductivity using the lowest possible temperature treatment. One of the most accepted bio-coatings, especially for permanently implantable devices in the body, an inert and hydrophobic “green” polymer, has shown to be successful as a substrate for this kind of devices.

This work is part of a research project entitled “Development of New Strategies for Treatment of Traumatic Spinal Cord Injury”, which aims to integrate professional areas of biological sciences and engineering in order to conduct researches which result in technologies capable to establish connections between organic microelectronic and other specific elements to provide an electrical interface implantable in the spinal cord. This project aims to enable the creation of a center of excellence for long-term production of organic chips with several applications.

In order to aggregate these promising technologies, this work proposes the fabrication of organic, flexible devices (electrodes), combining different materials using the technique of inkjet printing. For this purpose, a novel combination of materials (ink and substrate) was proposed. The materials (inks) chosen for printing are poly (3,4-ethylenedioxythiophene)/polystyrene sulfonate (PEDOT:PSS) ink, silver nanoparticle ink and polyimide ink, while the material chosen to be the substrate is the poly-(chloro-p-xylylene), PaC. The produced devices were electrically characterized and it was also intended to evaluate their interface with cells through neuronal cell culture. The developed device is a potential candidate for organic electrodes for several neuronal applications, such as brain activity assays.

1.1 OBJECTIVES

1.1.1 General Objective

This work aims the fabrication of organic, flexible devices, by inkjet printing technology through a novel combination of materials.

1.1.2 Specific Objectives

✓ To fabricate fully flexible organic devices using simple and low cost techniques.

- ✓ To produce devices which can be easily transferred from the original surface to a new substrate with an excellent conformation, keeping it in perfect conditions for use.
- ✓ To adequate the main printing parameters in order to improve the printability of the selected inks for printing.
- ✓ To ensure that the final device will be well insulated from the external environment by using only the printing of an insulating ink.
- ✓ To achieve the highest possible values of electrical conductive for both conductive inks using the lowest possible annealing temperatures.
- ✓ Electrical characterization of the final device and evaluation of its interface with biology (cells culture essays).

2. STATE OF THE ART

2.1 INKJET PRINTING TECHNOLOGY

Inkjet printing is a particularly attractive technique which has been heavily explored for fabrication of polymer flexible electronic circuits due to its advantages as its low cost, low temperature process, direct writing, non-contact, additive patterning, reduced material wastage, maskless approach and scalability to large area manufacturing (Tekin, E. et al., 2004; Liu, Z. et al., 2005; Singh, M. et al., 2009). This technique has become widespread in the graphics industry and nowadays is seeing significant use on functional printing (OE-A Roadmap White Paper, 2011). In this technology, droplets (liquid phase materials) are jetted from a small aperture directly to a specified position on a substrate using computer control to create an image (Le, H. P., 1998; Meier, H. et al., 2009). Another advantage is the great facility to change the design of the image (Singh, M. et al., 2009).

Solution-processable electronics has attracted considerable attention and research. Inkjet printing, a solution processing technique, has been demonstrated to be able to print all materials required for integrated circuits: conductors, semiconductors and dielectrics. It has the potential to significantly reduce the cost of integrated circuit fabrication, especially when compared to conventional silicon processing (Soltman, D. et al., 2008). Both organic (de Gans B. J. et al., February 2004; Yoshioka Y. et al., 2006; Mannerbro R. et al., 2008) and metallic (Liu Z. et al., 2005; Denneulin A. et al., 2011; Chiolerio A. et al., 2011) components have been manufactured using this novel technique (Liu, Z. et al., 2005). The inks used in this technology are elaborate formulations of solvents, plasticizers and surfactants, including the appropriate electronic materials. The solvents used in the preparation of these inks need to be compatible when printing subsequent layers (layer-by-layer) and still be environmentally safe for use in large scale production. Additionally, passivation of the printed device is also essential for long lifetime operation capabilities (OE-A Roadmap White Paper, 2011).

Organic and printed electronics depends on materials electrically active which may be used as conductors, semiconductors, electrochromic, electrophoretic or luminescent materials. The materials for this purpose have to be thoroughly selected since process conditions and the interplay with other layers have a great importance on the device's performance. Between these layers, both dielectrics and

passivation materials influence the device performance (Singh, M. et al., 2009).

Inkjet printing quality depends substantially on the behavior of ejected drops after the jetting action. These falling drops are affected by several factors including jetting conditions, such as the solvents, their concentrations, and the surface wettability of the substrate (Lim J. A. et al., 2008) and properties of the ambient (Singh, M. et al., 2009).

Industrial Inkjet Printing and specifically “Digital Fabrication” with inkjet printing impose a complex set of requirements, which are partially interdependent. Print resolution, reliability, placement accuracy and the resulting width of lines and gaps for printing are the main requirements. This claims for small drop volumes and a high printing addressability (Roadmap White Paper, 2011). Printing of thin lines is restricted by the size of the drop, which depends fundamentally on jetting conditions, surface energy of substrate, nozzle diameter and ink. Typically, the available nozzles vary between 1 pL and 10 pL and they should be chosen considering the line size required and the characteristics of the ink to be printed. Obviously, the nozzle diameter should form the lower bound on the drop size. Machining of smaller nozzles in inkjet cartridges is possible, the issue is smaller nozzles are easier to obstruct, as soon decreasing the reliability and repeatability of the jetting process. As well, care should be taken of the hydrodynamics (wind effects) at the location of drop formation in order to avoid drop placement errors (Yoshioka Y. et al., 2006). Industrial applications usually require high productivity, what implicates in a large number of nozzles per printhead and which is naturally in conflict with the requirements for printing with high resolution. To prove viable the inkjet technology there are determined requests beyond the inkjet process itself. Of key importance is the adaptation of the fluids to the printhead, so that their complex rheology is suited for a clean drop formation (avoiding satellite drops), that particles are kept in stable suspensions (avoiding partially or completely nozzle clogging), etc. Improved techniques and processes are demanded to accelerate the total inkjet printing fabrication process as required in industrial manufacturing lines (OE-A Roadmap White Paper, 2011).

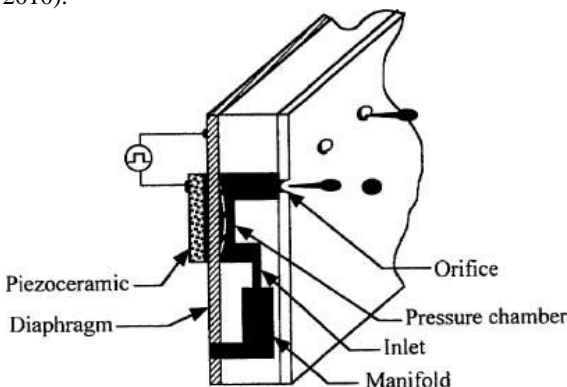
Functional device structures may be manufactured using inkjet printing technology, however, in most cases, it involves the use of prepatterned substrates at multiple levels of processing, and, sometimes, involving multiple materials. These situations result in complicated fluid flow patterns if compared to the simple case of a printed drop colliding on a flat substrate (Singh, M. et al., 2009).

The inkjet printing technology used to print the microelectronic devices in this work was the Drop-on-Demand inkjet (DOD). The DOD is a wide classification of inkjet technology where drops are ejected only when required. In general, the drops are produced by the creation of a pressure pulse. The subcategories on DOD are thermal, piezo and electrostatic (Magdassi S., 2010).

The printer used in this work uses the piezoelectric inkjet technology to eject the drops. This technology is most often selected for manufacturing processes such as printing electronic components and circuit board materials. Piezoelectric DOD printheads offer the demanding combination of high productivity, high reliability and homogeneous characteristics (such as drop volume stability and jet straightness) for jetting materials dispersed or dissolved in organic or aqueous media. Recently, it has proved achievable to project and fabricate highly productive and reliable printheads which assemble the exigent dispensing requirements for flat-panel display production (Le, H. P., 1998).

In piezoelectric DOD printer, a piezo crystal suffers distortion when an electric field is applied. The chamber filled with liquid is contracted in response to application of the external voltage and this distortion is used to mechanically generate a pressure pulse that induces a shockwave in the liquid, which ejects a liquid drop from the nozzle (Magdassi S., 2010; Singh, M. et al., 2009). Figure 1 displays the basic configuration of a piezoelectric printhead.

Figure 1: The basic configuration of a piezoelectric printhead (Magdassi S., 2010).



The ejected drop falls under action of gravity and air resistance until it collides with the substrate and spreads under momentum acquired in the motion; surface tension aids flow through the surface. The drop then dries by solvent evaporation, as shown in Figure 2 (Singh, M. et al., 2009). Advantages of piezo inkjet technology comprise the most elevated level of ink development freedom of any inkjet technology, in addition to long head life. (Magdassi S., 2010). The inks used in this technique consist of a solute dispersed or dissolved in a solvent (Singh, M. et al., 2009).

Figure 2: A schematic representation of the mechanism that occurs during the drop drying process after deposition with inkjet printing (Lim J. A. et al., 2008).



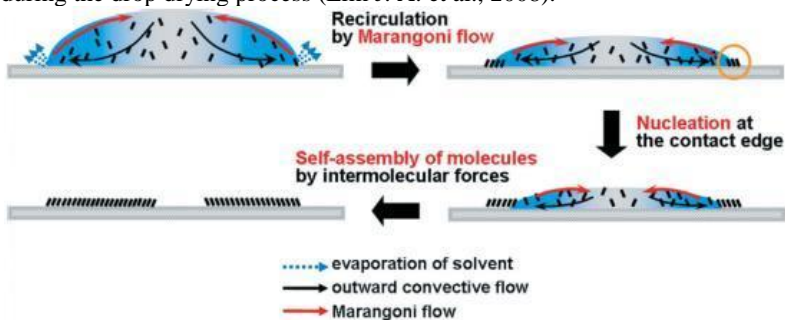
Polymer segment length, which is directly associated to the molecular weight and, consequently, to viscosity, has a crucial impact on the flow properties in piezoelectric inkjet printing, a situation that does affect compression of the fluid and shearing before its ejection from the nozzle (Hill E. K. et al., 2005). Polymers and other solutions and suspensions lend themselves easily to inkjet printing. Yet, printed nanoparticles behave differently from printed polymers and other solutions due to their higher density and elevated probability for phase segregation. The final assembly of such nanoparticles on the substrate relies on surface treatments which modify surface energy properties (Singh, M. et al., 2009).

Almost all traditional interpretation of the inkjet printing process relies on adopting the flow of the fluid ink as a Newtonian fluid, however, sometimes this supposition is invalid, particularly when occurs the rebound of a fluid due to the impact on a low surface energy substrate (Bartolo D. et al., 2007; Singh, M. et al., 2009). Research groups show the understanding of interaction between a non-Newtonian fluid and the substrate as a function of normal stress at the contact line between both (Bartolo D. et al., 2007). They showed that the rebound of the drop may be regulated or even avoided by adding a small quantity of flexible polymer to the solvent. Measurements such as surface tension, contact angle on the substrate of interest, viscosity and computational fluid dynamics modeling have been employed to investigate the flow process likewise the interaction of a falling drop with the substrate.

During the drying process, the evaporation behavior has a fundamental role in regulating the film morphology and the distribution of solute in inkjet-printed films. A ring stain of solute that signalizes the perimeter of the droplet is often observed in most of inkjet printed films, and is the result of known “coffee-stain” or “coffee-ring” effect (Deegan R. D., 1997, 2000). This effect occurs due to a flux of fluid that comes from center to edge of the drop. During drying, if a contact line is pinned, the drop has a fixed contact area which, induced by the differential evaporation rates across the drop, results in a capillary flow of the solvent from its center to the contact line in order to replenish the evaporation loss, leading to the buildup of solute in the periphery as the drop evaporated: liquid evaporating from the edge is replenished by liquid from the interior (Soltman, D. et al., 2008). This effect involves an undesirably irregular distribution of material across the printed drop, which might be prejudicial to device performance. The propensity of dissolved polymers and other nanoparticle species in suspensions and solutions to form coffee-ring-like structures is an unavoidable effect of the surface-tension-driven transport of solutes along a surface with an evaporating solvent. Significant advances have been obtained in recent studies to reduce the impact of such drawbacks on film uniformity and device performance (Singh, M. et al., 2009).

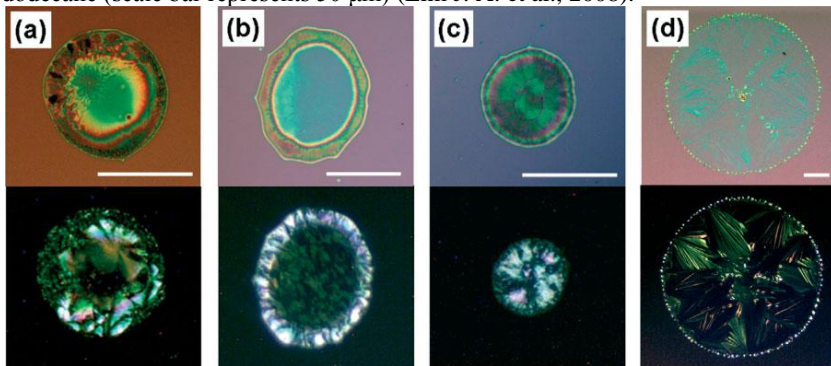
Therefore, one approach to ameliorate the uniformity of inkjet-printed deposits, which makes use of the evaporation-induced flow and, in special, the convective and Marangoni flows (schematized in Figure 3) that happen in a droplet during drying, involves printing from a mixed-solvent system (de Gans B. J. et al., August 2004; Tekin E. et al., 2007). The term "Marangoni flow" is given to spontaneous interfacial flows derived from interfacial tension gradients. These gradients can be generated by local changes of variables that affect the value of the interfacial tension, such as solute concentration, temperature and interfacial electrical potential.

Figure 3: A schematic representation of the convective and Marangoni flows during the drop drying process (Lim J. A. et al., 2008).



Depending on the solvent composition, the convective flow that conducts the solute towards the contact line may be counterbalanced or increased by the Marangoni flow, which as explained earlier is induced by the surface tension gradient between the periphery and the interior of the droplet from regions with low to regions with high surface tension. When the solvent in smaller amounts in the mixture has a higher boiling point and a lower surface tension than the solvent in greater amounts, a Marangoni flow with a direction counter to that of the convective flow may be produced. However, the Marangoni flow may equally raise the convective flow if a low boiling point solvent with high surface tension is included as the minor component. Based on this technique the evaporation-induced flow in droplets can be controlled by changing the composition of the solvent mixture (Lim J. A. et al., 2008). Figure 4 is part of a study using Triisopropylsilylethynyl Pentacene with different mixtures of solvents in order to corroborate the technique described above to reduce the coffee-ring effect.

Figure 4: Optical microscopy and polarized images of inkjet-printed TIPS pentacene droplets using chlorobenzene as the major solvent mixed with 25% of the minor solvent, a) chlorobenzene, b) hexane, c) o-dichlorobenzene, and d) dodecane (scale bar represents 50 μm) (Lim J. A. et al., 2008).



Studies show that employing different surface treatments, bigger particles accumulated closer to the centre of the droplet at high contact angles, while smaller particles under the same conditions moved closer to the contact line at the periphery of the droplet. Moreover, the use of highly hydrophobic substrates benefited in packing of nanoparticles, preventing coffee-ring formation (Perelaer J. et al., 2008). A significant parcel of work needs to be performed in fundamental understanding of the fluid flow process during inkjet printing to enable further progress in this promising field.

Given the intrinsic expense of lithography steps in industrial manufacture and the requirements to reduce the number and level of difficulty of such steps, inkjet printing yields an attractive, material-conserving alternative for various patterning applications. Moreover, inkjet printing is, in addition, an adequate process in circumstances where deposition of a given material must take place in predefined positions on a substrate owing pre-existing structures and devices that would, otherwise, be contaminated and/or deteriorated if a vacuum or spin-coating process were employed. In conclusion, given the impressive recent advances and magnification of inkjet printing to modern areas of materials deposition, this technology ensures a solid future in applied science and engineering.

2.2 SUBSTRATE AND INK INTERACTIONS

In inkjet printing technology, aimed to print a high quality printed device, good resolution, smoothness, evenness and straight patterns are key features. Therefore, it is essential to understand which parameters involved in printing have influence in these characteristics. In order to have a better understanding of this process, it will be introduced the most important parameters which have influence in this technology. Hence, the parameters that play an important role in this process are: physical parameters and physical-chemical properties of ink and substrate.

2.2.1 Substrate Printability

The different parameters which influence in substrate printability are porosity, permeability, roughness, smoothness, cleanliness (absence of impurities such as grease, waxes, etc.), surface energy and its hydrophobic or hydrophilic nature. These parameters will influence in its ability to produce a quality printing. The printability is dependent of the substrate properties as well as of the ink properties being used (as its composition, viscosity, surface tension, etc).

Other important physical parameters to inkjet printing process are the impact and the spreading of a drop on a substrate (Barret M., 2007).

2.2.2 Physical-chemical properties of ink

One of the most important points in inkjet technology is, surely, the physical-chemical properties of ink, especially its viscosity and surface tension. To achieve an optimum performance with the printer used in this work, some features are desirable to the ink, as:

- **Viscosity:** between $10-12 \times 10^{-3}$ Pa.s at jetting temperature. The ideal viscosity range enables an ink to be pulled into and pushed out of the chamber. The viscosity can be lowered somewhat by heating the print head or by adding certain humectants.

- **Surface Tension:** between 32-42 mN/m at jetting temperature. This is high enough to hold the ink in the nozzle without dripping.

- **Low Volatility** - Inks should not dry so quickly that they block the nozzles. Boiling points higher than 100°C are preferable.

- **Density** - Specific gravity greater than 1 is beneficial.

- **Particle Size (Solute)** – It is preferable to have solutes that are completely soluble. Care must be taken since colloidal suspensions or

inks with large particles bigger than 10 μm will clog the nozzles and partially dry, especially at the start of printing.

- **Acidity or Alkalinity** - A pH between 4 and 9 is recommended.

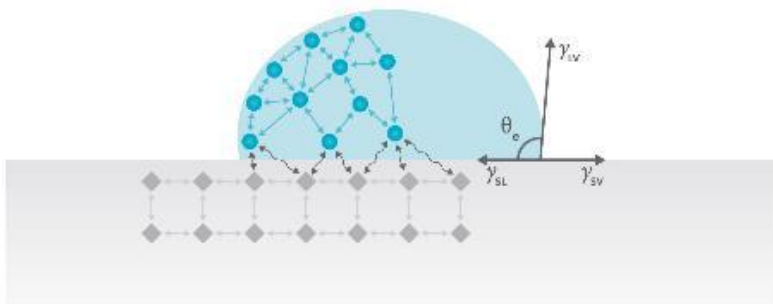
Some fluids out of this range can be jetted, but this implies additional difficulties and performance loss.

2.2.3 Wetting Phenomenon

The wetting phenomenon corresponds to the spreading of a liquid deposited without initial velocity on a substrate and it is quantified by measuring the contact angle of liquid/solid. There is a complex series of mechanisms behind this phenomenon. The most widely used method for determining the wettability is the sessile drop.

The sessile drop is a three-phase system: the solid surface, the drop of liquid and its vapor. These three elements are formed from three interfaces (solid-saturated vapor interface; liquid-saturated vapor interface and solid-liquid interface). The intersection between these three phases gives rise to the so-called line of contact. The goniometric contact angle (θ) is defined as the angle between the tangent to a drop of liquid and the line of contact. Depending on the contact angle, liquids can be classified as nonwetting, partially wetting or completely wetting (Fowkes F. M, 1964). Figure 5 shows schematically the wetting phenomenon, where γ_{SV} is the energy of solid-saturated vapor interface; γ_{LV} , energy of liquid-saturated vapor interface and γ_{SL} , energy of solid-liquid interface.

Figure 5: Representation of interfacial tensions during a wetting phenomenon at an ideal substrate with an angle θ . (www.attension.com/surface-free-energy, accessed October 02, 2012).



It was Young who defined the surface energy as the interaction between the cohesion forces and the adhesion forces. This interaction determines the surface wettability and the ability of a liquid to spread on the surface. By means of measuring the contact angle, the interaction between a surface and a given liquid can be studied. The liquid spreads through a solid surface when the forces of attraction liquid-solid equate or exceed those forces of attraction liquid-liquid (contact angle close to 0°). By conversely, when θ is close to 180° , the adhesion work solid-liquid is zero (spherical drop). This is the limiting case, when there is no adhesion between two surfaces. Based on measurements of contact angle, it is possible to determine the surface energy of a solid (using different liquids with characteristics polar and nonpolar) and the wettability can be defined by the value of static contact angle at the equilibrium, where the liquid will be classified as:

- if $\theta = 0$, completely wetting ;
- if $\theta < \pi/2$, partially wetting ;
- if $\theta > \pi/2$, nonwetting.

Surface free energy is divided into two parts: (a) a dispersive component and (b) a polar component. The surface tension is defined according to Young's equation (Hansen F. K., 2004).

$$\gamma_{LV} \cos\theta = \gamma_{SV} - \gamma_{SL} \quad (1)$$

Wu's harmonic mean method: This method utilizes a harmonic mean equation to sum the dispersive and polar components. Contact angles against two (or more) liquids with known values of γ^d and γ^p are measured. According to Wu, the harmonic mean is better appropriate for low energy surfaces, such as polymers (Hansen F. K., 2004). Wu's equation is presented in the equation 2:

$$\gamma_{SL} = \gamma_S + \gamma_L - 4 [(\gamma_S^p \gamma_L^p / \gamma_S^p + \gamma_L^p) - (\gamma_S^d \gamma_L^d / \gamma_S^d + \gamma_L^d)] \quad (2)$$

The resulting equation when combined with Young's equation yields:

$$(1 + \cos \theta) \gamma_L = 4 [(\gamma_L^d \gamma_S^d / \gamma_L^d + \gamma_S^d) + (\gamma_L^p \gamma_S^p / \gamma_L^p + \gamma_S^p)] \quad (3)$$

where γ indicates surface tension (surface free energy), the subscripts L and S indicate liquid and solid, and the superscripts d and p indicate dispersive and polar components.

In the inkjet printing, the chemical nature of the substrate affects the pattern size, since if the substrate and the ink have a hydrophilic nature, the drop will spread immediately on the substrate due to wetting phenomena. Thus, it is important to control these phenomena in order to have a better control of the pattern size. Sometimes a slight dewetting of ink on a substrate may be preferable to reduce the size of printed patterns and improve resolution (Barret M., 2007).

It is possible to change the chemical nature of a substrate, and thus its surface energy, doing some surface treatments, as plasma. For example, a CF_4 plasma can make the treated surface more hydrophobic whereas an oxygen plasma can make the surface more hydrophilic.

2.3 ORGANIC AND PRINTED ELECTRONICS

Organic electronics are based on the association of new materials and cost-effective, large area production processes that approximates new fields of application. It also allows a broad range of electrical components that can be fabricated and directly integrated in low cost reel-to-reel processes. Some of the key advantages which organic and printed electronics can offer are thin, light-weight and flexible products in addition to environmentally friendly processes. First organic and printed electronic products reached the market in 2005/2006 (OE-A Roadmap White Paper, 2011). While no organic and printed electronic products have really reached full mass market insertion, it seems that this is still likely for some products in the coming years.

The main applications of organic and printed electronics include organic photovoltaic cells (OPV), flexible displays, electroluminescent and OLED based lighting, printed RFID, organic memory devices, organic sensors, flexible batteries, smart objects and smart textiles. (OE-A Roadmap White Paper, 2011). Many of these applications demand inexpensive, often single-use devices that are ideally fitted to inkjet printing (Singh, M. et al., 2009). Several examples of promissory fields of application for organic and printed electronics established on new vast scale processable electrically conductive and semiconducting materials are intelligent packaging, rollable displays, flexible solar cells, transponders, energy efficient lighting, disposable diagnostic devices or games, low cost RFID, printed batteries and wearable electronics in garments (OE-A Roadmap White Paper, 2011). The large number of

applications reflects the complexity of the subject and the wide possible uses for organic and printed electronics and it is likely that the list will even grow in the future, since the technology is still in its early stage of development and is in the transition from lab-scale and prototype activities to production. Currently, only few products are commercialized in niche markets, however, many products are expected to establish in the near future and going to produce significant revenues in the medium and long term.

The Organic Electronics Association (OE-A), a working group which represents the whole value chain in organic and printed electronics, divides these applications in 5 main groups:

- **Organic Photovoltaics**
- **Flexible Displays**
- **Lighting** (including both OLED and electroluminescent (EL) products)
- **Electronics and Components** (including RFID, memories, batteries and other components)
- **Integrated Smart Systems** (ISS, including smart objects, sensors and smart textiles)

The potential to gather and assemble multiple electronics devices to called smart objects, integrating multiple organic devices, is the great benefit of organic and printed electronics. This process started with devices with simple functions, as an animated logo, and continuously will develop in complexity and size, allowing flexible complex systems, like smart cards or large area gameboards. These combinations are achievable thanks to the new processes and materials employed in organic and printed electronics. This enables the integration, onto one single substrate, of distinct devices such as transistors, memories, sensors, batteries or displays. The integration can be accomplished either by one process or by a hybrid arrangement of several apart fabricated devices (OE-A Roadmap White Paper, 2011).

All fields present particular vantages and restrictions with respect to current solutions based on conventional electronics. The capacity for high volume production at low cost and consequently the potential to qualify electronics in areas where today's conventional electronics are hardly integrated associated to their low thickness and great flexibility are the main advantages of organic and printed electronics in almost all application fields. However, some limitations exist as well. These are owing to the inherent lower electronic properties of the materials (e.g. conductivity, charge carrier mobility, life time) and the processes (printing vs. clean room processes). Thereby, organic and printed

electronics is in most cases not considered to replace standard electronics but will enable new application areas, where the properties of printed electronics provide important advantages.

The *Organic Electronics Association* anticipates the development of the performance potentials in nine application fields, which are briefly summarized in Table 1.

Table 1: Organic Electronics Association Roadmap for organic and printed electronics, with forecast for the market entry in large volumes (general availability) for the different applications.

	existing until 2010	Short-term 2011–2014	Medium term 2015–2019	Long term 2020+
Organic Photovoltaic	Consumer electronics	Outdoor recreational application and remote	Off-grid buildings facade and BIPV	Roof top grid connected
Flexible Display	Flexible segmented displays integrated into smart cards, price labels	Rollable colour displays, OLED TV	Electronic wallpaper	Rollable OLED TVs, telemedicine
OLED Lighting	Design lighting (prototype)	Decorative lighting (products)	Flexible lighting elements	General lighting technology
Electronics & Components	Printed RF-tags, primary batteries, printed memories for games	RFID for brand protection, advanced memories, transparent conductors for touch sensors	RFID and memories for logistics and smart applications, integrated batteries	RFID for item level, memories for multimedia, integrated batteries and components
Integrated Smart Systems	Simple physical and chemical sensors, textile photo-detectors, OPVs for battery charging	Sensor arrays, intelligent tickets, integrated displays, OPV in textiles	Complex smart packaging, fibre integrated sensors	Miniaturised diagnostics/lab on a chip

2.4 THE ADVENT OF ORGANIC ELECTRONICS WITH THE BIOLOGICAL INTERFACE

The goal of combine the advantages of organic electronics with biology, especially to explore new ways to reverse the solutions, sometimes restricted, offered by conventional technologies based on silicon, is the reason why large research groups aims to connect microelectronics to medicine, converging technologies that enable improve quality of life and lower costs in the health system.

“Synthetic metals” have lately passed for a fast development in electronics, especially because they are flexible, inexpensive and mostly easy processable (Forrest S. R., 2004; Malliaras G.G. et al., 2005; Müller D. et al., 2011, 2012). Several applications have used this class of materials, for example in flexible displays (Choi M-C. et al., 2008), flexible radiofrequency identity tags (Subramanian, V. et al., 2005), light-weight solar panels (Helgesen M. et al., 2010), smart labels (Jakimovski, P. et al., 2012), Field Effect Transistor (FET) (Wen Y. et al., 2010) and biomedical devices: in tissue engineering (Ndreu A., 2007), bionic interfaces (Wallace G., 2007), artificial sensors (Isaksson J. et al., 2007; Brochu P. et al. 2010) or implantable biosensors (Malhotra B. D. et al., 2006) and as components for ameliorating neural probes (Berggren M. et al., 2007; Guimard N. K. et al., 2007; Rogers J. A. et al., 2010).

Implantable electrodes and microelectrodes have been used for neuromuscular electrical stimulation (Sheffler L. R. et al., 2007), electrocorticography (ECoG) (Kim D. H. et al., 2010), spinal cord (Rodger D. C. et al., 2008), interfaces (Wallace G., 2007), deep brain stimulation (Coffey R. J., 2009), transducers for cardiac pacemakers (Curtis A. B., 2009), cochlear (Wilson B.S. et al., 2008) and retinal implants (Margalit E. et al., 2002), peripheral nerve (Navarro X. et al., 2005) and more generally, for brain-machine interfaces (Donoghue J. P., 2008; Stieglitz T. et al., 2009). Until recently, electrodes were made only of metals or inorganic semiconductors, or hybrids thereof, but studies demonstrate that these traditional conductors may be entirely replaced by highly flexible electroconductive polymers (Molina-Luna K. et al., 2007; Rodger D. C. et al., 2008; Rubehn B. et al., 2009; Blau, A. et al., 2011). Some of the reasons behind this replacement are that most of the classical microfabrication technologies demand access to expensive equipment and clean room infrastructure besides requiring carrier substrates that support the respective processing conditions,

which establish limitations onto device flexibility, biostability and biocompatibility and also in transparency (Stieglitz T., 2007).

Studies have shown the use of metal electrodes coated with conductive polymers, which are implanted in the central nervous system, perform an electrical interface with neurons, providing stimulation and recording the electrical activity of these neurons (Kim D.-H. et al., 2008; Wallace G. G. et al., 2009; Asplund M. et al., 2010). There are also researches testing the use of macroelectrodes produced in PPy: PSS (PoliPyrrol: Polystyrene-sulfonate) for tissue integration (George P. M. et al., 2005); and the diffuse electrical stimulation through nanofibrous scaffolds based on polyaniline (Ghasemi-Mobarakeh L. et al., 2009) and on microbial polyester (PHBV) (Ndreu A., 2007) have been reported to have a beneficial effect on cell proliferation and growth of nerve cells. Furthermore, conductive polymers may be functionalized with biomolecules which stimulate neural growth and minimize immune response to implants (Lin Y. et al., 1994; Kim D.-H. et al., 2008; Wallace G. G. et al., 2009; Asplund M. et al., 2010). Likewise, organic devices that accomplish transduction on a single-level cell with proper temporal resolution to recognize individual exocytosis events have already been developed. Several research groups have shown that coating metallic electrodes with conductive polymers such as PPy (Cui X. et al., 2001) and PEDOT (Ludwig K. A. et al., 2006), can decrease the electrical impedance of microelectronic devices (Chen, Y. et al., 2009; Yang, S. Y. et al., 2011; Blau, A. et al., 2011). In addition, there is evidence that conductive polymers expressively increase the electrode-tissue interaction (Green R. A. et al., 2009; Poole-Warren L. et al., 2010) and the electrical characteristics of conventional metal (Guimard N. K. et al., 2007; Abidian M. R. et al., 2010) or semiconductor-based bioelectric signal transducers (Bystrenova E. et al., 2008). Other examples are organic electronic ion pumps (Isaksson J. et al., 2007) and ion transistors (Margalit E. et al., 2002), which are newly created devices capable of the precise delivery of neurotransmitters to neurons. For this reason it can be said that conductive polymers may complement, or even replace, classical conductor materials in biomedical applications in a near future, since the ability of organics to transport ionic and electronic charge originate the opportunity to interface with electrically active cells in new ways (Isaksson J. et al., 2007).

In particular, researchers have focused efforts in order to replace partially or fully rigid implants (particularly with sharp edges) by flexible implants since the differences in mechanics and form between

this sort of devices and biological systems, conduct, almost always, to low-fidelity coupling at the biotic/abiotic interface in addition to limited long-term tissue health (Kim D-H. et al., 2010). Another important factor that motivates the fabrication of flexible implantable devices is soft and curvilinear nature of most human tissues, since the insertion of rigid devices may bring damages to adjacent tissues to the implant site or cause aversive reactions such as inflammations, encapsulation or even rejection or implant failure (Chen, Y. et al., 2009; Yang, S. Y. et al., 2011; Blau, A. et al., 2011). This conception can help in creating a modern generation of soft, minimally invasive, and curvature-adaptable *in vivo* probes and implantable electrodes (Blau, A. et al., 2011).

It is motivated in these studies that appears the intention of fabricate a flexible device that allows its use (implantation) in humans, combining their main characteristics: biocompatibility and flexibility, in application of new medical technologies that do not damage or endanger even more the parts of the body being treated.

2.5 SPECIFIC MATERIALS

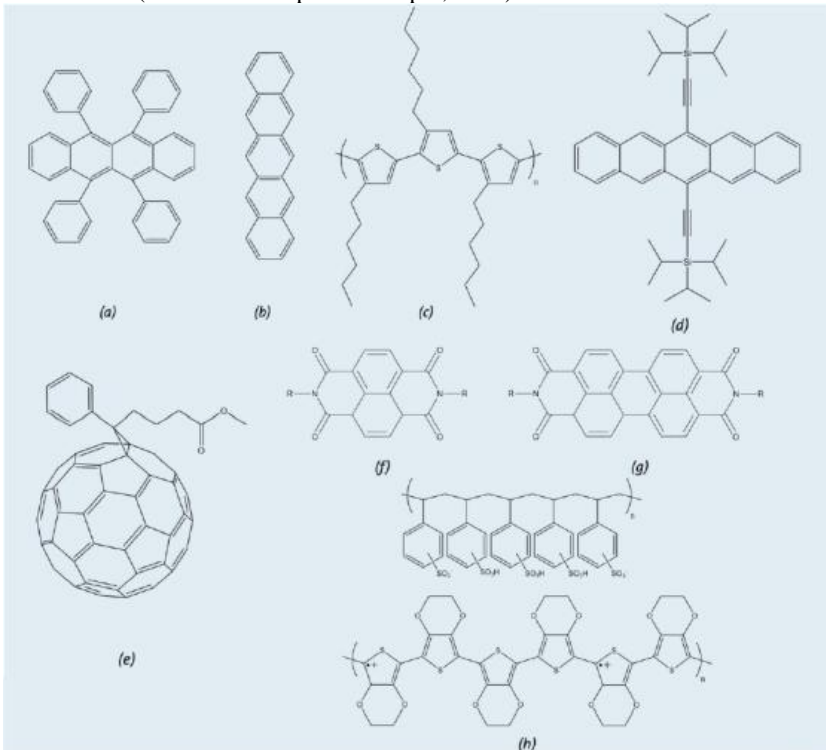
The choice of materials is an important step for a proper operation of the electronic device and to obtain a successful printing. For organic and printed electronics (usually semiconductor perspective) what is occurring is the development of materials that are easily and cost-effectively scale and that can conserve high power conversion efficiencies (PCEs) over long enough lifetimes when deposited with the thicker films necessary for high-volume manufacturing and subjected to real-world environmental conditions (OE-A Roadmap White Paper, 2011). The main examples of semiconductor and conductors materials used in producing organic and printed electronics devices are illustrated in Figure 6.

Novel material classes such as carbon nanotubes or hybrid (organic - inorganic) material combinations and device architectures are further new approaches to improve the performance of the devices. The selection of conducting materials is very dependent on their application. For high metallic conductivity it is still required to use filled materials, as silver inks. However, if conductivity is solicited in combination with high transparency, specific inorganic materials such as indium tin oxide (ITO) or the polymeric PEDOT:PSS represent state of the art solutions.

Transparent organic conductors are improving in performance but still present lower conductivities values compared to metal oxides like ITO. Advantageously the polymers admit for wet processing and the

flexibility of polymer coatings makes them the chosen candidates for substitution of conventional brittle inorganic materials, since researches have been done over the years in order to improve charge carrier mobility of these materials and it is forecast that it will have major improvements in the future, see Figure 7. Because their continuously improving properties, therefore, these materials are already qualified and used for determined sophisticated applications such as electrochromic displays and touch screens.

Figure 6: Structures of common materials for organic and printed electronics. The semiconductors a) Rubrene; b) pentacene; c) polythiophene P3HT; d) TIPSPentacene; e) PCBM; f) NTDI; g) PTCDI and the conductor h) PEDOT:PSS (OE-A Roadmap White Paper, 2011).

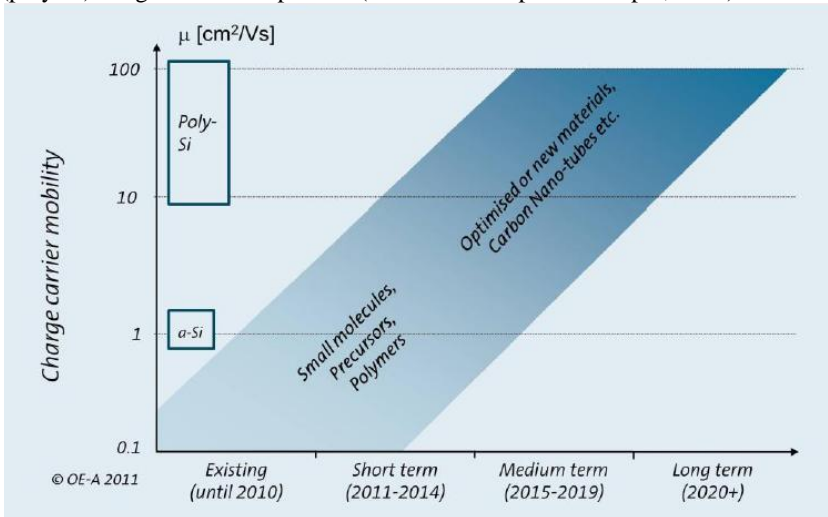


Recently, important progress has been made with solution based carbon nanotubes and other nano wire based concepts in terms of conductivity and transparency. Furthermore, for high metallic conductive nanoparticle inks silver and gold nanoparticles represent the

state of the art as well as organometallic inks. More recently, nanoparticle compositions have become available driven by the prospect of lower temperature sintering (and therefore increased conductivity) and fine line printing. As the trend goes to fully printed devices, printable dielectrics and passivation materials will complement wet chemical processing of semiconductors.

The wide number of applications of flexible electronics requests for each application their own specific requisites and, therefore, a suitable substrate. In general, glass, silicon and metal (usually stainless steel) are still the only substrates readily available with high and reliable barrier properties, a fundamental requisite for many applications. Among the polymer substrates, the most broadly employed nowadays in organic and printed electronics are the polyester grades (PET, PEN), however, also other polymers, paper and textiles have been used in these applications. In order to achieve physical and surface properties over a vast range, polymeric materials like PET, PEN or PC (polycarbonate) may be tailored so that they may suit as complete solutions. Other plastics like polyimide (PI, in particular [®]Kapton), polyethersulfone (PES), polyetheretherketone (PEEK) or Parylene are specialities and therefore higher priced materials with particular advantages like chemical stability.

Figure 7: Charge carrier mobility of semiconductors for organic and printed electronics applications. The values refer to materials that are available in commercial quantities and to devices that are manufactured in high throughput processes. The values for amorphous silicon (a-Si) and polycrystalline silicon (poly-Si) are given for comparison (OE-A Roadmap White Paper, 2011).



However, most materials used in organic and printed electronics need to be improved, concerning electrical performance, processability and stability. Materials also need improved environmental stability to enable operation in more robust environments and to reduce barrier requirements. Moreover, special formulations with non-toxic solvents are urgently needed for many materials.

To achieve a satisfactory performance, printed electrodes should satisfy a number of conditions, such as low resistivity, chemical stability and a low work function (energy needed to extract an electron) (Barret M., 2007).

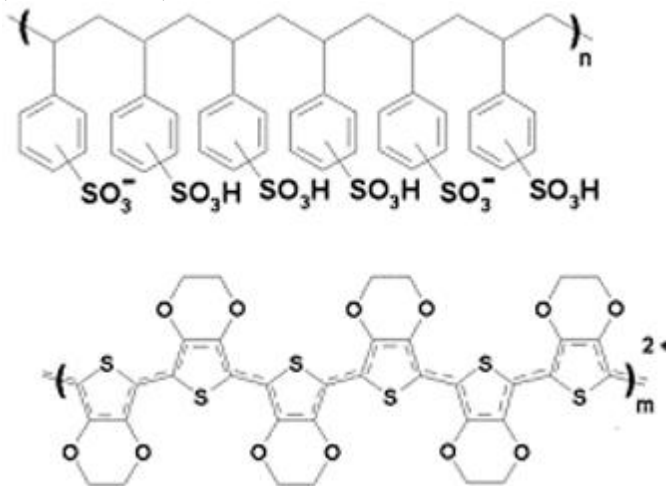
In this work it was used two different classes of conductive materials (inks) to print the electrodes: one based in conductive polymers and another based in metals. The goal of using this sort of materials is to obtain a printed device which exhibits a high conductivity using the lowest possible temperatures of post-treatment. Equally important, the final device should be insulated from the external environment and, to satisfy this requirement, a chemical resistant and waterproof polymer ink was used to print a thick film upon the device.

The substrate where these electrodes were printed is a “green” polymer chemistry and the most bio-accepted coating, principally for devices permanently implanted into the body (www.scscoatings.com, accessed August 20, 2011).

2.5.1 Conducting Polymer – PEDOT:PSS

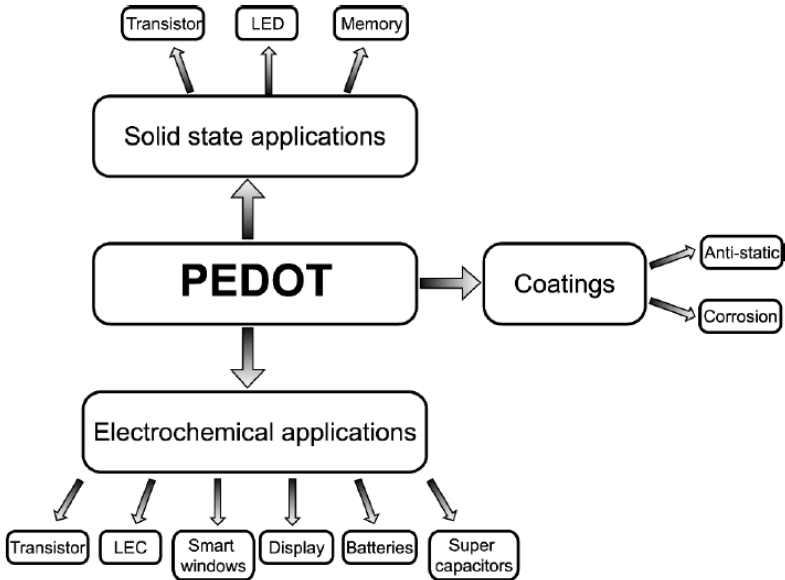
The conductive polymer chosen for this work was the poly(3,4-ethylenedioxythiophene) PEDOT, doped with poly(styrenesulfonate) PSS, one of the most studied and characterized conjugated polymers and the only conductive polymer commercially available for inkjet printing technology. The chemical structure of PEDOT and its dopant is shown in Figure 8.

Figure 8: Chemical structure of PEDOT (bottom) and of its dopant PSS (top) (Barret M. 2007).



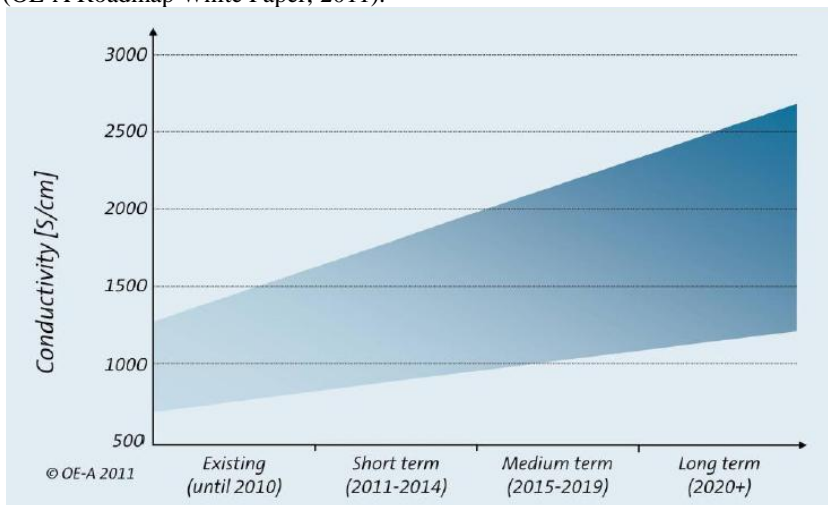
The most important features of PEDOT:PSS are its high conductivity, its excellent chemical stability and its low band gap. In addition, it absorbs strongly in the red part of the visible spectrum, which results in a deep blue color (Nilsson D., 2005). Some applications of PEDOT are shown in Figure 9:

Figure 9: Different applications where PEDOT can be applied (Nilsson D., 2005).



Furthermore, continuous advancement in enhancing the electrical conductivity of PEDOT:PSS polymer has been reached over the past years, as clear from Figure 10.

Figure 10: Past and predicted future progress in conductivity of PEDOT:PSS. (OE-A Roadmap White Paper, 2011).



Charge capacity and ionic conductivity of PEDOT associate to superior thermal and electrochemical stability (Yamato H. et al., 1995; White R.E. et al., 1999; Guangchun L. et al., 2000; Cui X. et al., 2003; Wang X. et al., 2004; Yang N. et al., 2006; Abidian M.R. et al., 2008) when compared to other semiconductor polymers, make this conducting polymer a more promising candidate for long-term implantation in the central nervous system (CNS), being also a good quality polymer to be used as a micro-neural interface material for electrostimulation (Seth J. W. et al., 2009). Some studies have shown that PEDOT coating of microelectrodes reduces the impedance modulus by approximately two orders of magnitude (Cui X. et al., 2003; Abidian M.R. et al., 2008) facilitating the activation of neurons (Nyberg T. et al., 2007) and the recording of neurophysiological signals (Cui X. et al., 2003; Ludwig K.A. et al., 2006). The purpose of coating with conducting polymer is to ameliorate the electrode tissue communication through a high surface area material more conductive to cell and tissue integration. Other studies showed that PEDOT films exhibit very low intrinsic cytotoxicity with NIH3T3 fibroblasts and that their inflammatory response upon implantation is good, making them ideal for biosensing and bioengineering applications (Luo S. et al., 2008). Further research revealed excellent adhesion and proliferation of neuronal cells on PEDOT-coated PET nanofibres (Bolin M.H. et al., 2009). The

interactions among PEDOT and neural cells aiming the development of electrically conductive biomaterials seeking for direct and functional contact with electrically active tissues, such as the nervous system, skeletal muscle and heart was also studied by polymerizing PEDOT around living cells (Richardson-Burns et al., 2007). Investigation of chemically deposit PEDOT on acellularized muscle tissue constructs revealed that *in situ* polymerization occurs all-over the tissue, transforming it into an extensive acellular, non-antigenic substrate which will be essential for *in vivo* tests associated to nerve repair and bioartificial prostheses (Peramo et al., 2008).

Examples such as an electrophoretic ion pump made of PEDOT:PSS to deliver ions (Ca^{2+} and K^+) or neurotransmitters (Isaksson J. et al., 2007; Simon D.T. et al., 2009) in quantities that induce biological signals highlight others advantageous features that allow this material to be used in biological applications. However, the application of PEDOT:PSS in neuroprostheses (devices that use electrical current to restore nerve function in patients who suffer from neural impairments) has been limited by its wanting biocompatibility considering the acidic and surfactant behavior of PSS (Asplund M. et al., 2008). Studies investigating PEDOT:PSS in applications as substrate for primary cerebral cortex neurons (J.E. Collazos-Castro et al., 2010), in neural probes applications - neural regeneration devices, neural stimulation and neural recording electrodes (Cui X. et al., 2003; Xiao YH. Et al.; 2004; Yang J. et a., 2005; Ludwig KA. et al., 2006; Cui X. et al., 2007; Green et al., 2008; Green et al., 2009; Subramaniam V. et al., 2011), in drug delivery devices (Abidian MR. et al., 2006) and its polymerization around living neural cells (Richardson-Burns SM. Et al., 2007) have been developed in the past years.

An important advantage of this polymer for use in organic devices is that PEDOT is the most commonly investigated polymer with several dopant types diversifying from polymers or small salt ions to biospecific dopants such as proteins, peptides and neurotrophins, thereby increasing its availability for applications in biological interfaces.

2.5.2 Conducting Metal – Silver ink

Metals are well-known materials for their conductivity. Due to their low resistivity and also to their weak oxidation ability, the principal materials employed to develop inkjet conductive inks are silver and gold (Denneulin, A. et al., 2011). Silver conductive materials have

been used for many years in printed flexible devices such as membrane touch switches, keyboards and RFID antennae. These have traditionally been screen printable formulations for enabling low cost (Xue F. et al., 2006) and high speed manufacture of highly conductivity printed tracks (Meier H. et al., 2009). These compositions usually contain micron sized silver particles, solvents, organic resins and rheology modifiers and are cured or dried at temperatures around 120°C. Because of their small size, nanoparticles exhibit low sintering temperatures (Lee C-L. et al., 2011; Denneulin A. et al., 2011; Liu Y-F. et al., 2012) compared to the melting point of bulk material, due to the bigger surface/volume ratio. During the sintering, the coalescence of nanoparticles creates a continuous percolation path for the passage of electrons through the material. These nanoparticles must present a high dispersion to prevent the aggregation and sedimentation of these particles in solution since that can lead to reliability problems of printing (nozzle clogging) (Barret M., 2007).

As advances in organic and printed electronics are made, there is an increasing demand for printable conductive tracks in many different application areas such as smart packaging, flexible displays, OLEDs, thin film transistors, OPV and smart textiles. Silver is still the material of choice due to its extremely high conductivity, stability and high volume manufacturability. There are now a variety of silver conductors available depending on the application and these can be applied by various techniques such as screen, flexography, gravure and ink jet (Kim D. et al., 2007; Chiolerio A. et al, 2011). Advances in particle and binder technology induced to a strong develop in performance of these silver inks in terms of conductivity, flexibility, line resolution, in addition to compatibility with several substrates.

In this work, the metallic conductive ink chosen was a Silver Nanoparticle Ink, not only because silver inks are the state of the art of metallic inks for inkjet printing, but equally because the conductive inks which provide the highest conductivity using the lowest post-processing temperatures (preventing subsequent damage to the underlying organic layer) are inks based on metallic nanoparticles. In addition, thermally deposited silver has been shown to form an ohmic contact with many semiconducting polymers (Liu Z. et al., 2005; Xue F. et al., 2006).

2.5.3 Insulating Polymer - Polyimide

After printing the complete conductive device, it is necessary to insulate it from the external environment to prevent short circuit as well

as to avoid the contact between the metal and the human body where the device will be employed or implanted. Moreover, this material should be waterproof, since most of the liquid present in the human body is composed of water, to avoid the contact between metallic material and these fluids. Thereby, to meet these requirements, the material chosen for this work was a Polyimide ink. This ink presents characteristics such as thermal stability, good chemical resistance and excellent mechanical properties (www.chisso.co.jp/english, accessed August 20, 2011). This is a commercial recently launched ink, already prepared for use in inkjet printing technology, and therefore there is no previous works reporting its applications. Until recently, polyimide had been used only as dielectric layer or as substrate materials.

2.5.4 Substrate – Parylene C

Parylene is the generic name for members of a unique polymer series. The basic member of the series, called Parylene N, is poly-para-xylylene, a completely linear, highly crystalline material. There is a variety of these polymers: Parylene N, C and D. Parylene C, the most popular among the three and the one used in this work, is a member of the series produced from the same monomer modified by the substitution of one of the aromatic hydrogens for a chlorine atom.

The Parylene C is a chemically inert, thermoplastic, hydrophobic, crystalline, optically clear (Chang T. Y. et al., 2007) biocompatible polymer coating material used in a wide variety of industries, in aerospace, chemical, automotive, consumer, pharmaceutical, and defense applications. Features as its all-carbon structural backbone, high-molar weight and nonpolar entities turn parylene C extremely resistant to most chemicals, as well as to fungal and bacterial growth. In addition to having conducive biochemical properties, parylene C has a Young's modulus of 3 GPa (Chen, P. J. et al., 2006) making it mechanically resistant and highly appropriate for fabricating stable and reusable microfluidic devices or stencils (Tooker, A. et al., 2005; Wright, D. et al., 2007; Jinno S. et al., 2008).

Parylenes exhibit high crystallinity and melting temperatures, in addition to their high molecular weight (~ 500.000), therefore they cannot be formed by conventional process such as molding or extrusion and thence it is deposited by vapor deposition. Therefore, PaC provides a conformal coating on virtually any substrate which is not achievable by other means, enabling that the entire object to be coated is uniformly impinged by the gaseous monomer. This is responsible for the surely

conformal nature of coating. One of the advantages of the Parylenes is that they can be formed in very thin layers. Its lubricity is close to that of Teflon however it can be applied uniformly in much thinner coatings. Parylene is transparent and colorless because it presents extremely little absorption in the visible region. Parylene's pinhole free conformal coating guarantees coated substrates will be protect from chemicals, moisture and electric charge. It can also be easily removed from the original surface allowing the transfer of devices (Rodger D. C. et al., 2008), for example, to a human body, with an excellent conformation with the new substrate, even upon irregular forms (www.scscoatings.com, accessed August 20, 2011). Furthermore, PaC is a “green” polymer chemistry and the most bio-accepted coating for stents and pacemakers (Peters M. S., 1984; Iguchi N. et al., 1997).

The chemical structure of parylene C is presented in Figure 11:

Figure 11: Chemical structure of Parylene C (www.scscoatings.com, accessed August 20, 2011).



Parylene may be annealed to enhance cut-through resistance, increase hardness and ameliorate abrasion resistance. This is the result of a density and crystallinity increase. Furthermore, the Parylenes are insoluble in all organic solvents up to 150° C, as well, they resist room temperature chemical attack. Good to excellent adhesion of Parylene to a large variety of substrates may be obtained by the easy treatment with a dilute solution of an organic silane anterior to Parylene coating.

Its mainly applications comprises conformal coating of printed circuit boards for protection against moisture and corrosive environments, surface passivation and environmental protection of semiconductor devices, conformal coating of biomedical devices for environmental protection (Schmidt, E. M. et al., 1988; Xie X. Z. et al., 2011) and electrical insulation requirements. Parylene C is the material of choice for coating critical electronic assemblies due to its ability to propitiate a true pinhole free conformal isolation (Noordegraaf J., 1997).

Studies have shown parylene C to be more hemocompatible and less thrombogenic than silicon (Weisenberg, B. A. et al., 2002). Furthermore, parylene C is a potentially utile material for studies with *in vitro* cell culture. Parylene C has also revealed great stability *in vivo* for a diversity of utilizations, such as cardiovascular implants (Eskin, S. G. et al, 1976; Schmidt, E. et al., 1988). Parylene C STF (Stratamet Thin Films) presents high surface area to volume ratio, what enables it to support high level of cell adhesion (Demirel, M. C. et al., 2007). Due to the importance in explore possible biomaterials which can be employed to produce biomedical microdevices, poly-(chloro-*p*-xylylene) became one such potential candidate for fabricating this sort of devices since studies show that the adhesion of mammalian cells, NIH-3T3 fibroblasts and AML-12 hepatocytes, among others, to surface-treated parylene C (including its variants) were similar to substrates used as standard tissue culture (Chang T. Y. et al., 2007; Wright, D. et al., 2007, 2008; Wei L. et al., 2010; Zhang C. et al., 2011), such as polystyrene. These results characterize parylene C and its surface-treated variants as a utile material for fabricating cell-based microdevices. (Chang T. Y. et al., 2007).

2.6 OXYGEN PLASMA TREATMENT

Plasma is a gas of neutral molecules which are energized. It can be done by the gas exposure to a high electric field until the moment where some electrons become free and the energized gas converts into a mix of ionized atoms, electrons, molecules, photons and residual neutral species. This mixture operates as a chemically active environment that may be completely controlled and reproduced. The plasma treatment changes the surface both in composition and roughness. Alteration of composition of polymer surfaces can make the surface to be highly hydrophilic, which mostly rely on enhancing the ratio of oxygen-containing group. The C=O bond is the fundamental factor to ameliorate the hydrophilicity of polymer surfaces. The roughness of the surface is also improved and it has an influence on the surface hydrophilicity (Lai, J. et al., 2006).

3. MATERIALS AND METHODS

3.1 MATERIALS

The fabrication of organic, flexible devices produced in this work comprises the use of three different inks and one substrate, which are described in the following sections:

3.1.1 Parylene C

The substrate used to print the devices is a chemical vapor deposited poly(p-xylylene) polymer, deposited on top of a glass slide. The chemical precursor used to the Parylene polymer deposition, di-para-xilylene dimer, was purchased from Specialty Coating Systems™. The PaC vacuum deposition is done with the SCS LABCOTER® equipment, supplied from the same company. The layer thickness obtained after deposition is around 2 μm. Table 2 is summarizing the main properties of Parylene C (Data provided by the supplier).

Table 2: Main properties of Parylene C.

Properties	PaC
Young's modulus (Pa)	2.8×10^9 (27.6×10^2 MPa)
Tensile Strength (Pa)	6.9×10^7 (68.9 MPa)
Yield Strength (Pa)	5.5×10^7 (55.2 MPa)
Elongation to break (%)	200
Yield Elongation (%)	2.9
Density (g/cm^3)	1.289
Water absorption (% after 24 h)	less than 0,1
Melting point ($^{\circ}\text{C}$)	290

3.1.2 Silver Nanoparticle Ink

The silver nanoparticle ink used in this work was purchased from Sun Chemical under the tradename Suntronic Jet Silver U5603. This ink is especially designed for piezoelectric inkjet printing. The metal loading is approximately 20% by wt. according to the supplier and the major liquid vehicle was identified to be ethanol. The average diameter of the silver nanoparticles is approximately 20 nm. Its viscosity is between $11 - 13 \times 10^{-3}$ Pa.s and its surface tension is 28 -31 mN/m (Data provided by the supplier).

3.1.3 PEDOT:PSS ink

The PEDOT:PSS ink used in this work is produced by AGFA with the trade name Orgacon IJ-1005. Its composition is 99% PEDOT inkjet-Ink and 1% Ethanol. It is odorless and completely miscible in water. Its relative density is 1.001 and its boiling point is $> 100^{\circ}\text{C}$. The solid content is 0.8 wt%, its viscosity range is $7 - 12 \times 10^{-3}$ Pa.s, the surface tension is 31 - 34 mN/m and its pH is 1.5 - 2.5 (Data provided by the supplier).

3.1.4 Polyimide Ink

The Polyimide ink was purchased from Chisso Petrochemical co. under the acronym PI 6302-002. It presents an excellent jettability and properties as viscosity of $8,6 \times 10^{-3}$ Pa.s, solid yield of 28,5wt% and surface tension of 27,6 mN/m. The solvent present is the Diethylene Glycol Methyl Ethyl Ether (EDM) (Data provided by the supplier).

3.1.5 Printer Dimatix DMP 2800

The printer used in this work to print the devices was the Dimatix Materials Printer, model DMP-2800 (Figure 12), purchase from Fujifilm Dimatix, Inc. This printer is a relatively low cost, highly featured printer that provides a good starting point for investigating a potentially method for electronics manufacturing. This printer presents features such as high resolution printing capabilities, a built in drop watcher, a maintenance station and a fiducial alignment camera.

The DMP 2800 is suited to print fluids (inks) containing proteins, nucleic acids, nanoparticles, conductive polymers, etc. The inks are filled into a disposable cartridge that has 16 individually tunable, piezo-actuated nozzles. Cartridges are available to dispense 10 pL or 1 pL drops. Drops are printed by voltage-driven deformations of a membrane wall of a chamber behind each nozzle. The segments of this action make up a waveform that is optimized for each ink as well as the intended print job. Others settings that can be adjusted are print height, nozzle firing voltage, meniscus volume, cartridge temperature, that can be adjusted up to 70°C , and temperature of the vacuum platen (which holds the substrate in place) that can be adjusted up to 60°C .

Figure 12: Dimatix Materials Printer, Model 2800. Fujifilm Dimatix, Inc., USA.



3.2 METHODS

The procedure executed until obtain the final printed device consists of four main steps:

1. Preparation of substrate

Parylene C (PaC) is deposited on glass slides via chemical vapor deposition (CVD), from the di-para-xylylene dimer. The process of vacuum deposition is performed with the equipment SCS LABCOTER[®] 2 Parylene Deposition System 2010, from the Specialty Coating Systems[™] company.

The process to cleaning the glass slides before the deposition of PaC consists of:

- ✓Washing the glass slides with soap and deionized water and drying with compressed air;
- ✓Permanence in ultrasound bath of acetone and drying with compressed air;
- ✓Cleaning in “multifunctional cleaning”, following the standard program to cleaning glass substrates. Equipment used: Ultra-100 Integrated Cleaner & Vapor Coater, from Nanonex company.

2.Characterization of substrate and inks

Before starting the printing process, it is essential to characterize the substrate to measure its surface energy as well as to characterize the inks regarding their wettability on the substrate (contact angle) in order to predict their behavior during the printing process. These measurements are performed in the Goniometer DataPhysics, Contact Angle System OCA.

3.Optimization of Printing Parameters

To obtain high quality printed patterns, several relevant parameters should be taken into account, involving printing parameters, parameters of ink and substrate parameters. Among the printing parameters, three of them were optimized (at the printer) and performed separately for each ink: waveform, drop spacing and substrate temperature. These parameters will be explained in more details on section 3.2.2.

4.Printing the final device

Only after all the aforementioned parameters are adjusted for each ink, is possible start the step of printing the final device. All designs printed must be perfectly aligned to obtain a successfully printed device. The printing process consists of following steps:

- i) Printing of silver nanoparticle ink (forming conductive tracks), followed by sintering process.
- ii) Printing with PEDOT:PSS ink (small opened rectangles that will be in contact with the tips of silver tracks), followed by the annealing.
- iii) Printing of polyimide ink (forming a thick film upon the device, leaving opened only the rectangles of PEDOT:PSS), followed by solvent evaporation and annealing.

The procedure adopted for the preparation of inks to ensure that the cartridge will be able to produce stable jets and the nozzles will be free of clogging, further the description of heat treatments used are described below:

➤ **PEDOT:PSS ink:**

To printing with PEDOT:PSS ink, the first step to be realized is

degassing/filtration of the ink. This was found after trying to print the ink without its previous degassing/filtering, which resulted in printing nozzles completely clogged after a few minutes. Thus, the steps to be followed before start printing are:

1. Degas the ink in an ultrasonic bath for 15 minutes (to ensure the separation of any agglomerate possibly formed, thus avoiding a material loss during filtering);

2. Filter the ink with a PTFE (or PVDF) syringe filter, pore-size 0.2 μm (to prevent clogging nozzle, the particle size should be smaller than 1% of the nozzle diameter – the nozzle of the 10pL cartridge has a diameter of 21.5 μm);

3. Fill the 10 pL cartridge with approximately 3 - 4 mL of ink.

The annealing conditions indicated by the supplier are 3 minutes at 120°C on hot plate.

➤ **Silver Nanoparticle Ink:**

This ink must remain all the time on the rotating rolls to avoid the aggregation of nanoparticles. Before fill the cartridge it is important to follow almost the same steps needed to print PEDOT:PSS. Steps to be followed are described below:

1. Degas the ink in an ultrasonic bath for 10 minutes;

2. Filter the ink with a PTFE (or unreactive material) syringe filter, pore-size 0.45 μm ;

3. Fill the 10 pL cartridge with approximately 3-4 mL.

The annealing conditions are dependent of the time and the temperature used. Varying these parameters, the sintering process is varied and consequently the electrical resistivity of the material. The greater is its sintering, the greater is its electrical conductivity. To avoid PEDOT:PSS and PaC degradation, the annealing condition was set in 2.5 h at 130°C in atmospheric oven.

➤ **Polyimide Ink:**

PI 63002 must be kept in a freezer (temperature less than minus 15°C). Before fill the cartridge no filtration is required. Thus, the steps to be followed before start printing are:

1. Thaw the frozen ink to room temperature before use. This process consists in leave ink bottle standing for 1 to 2 hours;
2. Fill the cartridge with approximately 3-4 mL of ink at room temperature;
3. Leave the filled cartridge at rest for 1 hour to remove microbubbles from ink.

The curing conditions indicated by the supplier are 5 minutes at 80°C on hot plate (to volatile solvents) more 30 minutes at 230°C in atmospheric oven. However, to prevent PEDOT:PSS and PaC degradation, instead of use 230°C for 30 minutes, the curing was realized at 150°C for 1 hour.

3.2.1 Oxygen Plasma Treatment

The oxygen plasma treatment performed in this work was realized in a Reactive-Ion Etching (RIE) equipment using a standard cleaning program used by the researchers from CMP (Centre Microelectronique de Provence, France) to clean the silicon wafers. The equipment used was the Plasmalab 80 Plus, from Oxford Instruments. The power used was 100 W and the operating pressure used was 0.3 mbar.

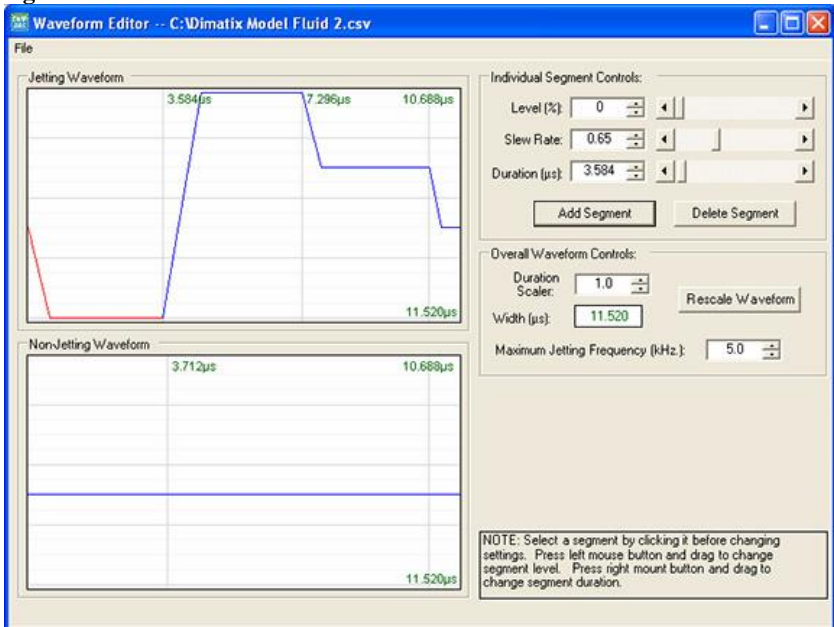
3.2.2 Evaluation of printing parameters

Before start printing the complete device, it is important to adjust several parameters involved in the printing process. There are lots of relevant parameters which can be optimized to obtain a high inkjet printing quality, involving printer parameters, such as pulse voltage, drop spacing and waveform settings; ink parameters, such as composition, viscosity, and temperature and, finally, substrate parameters, such as surface energy, temperature, porosity and roughness, among others.

In this work, the improvement of only few parameters was focused because this process could take a long time to be fully completed. Therefore, for each ink used, it was realized the improvement/adjustment of the following parameters:

i) Waveform: sets the sequence of drive pulses applied on a piezoelectric chamber wall to generate a variable-size drop. A model of a Dimatix waveform is shown in Figure 13:

Figure 13: Waveform editor on Dimatix Control Panel.



The typical waveform is divided into four segments, each with adjustable settings: duration, level and slew rate. The applied voltage (amplitude) is related to bending the fluid chamber membrane. The slew rate controls how fast you are bending it, and the duration is how long it stays in that position. The applied voltage and the first two segments have the most impact on jetting. The first voltage pulse deforms the piezoelectric channel walls so as to increase the volume of the ink chamber and create a negative pressure in the ink chamber; a subsequent voltage pulse decreases the volume of the ink chamber and increases the pressure in the ink chamber thereby ejecting a droplet from the ink chamber. The voltage pulses are then removed from the electrodes to bring the ink chamber back to its original volume. This sequence of drive pulses may be repeated a number of times corresponding to the number of droplets to be ejected successively for merging into a drop.

ii) Drop Spacing: the Drop Spacing is the center to center distance from one drop to the next drop in X and Y axis to create the pattern. The X spacing is controlled by the X axis encoder, while the Y

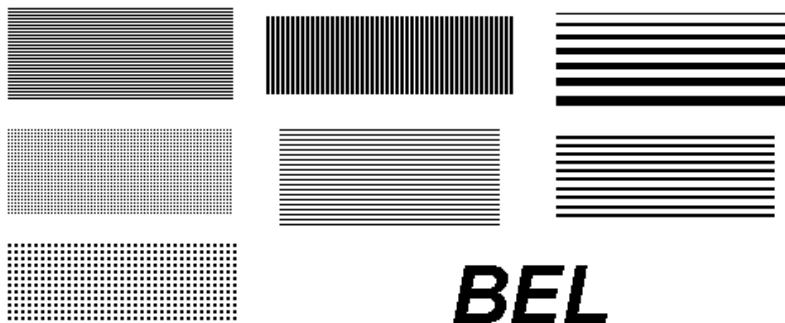
axis is controlled by the cartridge angle. The drop spacing is responsible for the pattern resolution and it should not have very high values, to avoid the separation between the drops (if the goal is printing a continuous line, for example) but also should not have very small values, to avoid a super overlap between the drops, which can lead to a loss of the pattern design. In the printer Dimatix, the drop spacing can be adjustable between 5 and 254 μm .

iii) Substrate temperature: if the substrate is at room temperature, there will be a greater spread of ink upon the surface of the substrate when compared to a heated substrate. A heated substrate will lead to a faster evaporation of the solvent present in the ink, which allows a better shape control of the design by reducing the ink spread. Playing with this parameter, it is possible to print superposed lines to, for example, create thicker lines to decrease the resistance of a conductive line. The thickness and width increases linearly with the number of passes, and in this case, the control of line's geometry can be done by the control of substrate temperature. However this heating should not be exceedingly elevated, because to maintain a good control of the drops positioning, the distance between substrate and cartridge should be typically less than 2 mm, but, if the substrate is excessively hot, the heat transfer from the substrate to the nozzle can cause a partially or completely clog nozzle.

To perform this optimization a pattern containing vertical lines, horizontal lines, lines of different thicknesses and dots were used. Figure 14 shows the pattern utilized to perform this parameters optimization.

The results of the development of improved printing parameters for each ink are discussed in section 4.

Figure 14: Pattern used to perform the parameters optimization. (BEL: Departmente of Bioelectronics)

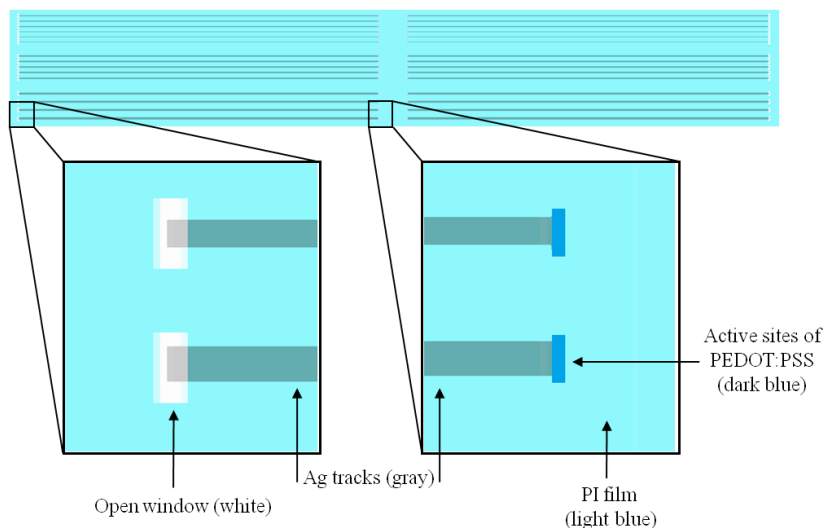


3.2.3 Printing the Final Device

To print the final device, it is imperative to take into account the drop spacing used to print all the 3 materials, because to keep the original pattern and to ensure the perfect alignment between them, it is necessary to use the same drop spacing value for all printings.

The final device consists in printing 3 different materials: silver ink, responsible for the electrode tracks; PEDOT:PSS, responsible for the active sites (rectangles) and polyimide ink, responsible for the protective layer. The pattern of polyimide ink is a rectangle, forming a film above the device, with small opened windows i) upon the PEDOT:SS rectangles in the middle of the device (PEDOT:PSS will be in contact with external environment) and ii) upon the outer silver tracks edge. The design of the device is shown in Figure 15:

Figure 15: Design of the final device.

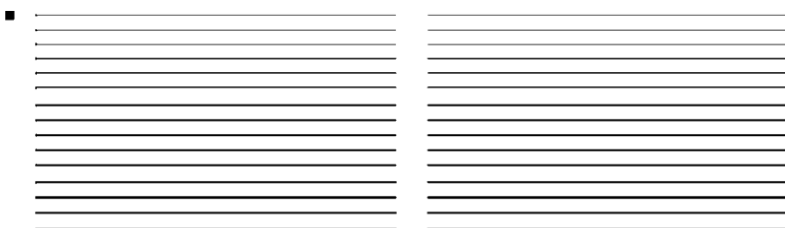


All PEDOT:PSS rectangles have the same area but the width of silver lines increase from top to bottom. The pattern was design purposely in this way to verify if a variation in contact area between PEDOT:PSS and Silver will implicate in a significant difference in impedance values obtained from the electrochemical impedance spectroscopy (see Appendix A).

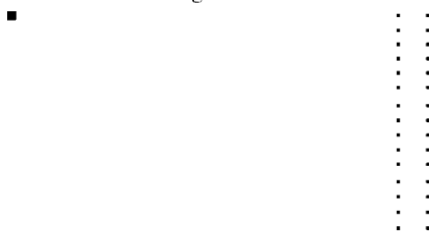
The patterns used in Dimatix to print every separated part of the device are shown in Figure 16.

Figure 16: Patterns of each step of printing for silver nanoparticle ink, PEDOT:PSS ink and polyimide ink, respectively.

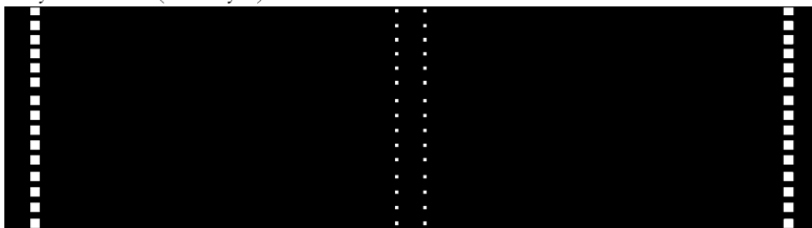
Silver tracks



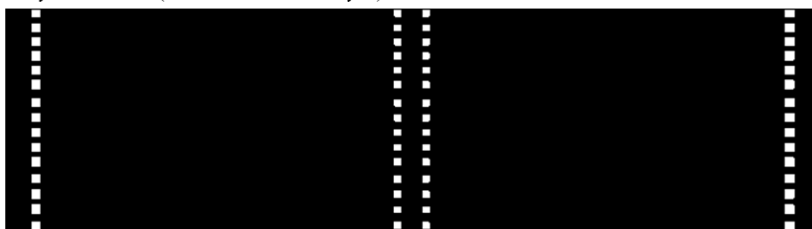
PEDOT:PSS rectangles



Polyimide film (first layer)



Polyimide film (second and third layer)



To ensure that windows of PEDOT:PSS will be open at the end of Polyimide printing, it is necessary to print the second and third layers (of PI) with slightly bigger windows than the first layer. If the printing is not realized in this way, at the end of printing the third layer of PI, PEDOT rectangles will be completely covered by PI ink, due to its spread on the surface (the wettability between polyimide-polyimide is

much higher than the wettability between polyimide-parylene and polyimide-PEDOT:PSS).

3.3 CHARACTERIZATION

The equipments utilized to characterize the inks, substrate and the final device are listed below:

3.3.1 Determination of Surface Energy and Contact Angles

The measurements of surface energy and contact angles were performed with the Goniometer DataPhysics, Contact Angle System OCA.

The equipment provides different results of surface energy, which are obtained from different methods. The chosen method was the Wu method (Kapur D. et al., 1988). This method uses the harmonic mean and is better suited for low energy surfaces, such as polymers (Hansen F. K., 2004).

The surface energy characterization of the substrate Parylene C was made using the sessile drop technique. In this method the Young-Laplace equation is used to calculate the surface tension by adjusting the shape of the drop (captured by video image) to the equation, since the Young-Laplace equation relates interfacial tension to drop shape. Liquids with known surface energy are used. The shape of the drop, specifically the shape in the contact liquid/solid (contact angle) and the known surface energy of the liquids are the parameters which can be used to calculate the surface energy of the solid sample. It is necessary the use of several different liquids and the software executes the calculations automatically (Woodward R. P., 2007). The liquids with known surface energy used in these measurements were: ethylene glycol 40%, diiodomethane and deionized water.

In the measure of contact angles, three measurements were performed for each sample, and values are expressed in terms of mean value and standard deviation.

3.3.2 Optical Microscopy

The optical microscope was used to obtain quality images of the printed devices, after the heat treatment. The equipment Eclipse L200, from Nikon enabled to acquire images with 50 X the real magnitude.

3.3.3 Mechanical and Optical Profilometer

The mechanical and optical profilometers were the equipments used to measure the thickness of printed layers for each ink. The mechanical profilometer utilized was the XP-2 Profiler, from Ambios Technology, and the Optical Profilometer was the WYKO NT1100 Optical Profiling System, from Veeco.

3.3.4 Electrical Resistivity

For thin samples the most commonly used measurement to calculate the electrical resistivity of a material is the sheet resistance, measured in ohms per square (as the size of the square is not relevant to this measurement, there is no unit for sheet resistance).

The sheet resistance of Silver and PEDOT:PSS printed patterns was measured with a 4-point probe measurement in a Multi Height Microposition Probe equipment from Jandel, and the resistivity values were obtained from the RM3000 Four Point Probe Test Unit equipment, from Jandel as well.

The equations used to calculate the electrical resistivity (equation 4) and conductivity (equation 5) of a material was:

$$\text{Resistivity [ohm.cm]} = \text{sheet resistance} \times \text{thickness (in cm)} \quad (4)$$

$$\text{Conductivity [S.cm}^{-1}] = 1 / \text{Resistivity} \quad (5)$$

Five measurements were performed for each sample, and values are expressed in terms of mean value and standard deviation.

3.3.5 Scanning Electron Microscopy (SEM)

Scanning electron microscopy was employed in order to analyze the microstructures of silver layers printed to verify the degree of sintering. The equipment used to capture the images was the microscope Ultra 55, from Carl Zeiss.

3.3.6 Cell culture assays

One of the cells used in this experiment were the Caco-2, a continuous line of heterogeneous human epithelial colorectal

adenocarcinoma cells. Each tested sample was placed in a Petri dish and a sterilization process was performed leaving each sample immersed in ethanol for 20 minutes; posteriorly, these samples were rinsed three times with PBS for 5 minutes each rinse. The number of cells put in each Petri dish was 1.1×10^5 cells and the samples were kept in a cell incubator at 37°C containing 5% of CO_2 . The medium was changed twice per week (Medium: DMEM, add 10% of Foetal Bovine Serum (FBS); 0.1% of Gentamicin; 1% of PenStrep and 1% of Glutamax).

The other cell used in this experiment was the PC-12, a cell line derived from a pheochromocytoma of the rat adrenal medulla. PC-12 cells stop dividing and terminally differentiate when treated with nerve growth factor, what makes PC-12 cells useful as a model system for neuronal differentiation. The experiment was conducted in the same mode as with the Caco-2 cells; however, this time the number of cells put in each Petri dish was 2.7×10^5 cells and the medium used was RPMI (add 5% of Foetal Bovine Serum (FBS); 10% of Horse Serum; 1% of PenStreo and 1% of Glutamax).

For each test, five squares of different sizes were printed in five different glass slides coated with PaC. Parameters used to print and to annealing the samples were the same used to print the device (including the same number of layers). Squares were printed with areas multiplied by a factor of 2.

Viability and cell proliferation were determined by the mitochondrial activity of cells through MTS colorimetric assay [(3-(4,5-dimethylthiazol-2-yl)-5-(3-carboxymethoxyphenyl)-2-(4-sulfophenyl)-2H-tetrazolium)].

For MTS assay the cells used were B16F10 mouse melanoma cells - a strain of spontaneous melanoma of rats C57BL / 6 selected by Fidler (1973). The melanoma cells were kept in a cell incubator at 37°C containing 5% of CO_2 , in DMEM medium (Dulbecco's modified Eagle's medium) supplemented with 10% of foetal bovine serum (FBS), 2 mM of L-glutamina, $4.5 \text{ g}\cdot\text{L}^{-1}$ of glucose, $1.5 \text{ g}\cdot\text{L}^{-1}$ of sodium bicarbonate, 1% of penicillin and streptomycin. For viability and cytotoxicity tests the number of cells seeded upon the devices was $5 \times 10^5 \text{ cells}/\text{cm}^2$.

B16F10 cells were seeded onto the surface of the device utilizing a cell density of $5 \times 10^5 \text{ cells}/\text{cm}^2$. Viability and cell proliferation were evaluated after 24 hours of culture. Carrying out the MTS assay, the medium was removed and the samples were rinsed three times with PBS and moved to a new culture plate. Then, 8 mL of medium and 1600 μL of MTS reagent were added to each culture plate containing the device. The culture plates were kept in a cell incubator at 37°C containing 5%

of CO₂ for 1 hour. Thereupon, the solution (medium/MTS) was homogenized, and 100 µL of solution of each sample were transferred to a new 96-well cell culture plate. The solution absorbance was measured at 490 nm and analyzed in a microplate reader (equipment TP Reader NM, from Thermo Plate).

Simultaneously to the MTS assay, a qualitative analysis of Live/Dead assay was also performed. The Live/Dead@Viability/Cytotoxicity (Invitrogen) Kit is used only with mammalian cells and measure intracellular esterases (calcein) activity and plasma membrane integrity (ethidium homodimer). A calcein solution: ethidium homodimer (4:1) in PBS was prepared and 500 µL of this solution were added to each sample containing approximately 1000 µL of incomplete medium. Thereupon, the culture plate was kept at 37°C containing 5% of CO₂ for 45 minutes. After incubation, the samples were prepared and analyzed by the fluorescence microscope (equipment Ecliose Ci, from Nikon). The images from Fluorescence microscopy determines the live cell number (green color) and the dead cell number (red color).

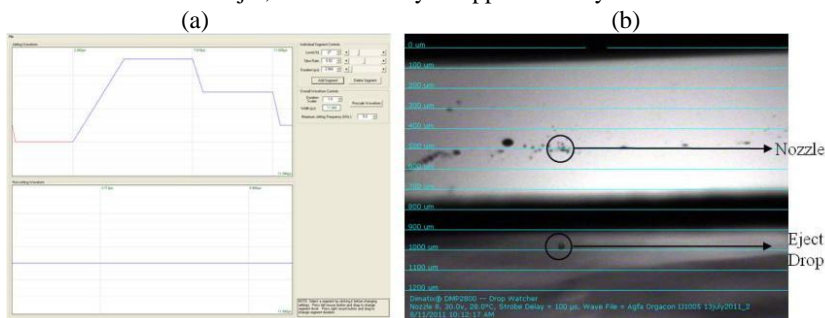
4. RESULTS AND DISCUSSION

4.1 PEDOT:PSS PARAMETERS EVALUATION

The first parameter to be adjusted is the waveform. There are several standard waveforms provided for model inks or common solvents and in most cases they are provided by the ink supplier. This waveform can be used as a starting point and only some adjustments are required. The main requirements to be met are obtain a high velocity jet and a good drop formation, avoiding satellites drops and tails.

The waveform optimized for the PEDOT:PSS IJ 1005 ink and an image of its jets are shown in Figure 17.

Figure 17: (a) Optimized waveform for PEDOT:PSS IJ 1005 ink. (b) Image of a PEDOT:PSS IJ 1005 jet, with a velocity of approximately 5m/s*.



To show the important effect of the waveform in jet velocity, a different waveform and its drop ejection are shown below for the same ink. Only changing the waveform parameters, the drop velocity was changed from 5 m/s to 2 m/s (Figure 18).

*This image was taken freezing the drop 100 μs after drop ejection (see Strobe Delay on the image). As the drop traveled approximately 500 μm (see the gratificate screen), its velocity is around 5 m/s.

Figure 18: (a) Modified Waveform for PEDOT:PSS IJ 1005 ink. (b) Image of a PEDOT:PSS IJ 1005 jet using the waveform showed in (a); velocity reduced to approximately 2 m/s.



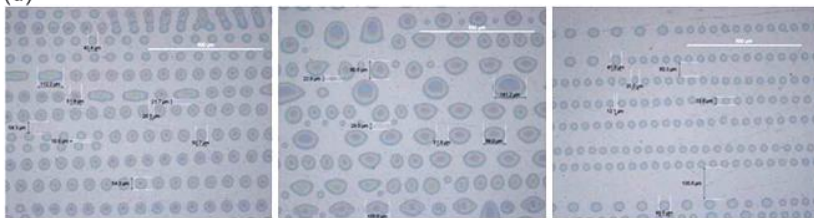
After optimizing the waveform, it is necessary to adjust the drop spacing and substrate temperature. Only the most relevant images of each combination of parameters will be presented (normally, vertical and horizontal lines and single dots). The optical microscopy images were always taken after the heat treatment.

Figure 19 shows the printing at room temperature (28°C), where the parameter changed was the **Drop Spacing**.

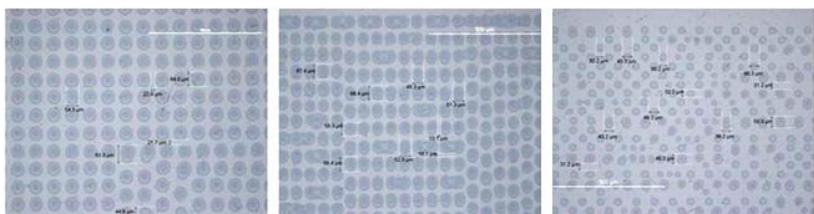
As it is possible to verify from Figure 19, it is not possible to obtain an impression of the desired patterns utilizing these values of drop spacing. What is supposed to be horizontal lines (left) and vertical lines (middle) are just an agglomerate of connected droplets. From the image of single dots (right), it is possible to observe that a unique droplet has a diameter of approximately 25 μm. The printed pattern similar to the original pattern was the vertical line using 15 μm of drop spacing (Figure 19 (d)). The closer are the drops (decreasing the drop spacing), the bigger are the agglomerates, because, printing with 25 μm of drop spacing, 1 agglomerate corresponds to 1 drop (2 drops at maximum) however printing with 14 μm of drop spacing, 1 agglomerate corresponds to 4 or 5 drops (it is possible to see this evolution from the first to the last photo representing the horizontal lines)

Figure 19: Printing with (a) 25 μm, (b) 20 μm, (c) 17 μm, (d) 15 μm and (e) 14 μm of Drop Spacing (Left: horizontal lines; middle: vertical lines and left: single dots). Scale bar: 500 μm.

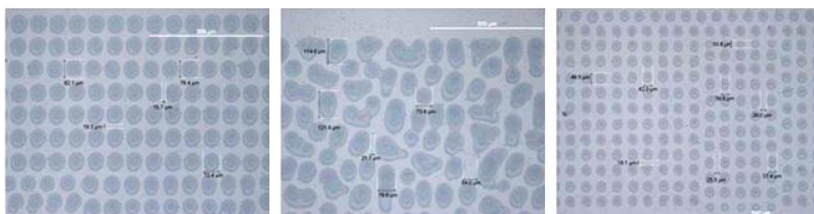
(a)



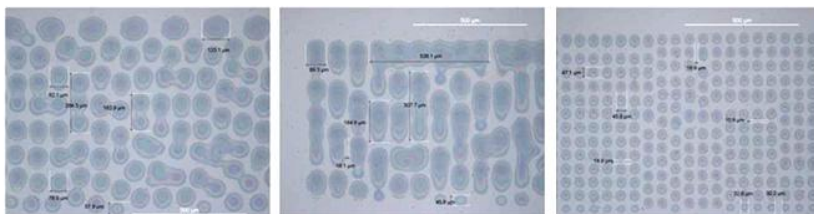
(b)



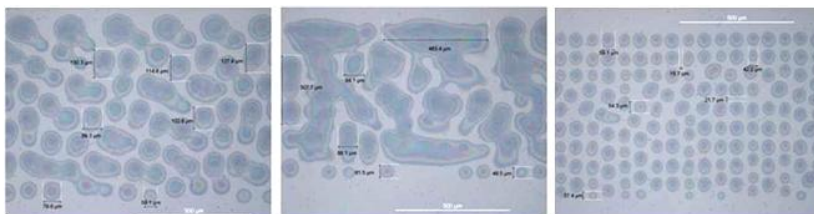
(c)



(d)



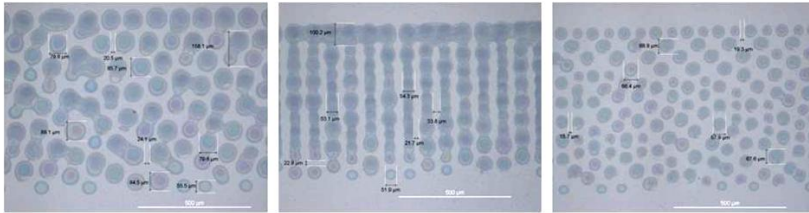
(e)



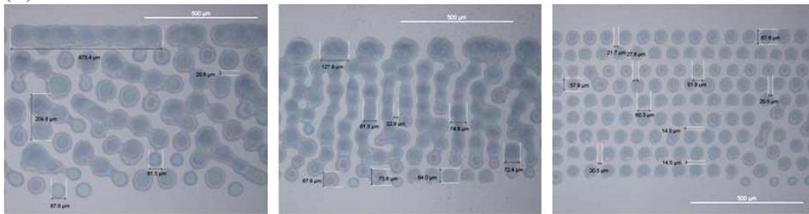
In order to verify if there are any changes in this behavior, the substrate temperature was increased. Figure 20 shows the printing at 35°C, where the parameter changed was the **Drop Spacing**.

Figure 20: Printing with (a) 14 μm and (b) 13 μm of Drop Spacing (Left: horizontal lines; middle: vertical lines and left: single dots). Scale bar: 500 μm .

(a)



(b)

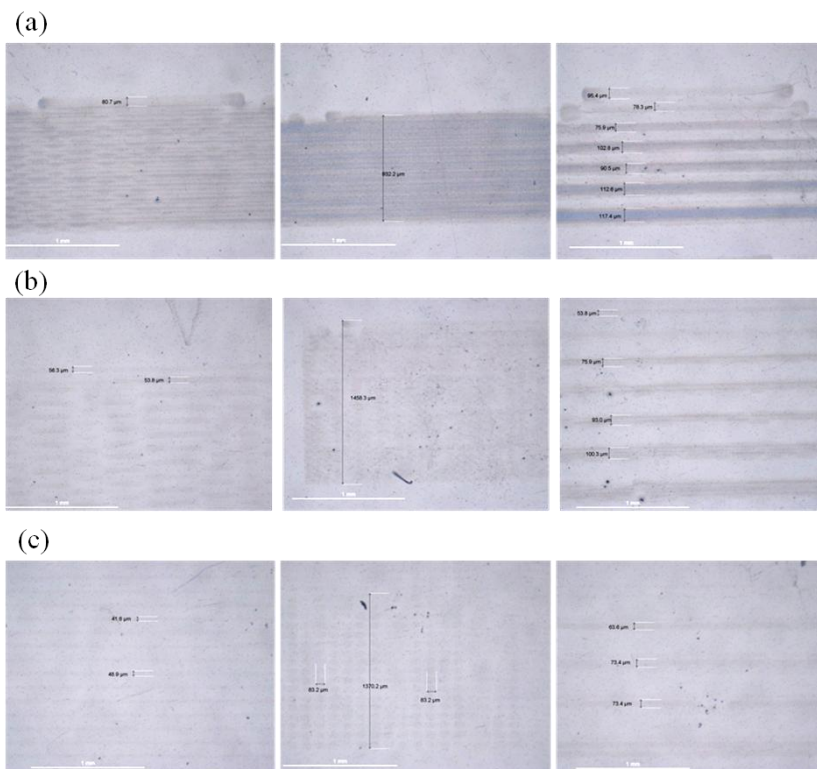


Even increasing the temperature to 35°C, it was not possible to reach satisfactory printed patterns. The printed pattern which exhibited a closer pattern from the original was the vertical line using a drop spacing of 14 μm (Figure 20 (a)). For this reason, it was decided to use this value as drop spacing and only continue increasing the temperature to verify the adequate condition for printing line-patterns. Figure 21 shows the printing using only 14 μm as Drop Spacing value, varying the **temperature**.

From these images, it is possible to observe that the only pattern which approximates of the original pattern is the vertical line (images on the middle). The best printed pattern for the vertical lines is the pattern printed at 40°C using a drop spacing of 14 μm (Figure 21 (a)). For the horizontal lines, none of the printed patterns approximates from the original pattern.

Figure 21: Printing with (a) 40°C, (b) 45°C, (c) 50°C, (d) 55°C and (e) 60°C of temperature. (Left: horizontal lines; middle: vertical lines and left: single dots). Scale bar: 500 μm .

Figure 23: Printing with (a) 20 μm , (b) 30 μm and (c) 40 μm of Drop Spacing. (Left: horizontal lines; middle: vertical lines and left: lines of different thicknesses). Scale bar: 1 mm.

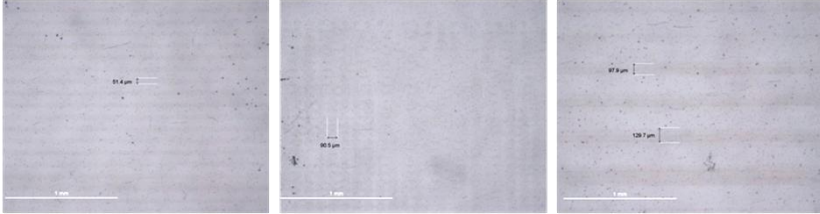


Even printing utilizing a big drop spacing (if compared with the drop spacing values used before), as wide as 40 μm , it can be observed that it is possible to obtain line-patterns, especially for horizontal lines. These printed samples have a lighter color when compared with the samples printed without plasma treatment because this time the ink spread is much higher and, consequently, the layer is thinner (the thicker is the layer, the darker blue is the pattern).

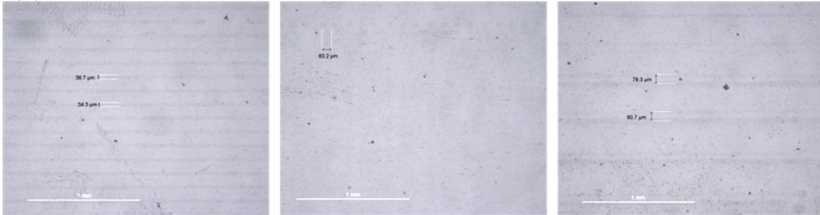
For other sample group, the drop spacing was kept in 40 μm and the substrate temperature was increased. Figure 24 shows the printed patterns using 40 μm of Drop Spacing, varying the **temperature**.

Figure 24: Printing with (a) 35°C and (b) 40°C of temperature. (Left: horizontal lines; middle: vertical lines and left: lines of different thicknesses). Scale bar: 1 mm.

(a)

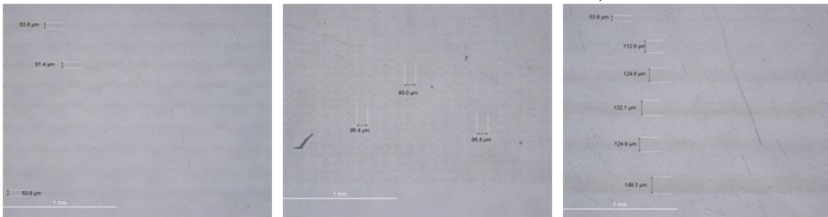


(b)



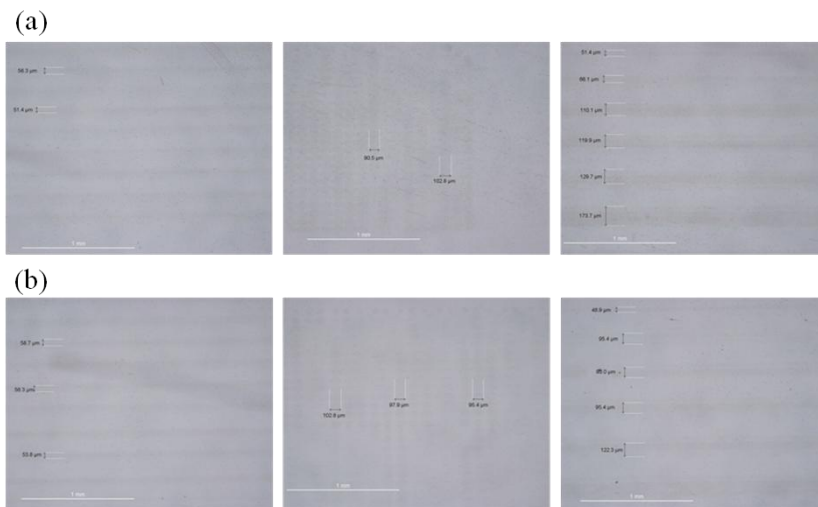
As the ink spreading is very large, what makes it difficult to control the pattern size and, sometimes, the form (design) of the pattern, it was decided to decrease the time of plasma treatment from 3 to 1 minute to verify the effect of plasma treatment on the pattern quality. Figure 25 shows the printing at room temperature (28°C), using a drop spacing of 35 μm and oxygen plasma treatment for 1 minute.

Figure 25: Printing with 35 μm of Drop Spacing. (Left: horizontal lines; middle: vertical lines and left: lines of different thicknesses). Scale bar: 1 mm.



Printing with a slightly increase in substrate temperature, now using 32°C, is shown in Figure 26, varying the **Drop Spacing**, for the same time of oxygen plasma treatment used previously (1 minute).

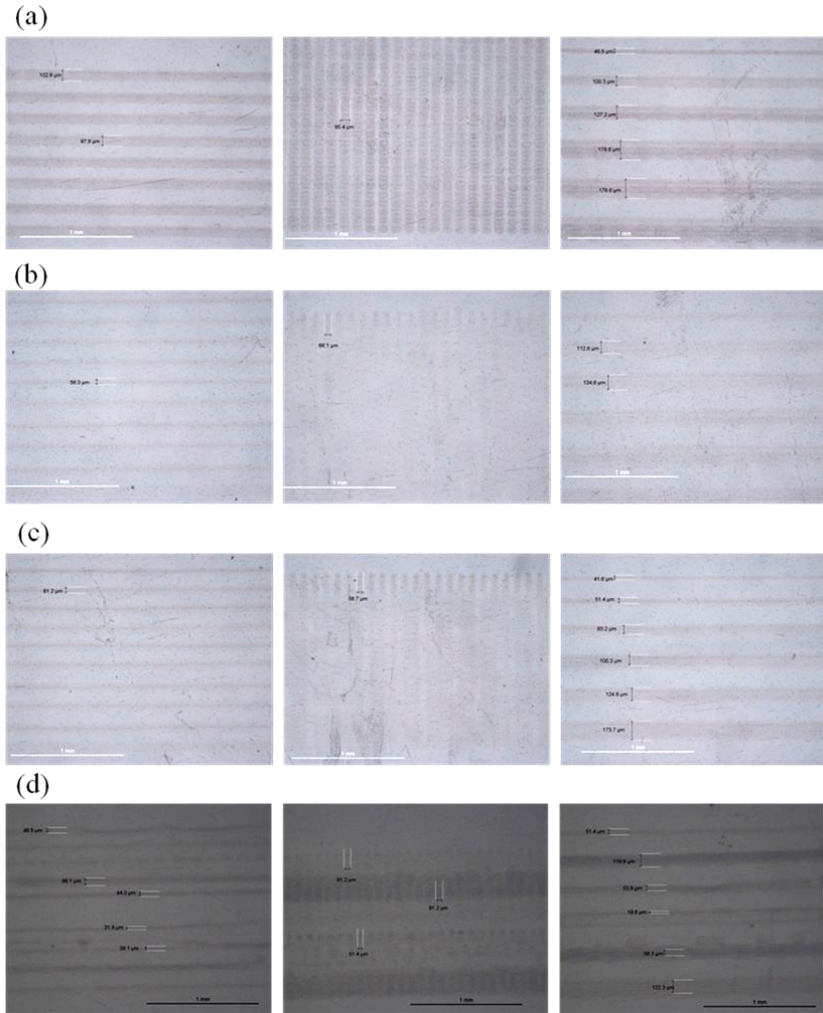
Figure 26: Printing with (a) 35 μm and (b) 38 μm of Drop Spacing. (Left: horizontal lines; middle: vertical lines and left: lines of different thicknesses). Scale bar: 1 mm.



There are no considerable differences among the last printed patterns and the patterns printed with 3 minutes of plasma treatment, even printing with different substrate temperatures and different drop spacing values. For this reason, it was decided decrease furthermore the time of plasma treatment to discover if a significant difference could be reached in printing or not. This time, plasma treatment was performed for only 30 seconds. Figure 27 shows the images of printing at 32°C, varying the Drop Spacing and using an oxygen plasma treatment for 30 seconds.

From the results of Figure 27 one can observe that a slight improvement was achieved in the size and shape control of the pattern performing a plasma treatment only for 30 seconds. Treatment times shorter than 30 seconds will not result in relevant differences. Since it is always better to use a reduced time to this sort of treatment, reducing costs and time, 30 seconds of treatment was kept as the adequate value for oxygen plasma treatment for the next printings.

Figure 27: Printing with (a) 38 μm (2 layers), (b) 35 μm , (c) 33 and (d) 38 μm of Drop Spacing. (Left: horizontal lines; middle: vertical lines and left: lines of different thicknesses). Scale bar: 1 mm.



After this optimization, it is possible to choose which combinations of parameters use depending on the design/size desired.

Table 3 summarizes all substrate temperatures and drop spacing values used during the process of parameters adjustments for PEDOT:PSS ink.

Table 3: Substrate temperatures and Drop Spacing values used for parameters adjustments of PEDOT:PSS ink.

Before Oxygen Plasma Treatment							
Temperatures [°C]	28	35	40	45	50	55	60
Drop Spacing [μm]	25, 20, 17, 15, 14	14, 13	14	14	14	14	14, 13,12
Oxygen Plasma Treatment for 3 minutes							
Temperatures [°C]	28		35			40	
Drop Spacing [μm]	20, 30, 40		40			40	
Oxygen Plasma Treatment for 1 minute							
Temperatures [°C]	28			32			
Drop Spacing [μm]	35			35, 38			
Oxygen Plasma Treatment for 30 seconds							
Temperatures [°C]	32						
Drop Spacing [μm]	30, 33, 35 and 38						

4.2 SILVER NANOPARTICLE PARAMETERS EVALUATION

The first parameter optimized, as reported earlier, was the waveform. The waveform provided by the supplier for this ink was used as base and some adjustments were made to obtain a high velocity jet and a good drop formation, always avoiding satellite drops and tails.

The waveform optimized for the Silver Nanoparticle ink U5603 and an image of its jets are shown in Figure 28.

Figure 28: Optimized waveform for Silver Nanoparticle U5603 ink (on the left) and image of Silver Nanoparticle ink U5603 jet, with a velocity of approximately 4 m/s (on the right).



As already discussed, after adjustment of the waveform, the optimization of drop spacing and substrate temperature were started. All the combinations performed with these parameters until obtain the best possible printed pattern will be shown by the optical microscopy images taken from these printed patterns. The Silver Nanoparticle ink presents a good jet formation and exhibits a good behavior on PaC, therefore it is relatively easy to be optimized. All the samples were printed at room temperature to perform the optimization. For this parameters optimization, the same pattern used to PEDOT:PSS optimization was employed.

Figures 29 and 30 show the printing of silver ink at room temperature (28°C), varying the **Drop Spacing**.

Figure 29: Printing with (a) 100 μm , (b) 50 μm and (c) 45 μm of Drop Spacing. (Left: horizontal lines; middle: vertical lines and left: lines of different thicknesses). Scale bar: 1 mm.

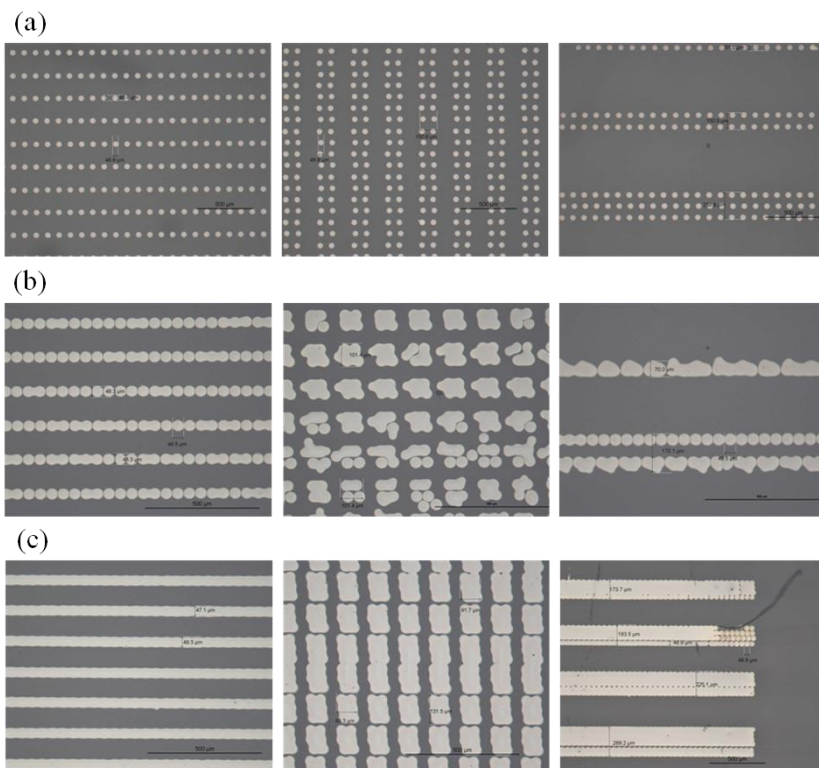
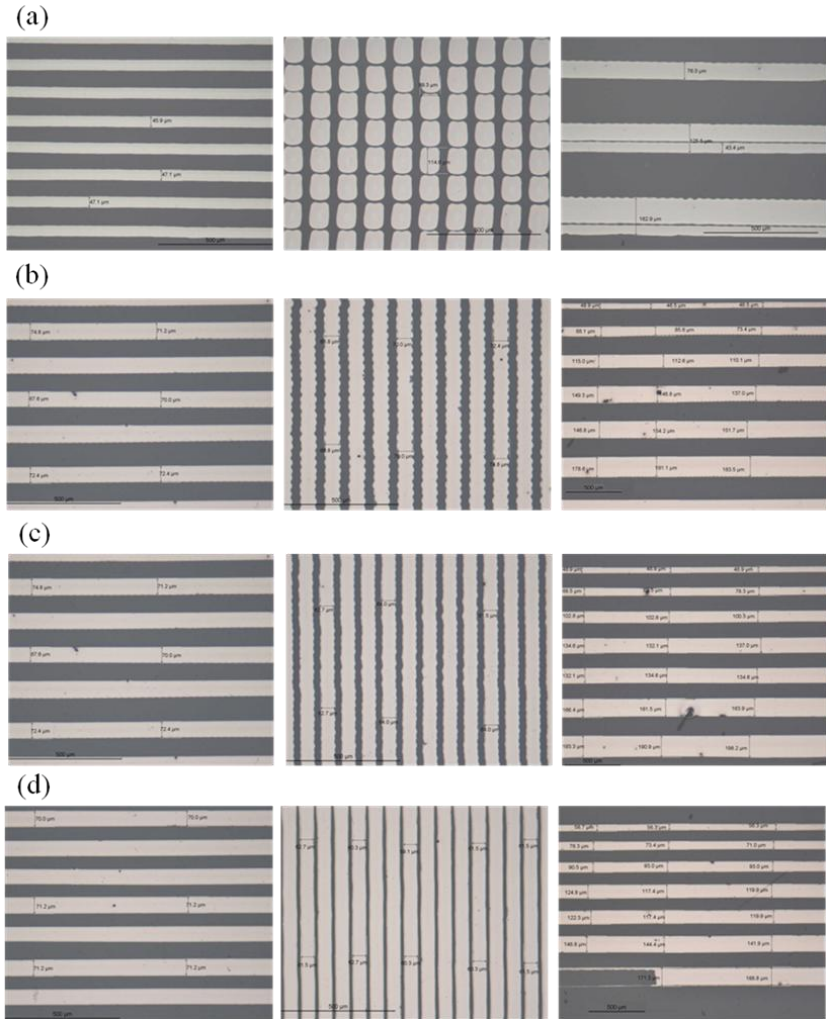


Figure 30: Printing with (a) 40 μm, (b) 35 μm, (c) 30 μm and (d) 25 μm of Drop Spacing. (Left: horizontal lines; middle: vertical lines and left: lines of different thicknesses). Scale bar: 1 mm.



From Figure 31 (single dots), it is possible to see that one droplet has a diameter of approximately between 45 μm and 48 μm. Therefore, since the drop spacing is greater than the diameter of a single drop, it is expected that the printed pattern will not form a continuous line (case of Figure 29 (a) 100 μm and (b) 50 μm of drop spacing). For all lines, the

line width becomes more uniform by decreasing the drop spacing. For horizontal lines, a continuous line can be obtained from a drop spacing of $45\ \mu\text{m}$. When the line has only one pixel of width, printed pattern is uniform even using a drop spacing of $35\ \mu\text{m}$. However, if the line has more than one pixel, as in Figure 32, the bottom of the line is scalloped for elevated values of drop spacing but is straighter by its decreasing, reaching relative uniformity at $25\ \mu\text{m}$ of drop spacing. Vertical lines present the same behavior, but the pattern starts to form a line just from $35\ \mu\text{m}$ of drop spacing and to obtain a perfect straight line it is necessary to print using a drop spacing even smaller than $25\ \mu\text{m}$.

Figure 31: Single dots of Silver Nanoparticle ink. Scale bar : $500\ \mu\text{m}$.

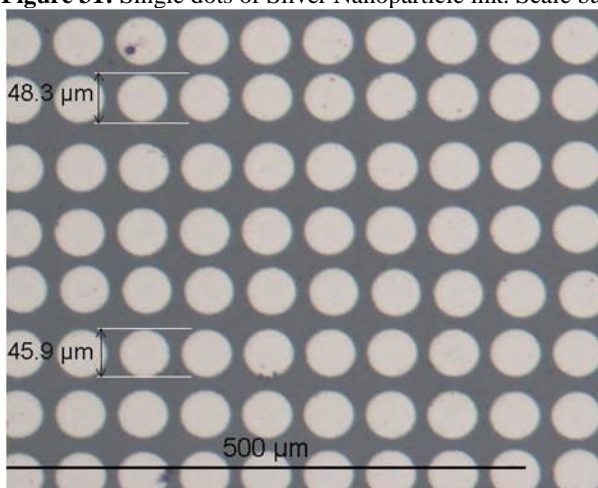
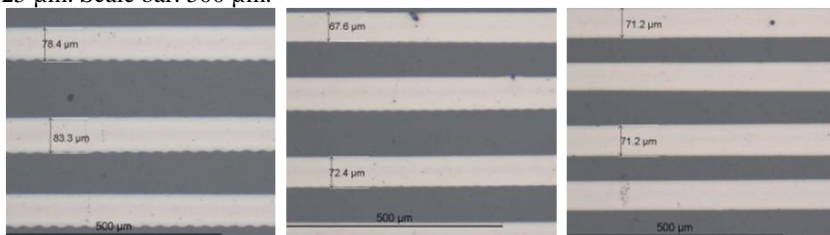


Figure 32: Horizontal line with 2 pixels of width. On the left, drop spacing of $35\ \mu\text{m}$, in the middle, drop spacing of $30\ \mu\text{m}$ and on the right, drop spacing of $25\ \mu\text{m}$. Scale bar: $500\ \mu\text{m}$.

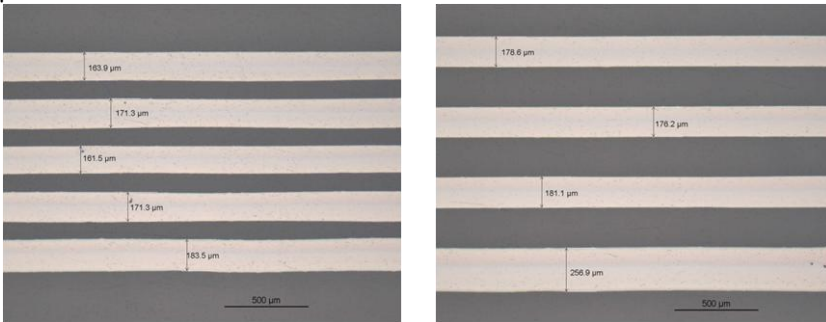


To ensure that this ink will keep an adequate behavior even being printed on PaC treated with oxygen plasma, a printing test was

performed using a substrate (PaC) treated for 30 seconds in RIE. The printed patterns did not present significant differences when compared to the samples printed on PaC untreated, though a slightly larger spread might be expected due to the low contact angle measured.

Figure 33 shows the images of silver ink printed upon oxygen plasma treated PaC (for 30 seconds), using a drop spacing of 23 μm .

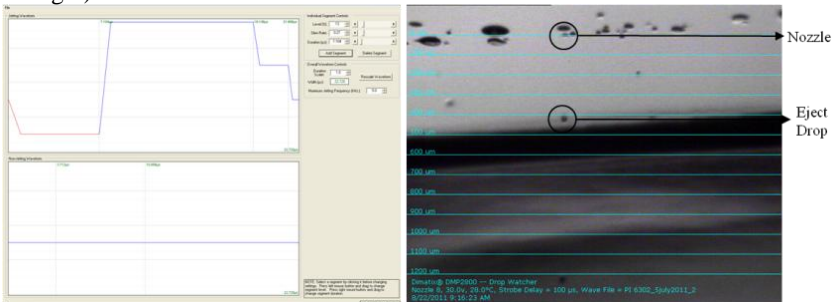
Figure 33: On the left, horizontal lines (same thickness) and on the right, horizontal lines with different thicknesses. Drop Spacing 23 μm . Scale bar: 500 μm .



4.3 POLYIMIDE INK PARAMETERS OPTIMIZATION

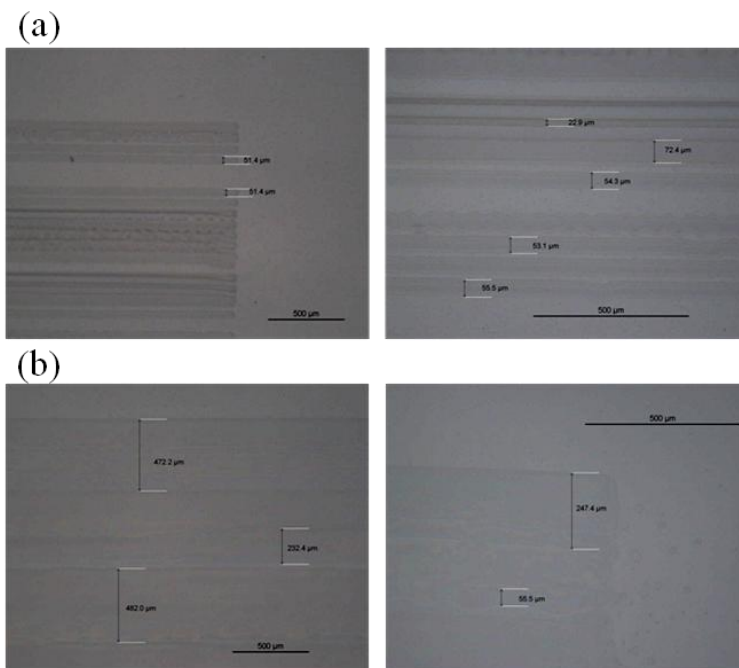
The optimized waveform was adjusted from a waveform provided by the ink supplier. This ink presents very stable jets and a good drop formation. The waveform optimized for PI 63002 ink and an image of its jets are shown in Figure 34.

Figure 34: Optimized waveform for Polyimide ink PI 63002 (on the left) and image of Polyimide PI 6302 ink jet, with a velocity of approximately 4 m/s (on the right).



After adjustment of the waveform, the optimization of drop spacing and substrate temperature can be started. For PI ink, the purpose of adjustment is different from the other inks; for PI ink it is necessary to find parameters that allow printing a homogeneous thick film to ensure the complete isolation of the device from external environment. The combinations performed to obtain a uniform printed film will be shown by the optical images taken from the printed samples. The pattern used for this optimization was a square. Figure 35 shows the printing at room temperature (28°C), using a cartridge of 1 pL (instead of 10 pL, as used previously). The parameter changed was the **Drop Spacing**.

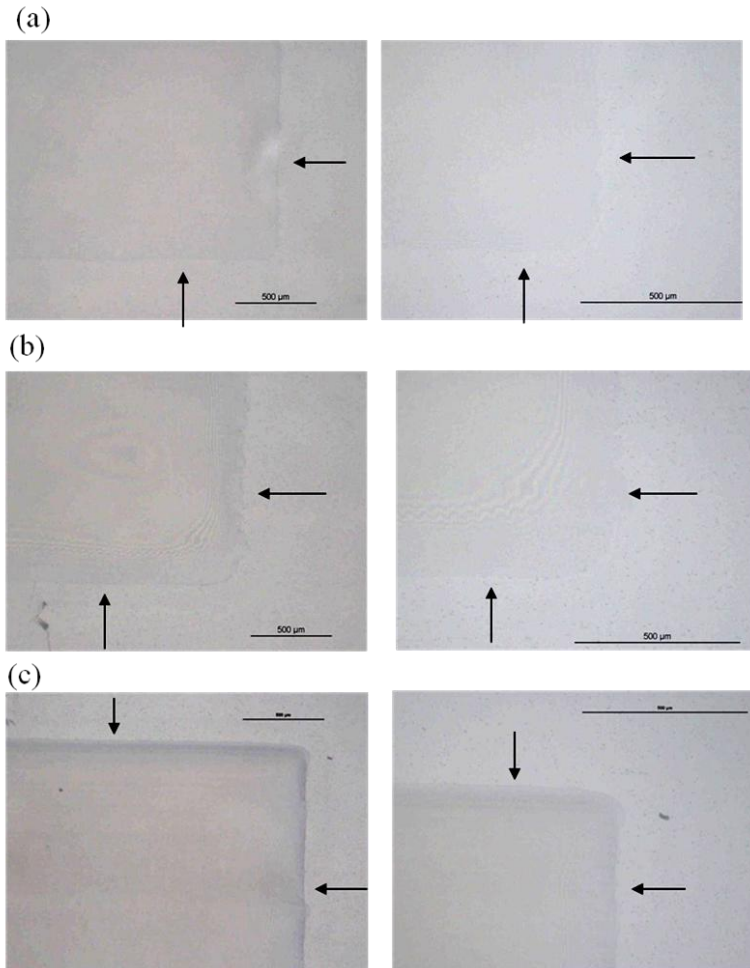
Figure 35: Printed square of Polyimide ink, using a drop spacing of (a) 35 μm and (b) 25 μm . Magnification of 5X (on the left) and 10X (on the right). Scale bar: 500 μm .



Using a cartridge of 1 pL and a drop spacing of 35 μm it is evident that it is not possible to print a homogeneous and continuous film. Decreasing the drop spacing down to 25 μm , it is observed a significant improvement to form a film. However, this drop spacing is not short enough to satisfy the necessary requirements. Therefore,

cartridge of 10 pL was used to increase the drop size. Additionally, drop spacing was also decreased (using 23 μm) and the substrate temperature increased. The number of layers was increased until certify that thickness is enough to protect the device properly. Figure 36 shows the printing of polyimide ink at 35°C, using a cartridge of 10 pL, only varying the **number of layers**.

Figure 36: Polyimide printed square with drop spacing of 23 μm . (a) 1 layer, (b) 2 layers and (c) 3 layers. Magnification of 5X (on the left) and 10X (on the right). Scale bar: 500 μm .

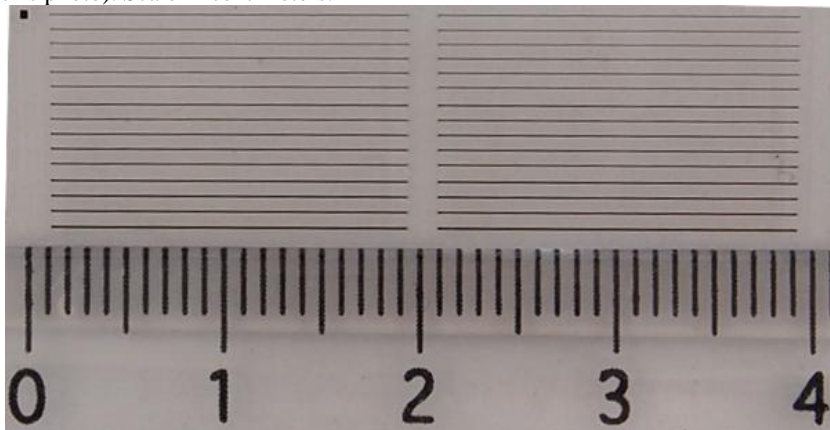


From the images shown in Figure 36 a uniform and continuous film obtained after printing 3 layers using 23 μm of drop spacing can be observed. The slightly heated substrate keeps the shape of the pattern well controlled, as can be noticed in Figure 36 (c).

4.4 FINAL DEVICE

The complete device was printed in two different ways. In the first way (Device S), silver tracks were printed first, on top of PaC untreated, and then the PEDOT:PSS rectangles were printed over it, finalizing with the polyimide printing. In the second way (Device P), the sequence of silver and PEDOT printing is inverted, therefore, an oxygen plasma treatment for 30 seconds was realized on the PaC surface; next, PEDOT:PSS was printed, then, silver tracks printing were performed and, finally, polyimide printing was realized. Figure 37 shows a photograph of the full-size printed device.

Figure 37: Photograph of a full-size printed device, showing a size of approximately 4 cm (including the polyimide printing, which is not visible in this photo). Scale in centimeters.



Since there is not any visible difference between the devices, only the photo of one way of printing was shown (device S). However, the images obtained from the optical microscope of both ways of printings show a considerable difference, especially in PEDOT:PSS printings. Figure 38 shows an optical microscopy image of the contact between silver and PEDOT in each way of printing.

Figure 38: Optical microscopy image of the device using a magnification of 50X when silver tracks were printed first (on the left) and when PEDOT rectangles were printed first (on the right). This magnification shows clearly the contact between silver and PEDOT in each way of printing. Scale bar: 100 μm .

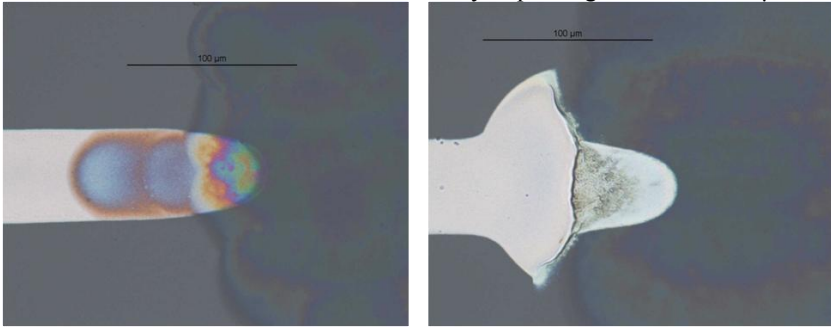


Figure 39 shows the optical microscopy image of Device S, highlighting the contact between silver ink and PEDOT:PSS ink, before the polyimide printing.

Figure 39: Optical microscopy image of final device where the silver tracks were printed before the PEDOT:PSS rectangles (without polyimide printing). (a) First lines of the device and (b) last lines of the device. Scale bar: 1 mm.

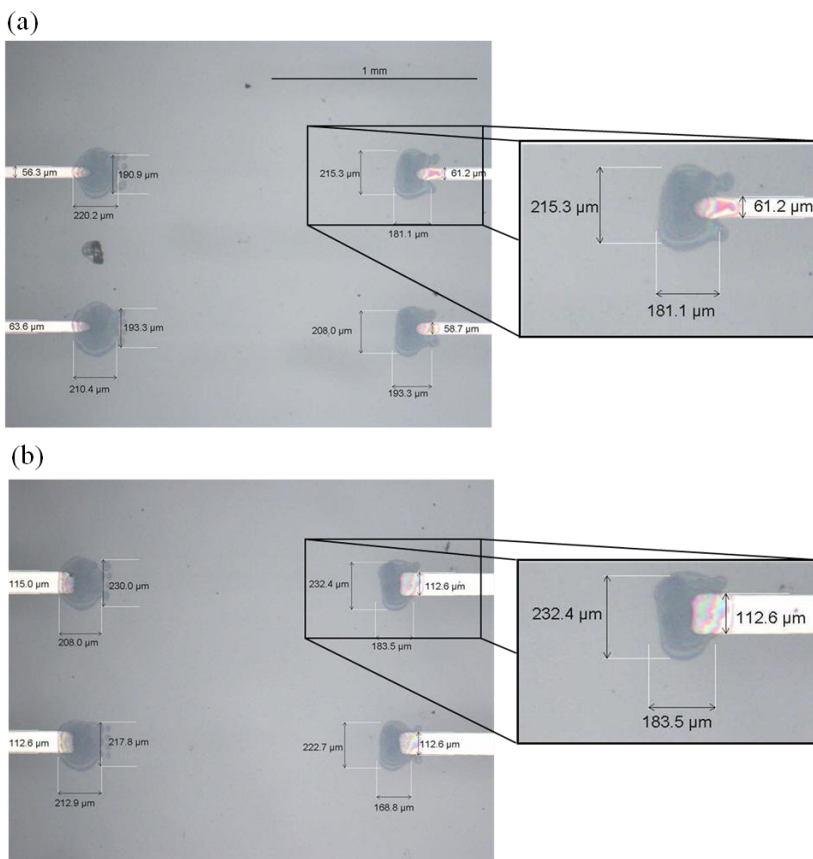
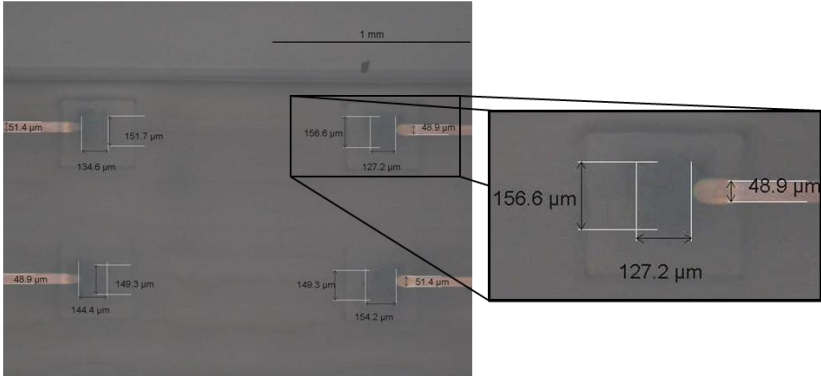


Figure 40 shows the optical microscopy image of Device S, highlighting the contact between silver ink and PEDOT:PSS ink, after polyimide printing.

Figure 40: Optical microscopy image of complete device shown in Figure 39 after polyimide printing. Silver tracks were printed before the PEDOT:PSS rectangles. (a) First lines of the device and (b) last lines of the device. Scale bar: 1 mm

(a)



(b)

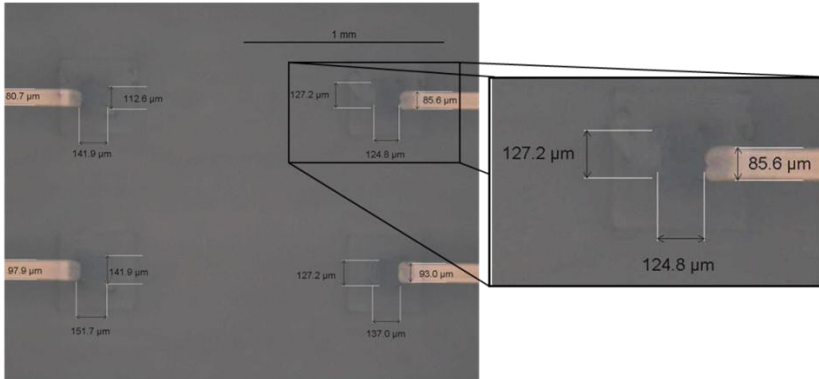


Figure 41 shows the optical microscopy image of Device P, highlighting the contact between PEDOT:PSS ink and silver ink, before polyimide printing.

Figure 41: Optical microscopy image of final device where the PEDOT:PSS were printed before the silver tracks (without the polyimide printing). (a) First lines of the device and (b) last lines of the device. Scale bar: 1 mm

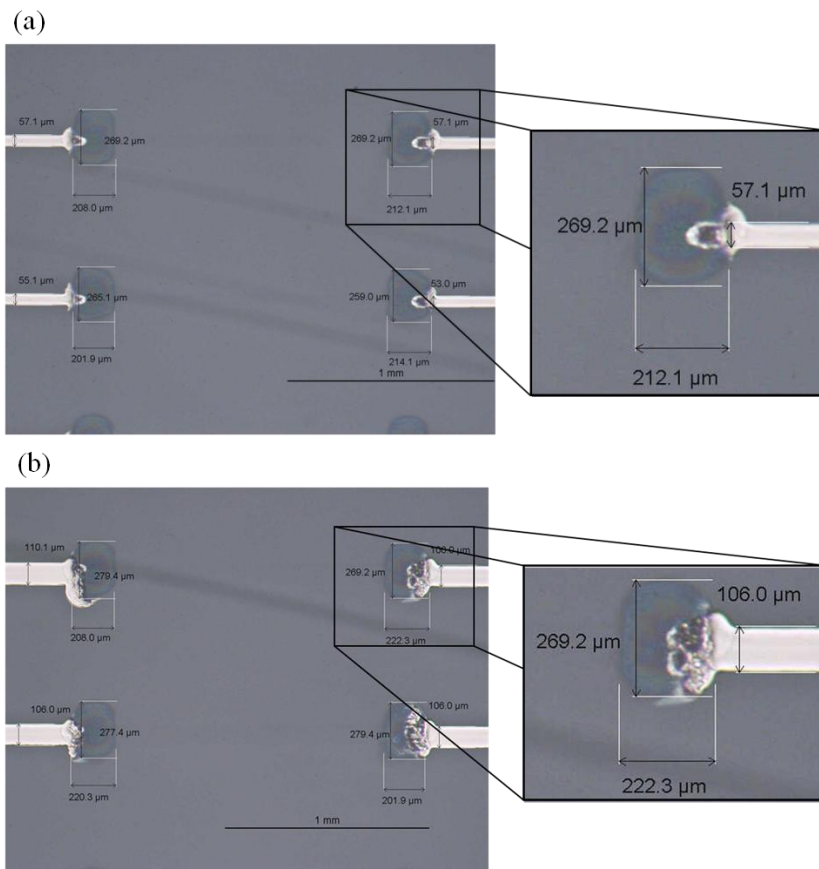
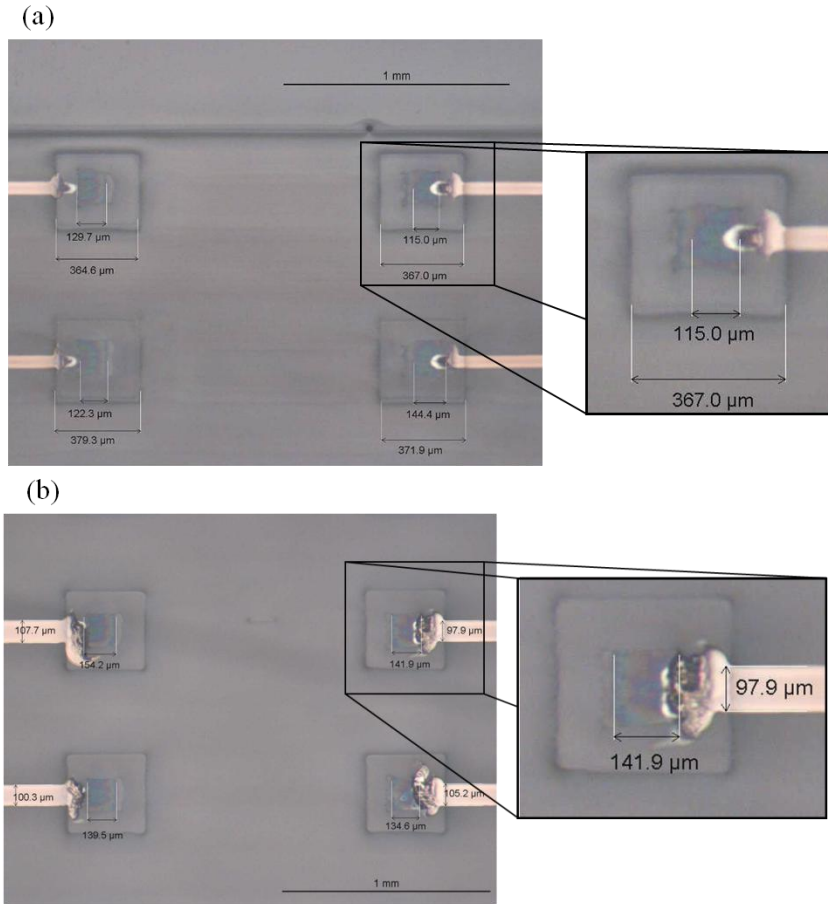


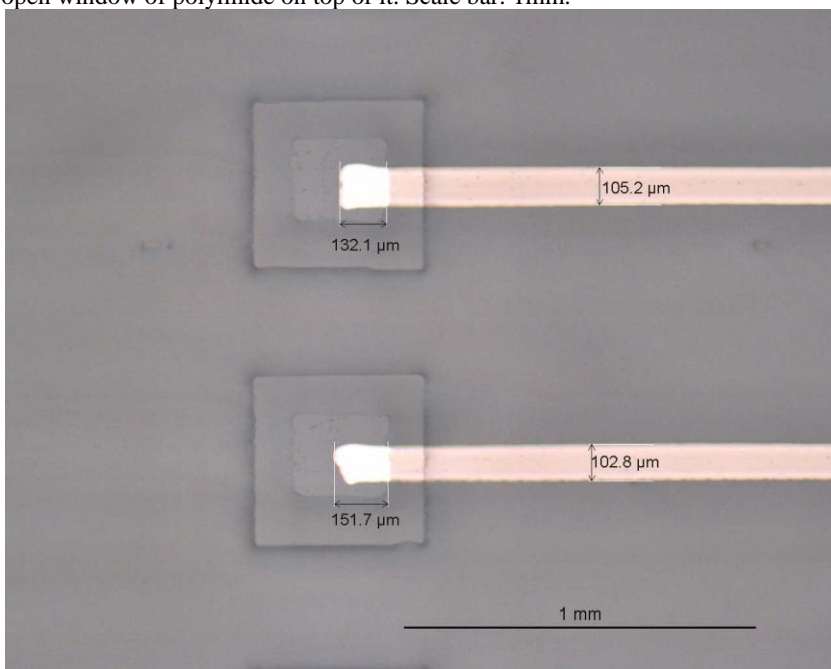
Figure 42 shows the optical microscopy image of Device P, highlighting the contact between PEDOT:PSS ink and silver ink, after polyimide printing.

Figure 42: Optical microscopy image of complete device shown in Figure 41 after polyimide printing. The PEDOT:PSS rectangles were printed first. (a) First lines and (b) last lines of the device. Scale bar: 1 mm.



In Figure 43, it is possible to visualize the external edges of silver tracks and the open window of polyimide on top of it (external part of the device). In this image, the difference between the windows size of the first and second/third layers of polyimide is evidenced.

Figure 43: Optical microscopy image of external edges of silver tracks and the open window of polyimide on top of it. Scale bar: 1mm.



4.5 SURFACE ENERGY OF PARYLENE

The surface energy of Parylene C was obtained through calculations based on contact angles between PaC and different liquids with polar and nonpolar nature. Figure 44 shows the results of contact angle measurements for Parylene C.

Figure 44: Contact angles between PaC and ethylene glycol 40% (on the left), Diiodomethane (in the middle) and deionized water (on the right).



It was observed that ethylene glycol ($70.9^\circ \pm 2.3^\circ$) and water ($90.8^\circ \pm 1.9^\circ$) do not wet significantly the PaC surface, while

Diiodomethane wets it by an angle of $34.1^\circ \pm 1.2^\circ$, corroborating the hydrophobic nature of Parylene C.

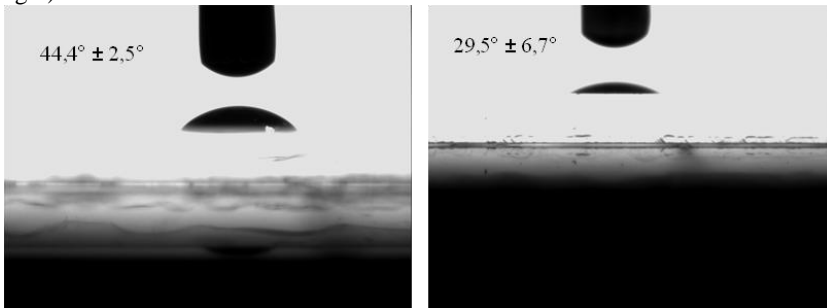
The surface energy obtained from the Wu's method (see Appendix B) for PaC is 39.97 mN/m (dispersive fraction: 37.75 mN/m, polar fraction: 2.22 mN/m).

4.6 CONTACT ANGLE BETWEEN PaC AND INKS

After characterizing the surface energy, the contact angles of all the available inks which could be printed on PaC were performed.

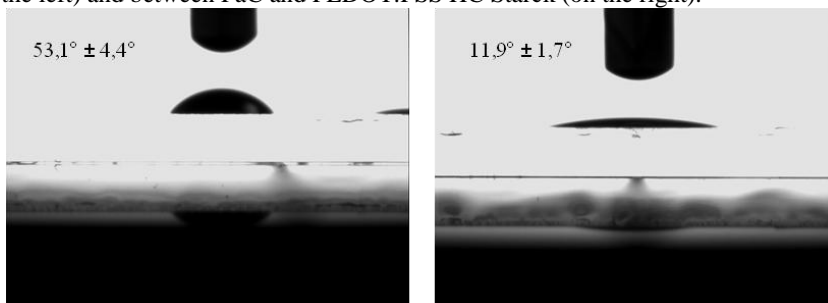
The measurements were carried out with the same goniometer used to characterize the surface energy. Images and results obtained from these measurements for metal inks are shown in Figures 45.

Figure 45: Contact angle between PaC and Silver Nanoparticle Ink U5603 (on the left) and between PaC and Silver Organometallic Ink TEC-IJ-010 (on the right).



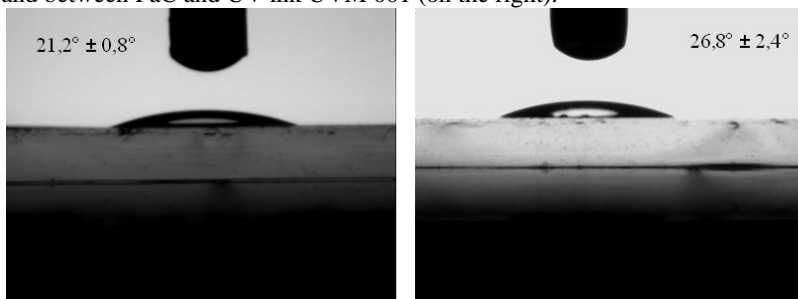
Images and results obtained to contact angle measurements for conducting polymers are shown in Figures 46.

Figure 46: Contact angle between PaC and PEDOT:PSS Orgacon IJ 1005 (on the left) and between PaC and PEDOT:PSS HC Starck (on the right).



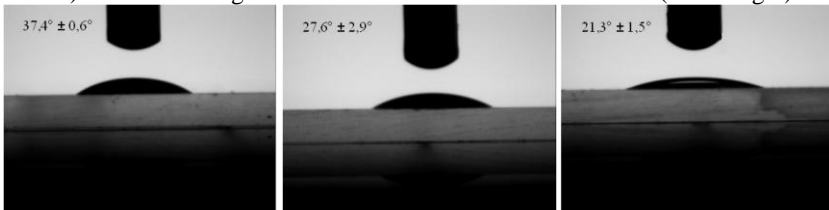
Images and results obtained to contact angle measurements for passivate inks are shown in Figures 47.

Figure 47: Contact angle between PaC and Polyimide PI 6302-002 (on the left) and between PaC and UV ink UVM 001 (on the right).



Throughout the work, as a surface treatment in PaC surface was necessary to convert its hydrophobic nature to hydrophilic, in order to improve the quality of PEDOT:PSS Orgacon printing, measurements of contact angle between PaC treated with oxygen plasma and the main inks, U5603, IJ 1005 and PI 6302-002, were carried out. A significant difference between the results before and after the plasma treatment was observed only for PEDOT:PSS Orgacon. For Silver Nanoparticle Ink and Polyimide ink the results remained virtually the same. These results are shown in Figure 48.

Figure 48: Contact angle between treated PaC and U5603 ink (on the left), contact angle between treated PaC and PEDOT:PSS Orgacon IJ 1005 (in the middle) and contact angle between treated PaC and PI 6302-002 (on the right).



As a comparison between the substrate Parylene C and another biocompatible substrate, Kapton[®], a polyimide substrate widely used in microelectronic and largely used in the research works developed at CPM, the contact angle measurements for both kinds of PEDOT:PSS on this substrate were carried out as well. Kapton[®] was purchased from Dupont in a form of a film ready to be used. The results of the contact angles are shown in Figure 49.

Figure 49: Contact angle between Kapton and PEDOT:PSS IJ 1005 (on the left) and between Kapton and PEDOT:PSS HC Starck.

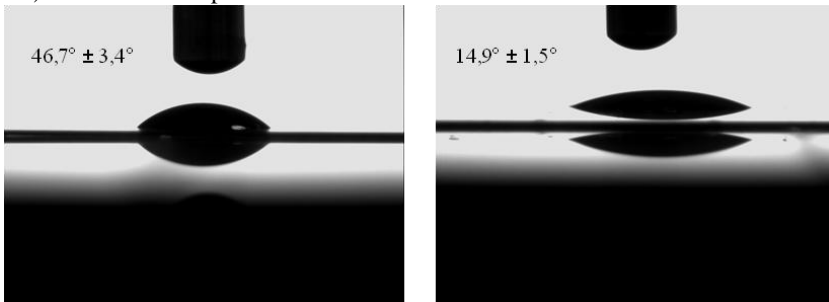


Table 4 summarizes all the measured contact angles.

Table 4: Contact angle between PaC and all the tested inks.

Ink		Parylene C	Kapton
PEDOT:PSS IJ 1005	Without plasma	$53.1^\circ \pm 4.4$	$46.7^\circ \pm 3.4$
	With plasma	$27.6^\circ \pm 2.9$	
PEDOT:PSS HC STARCK		$11.9^\circ \pm 1.7$	$14.9^\circ \pm 1.5$
U5603	Without plasma	$44.4^\circ \pm 2.5$	
	With plasma	$37.4^\circ \pm 0.6$	
TEC IJ 010		$29.5^\circ \pm 6.7$	
PI 6302-002	Without plasma	$21.2^\circ \pm 0.8$	
	With plasma	$21.3^\circ \pm 1.5$	
UVM 001		$26.8^\circ \pm 2.4$	

4.7 THICKNESS

Thickness of silver tracks was characterized in both profilometers to compare the results and to ensure the reliability of obtained values. Thickness was measured for each line with different widths: 1, 2, 3, 4 and 5 pixels.

Results obtained from both profilometers are very close and exhibit only a small difference of few nanometers. Table 5 shows the results obtained for thickness measurements.

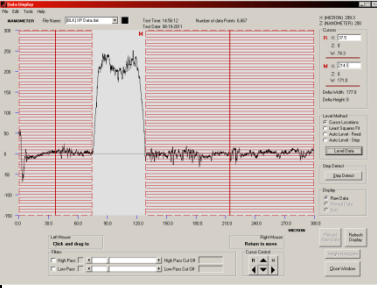
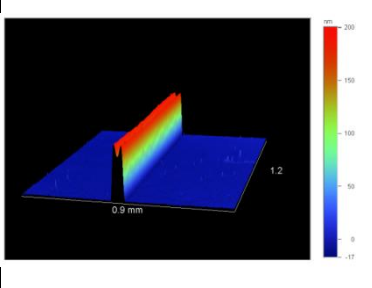
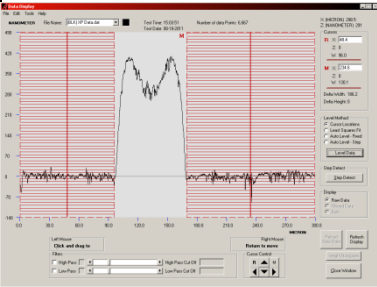
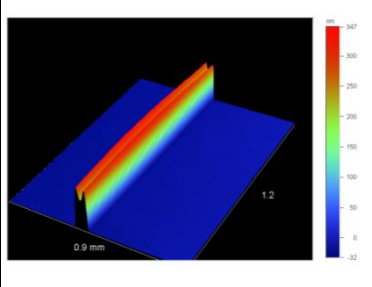
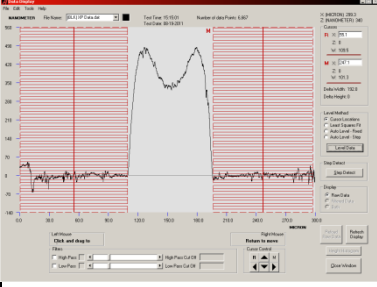
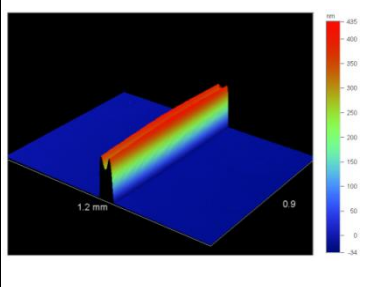
Table 5: Thickness values for silver lines.

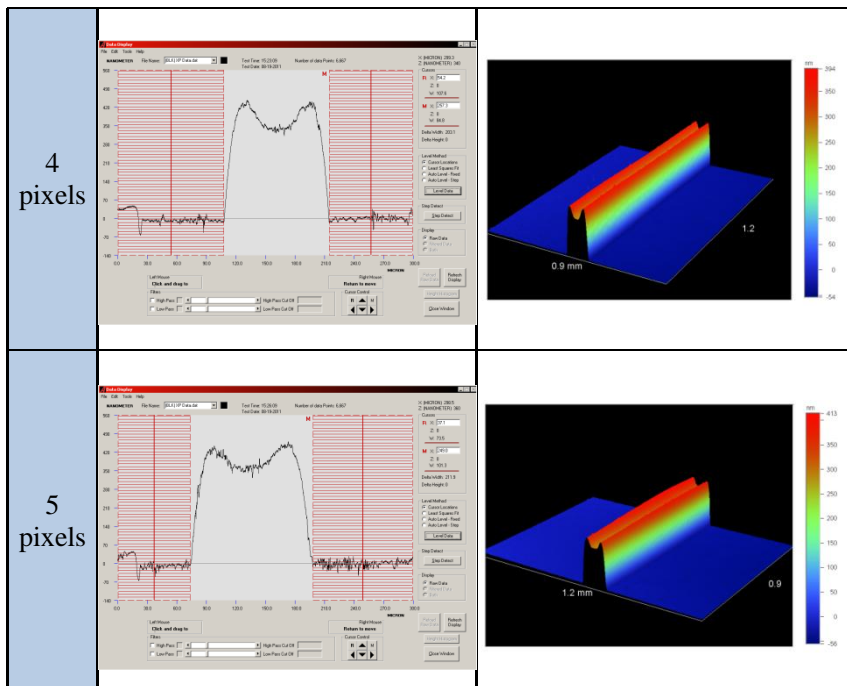
Width	Thickness [nm]	
	Mechanical Profilometer	Optical Profilometer
1 pixel	200 - 230	190 - 220
2 pixels	290 - 400	280 - 380
3 pixels	340 - 480	330 - 470
4 pixels	340 - 440	350 - 450
5 pixels	360 - 440	360 - 460

The range of thicknesses values is due to the difference in height found between the middle and the edge of line due to coffee-ring effect, a very common problem found in inkjet printing devices. This effect is evident in the profiles obtained in both profilometers.

Table 6 shows the results of silver lines profile obtained from both mechanical and optical profilometers.

Table 6: Silver lines profile obtained from the mechanical and optical profilometers.

Width	Mechanical Profilometer	Optical Profilometer
1 pixel		
2 pixels		
3 pixels		

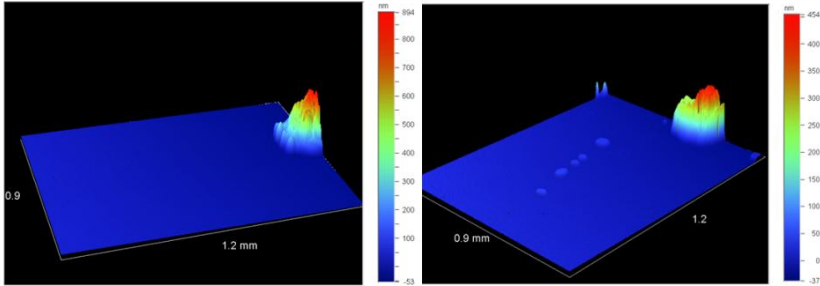


Thickness of PEDOT:PSS rectangles was measured only in optical profilometer, because of its “soft” nature, since the mechanical profilometer touches the material to run the measurement and this could damage the device. Thickness was measured for both ways of printing – with and without plasma treatment on PaC. Results are an approximate average of values obtained, because the profiles are very irregular, especially for the device without plasma treatment. Table 7 shows average values for PEDOT:PSS thickness and Figure 50 shows the 3D profiles obtained from the optical profilometer.

Table 7: Thickness average values obtained for PEDOT: PSS printed with and without plasma treatment.

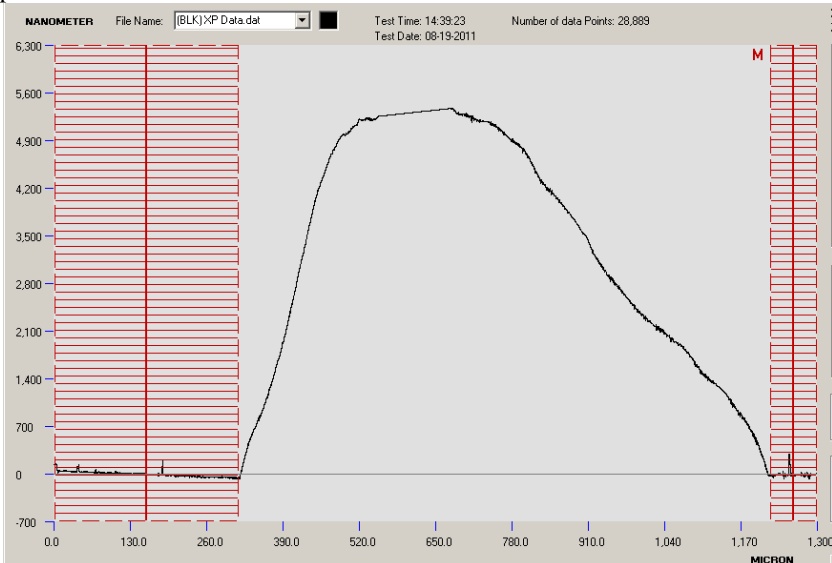
	Number of layers	Thickness [nm]
PEDOT:PSS without plasma treatment	6	~ 700
PEDOT:PSS with plasma treatment	4	~ 400

Figure 50: 3D profiles obtained for PEDOT:PSS printing without plasma treatment (on the left) and with oxygen plasma treatment (on the right).



Thickness of polyimide film cannot be measured in optical profilometer because of its transparency. Thus, to not damage the device, an impression of a polyimide sample was printing using the same parameters used to print the device, however, in a smaller dimension, so it could be measured in the mechanical profilometer. With 3 printed layers, the film presents an approximately thickness of $5.5 \mu\text{m}$. The profile obtained from the mechanical profilometer is shown in Figure 51.

Figure 51: Profile of polyimide printed sample obtained from the mechanical profilometer.



4.8 SHEET RESISTANCE

Sheet resistance of PEDOT:PSS were measured in samples with and without plasma treatment. One sample of Silver annealed using a different sintering condition (1 h at 130°C more 15 minutes at 200°C instead of 2,5 h at 130°C) was measured as well to compare the results.

To measure the sheet resistance, squares (1.5 cm x 1.5 cm) of each material were printed using the same printing conditions used to print the final device, in order to obtain a sufficient size to perform the measurements.

A table containing the electrical resistivity and conductivity values obtained for Silver and PEDOT:PSS printed patterns are shown in Table 8.

Table 8: Electrical Resistivity and Conductivity for Silver and PEDOT:PSS samples.

	Resistivity [$\Omega \cdot \text{cm}$]	Conductivity [$\text{S} \cdot \text{cm}^{-1}$]
Silver (2.5 h at 130°C)	$3.4 \pm 1.6 (\times 10^{-4})$	$2.9 \pm 0.6 (\times 10^3)$
Silver (1 h at 130°C + 15 min at 200°C)	$1.0 \pm 0.6 (\times 10^{-3})$	$9.6 \pm 1.7 (\times 10^2)$
PEDOT:PSS without plasma treatment	$5.4 \pm 3.7 (\times 10^{-3})$	$1.9 \pm 0.3 (\times 10^2)$
PEDOT:PSS with plasma treatment	$3.0 \pm 1.3 (\times 10^{-3})$	$3.3 \pm 0.8 (\times 10^2)$

There is a small difference in the conductivity values between Silver samples, as expected, due to the difference in sintering conditions. However, the electrical conductivity obtained with the heat treatment used in the final device was still satisfactory, presenting values one order of magnitude lower than the electrical conductivity of the bulk material.

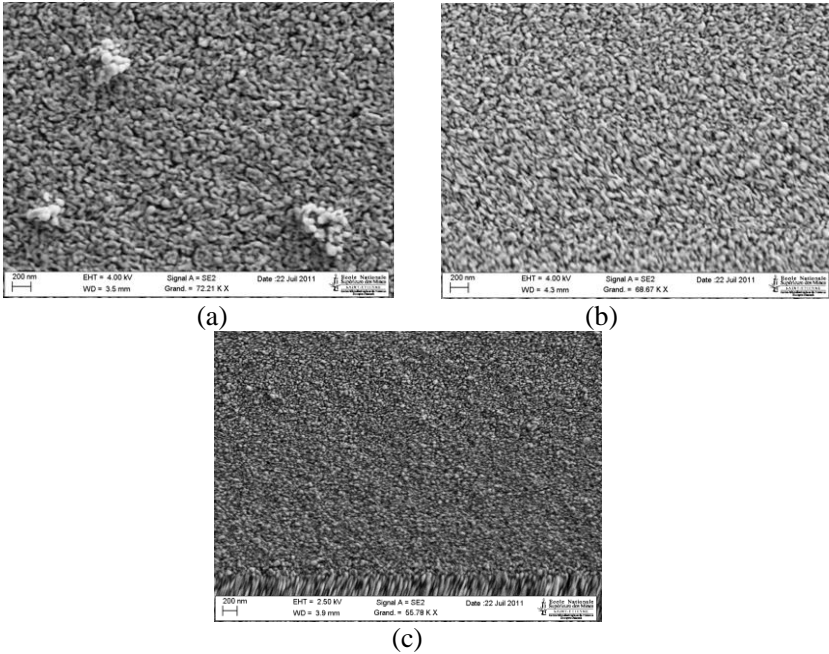
In order to analyze the microstructures of silver tracks in the microscope to verify its degree of sintering, it was decided to increase the sintering temperature and decrease the time of treatment. Sintering conditions that were performed are:

- 60 minutes at 200°C

- 10 minutes at 200°C
- 30 minutes at 150°C

From Scanning Electron Microscopy (SEM) images (Figure 52) taken of each sample, it is clear from the microstructures that there is a gradual increase, as expected, in the evolution of neck growth with increasing the sintering temperature, leading to a higher material densification, which consequently leads to a higher electrical conductivity. However, during the annealing process in these other temperatures, a considerable shrinkage succeeded in the printed patterns, leading to a loss of original design/form. Hence, it was preferable to keep the annealing condition at 130°C for 2.5 h, even possibly losing magnitude in the electrical conductivity values, but maintaining the shape/design.

Figure 52: SEM images to different annealing conditions: (a) 60 minutes at 200°C, (b) 10 minutes at 200°C and (c) 30 minutes at 150°C. Scale bar: 200 nm.



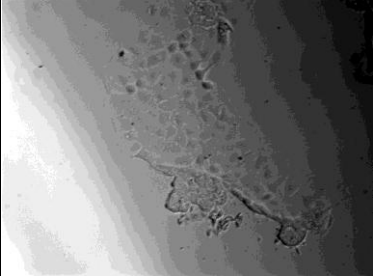

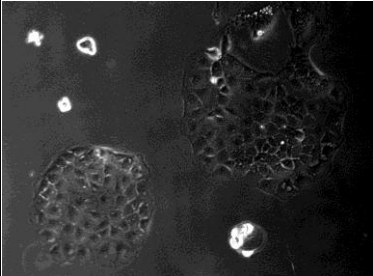
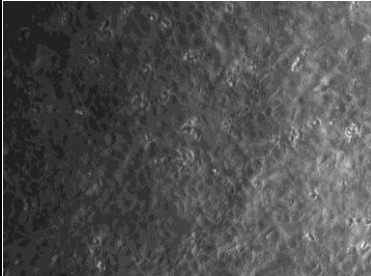
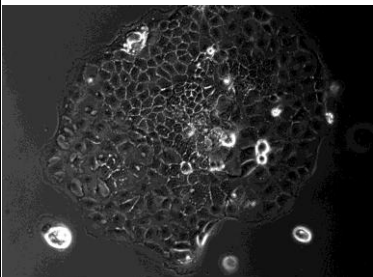
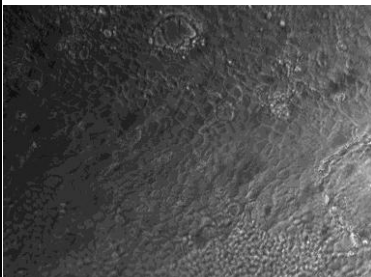
4.9 CELL CULTURE ASSAYS

As the polyimide ink had never been used in any previously reported work involving bioelectronics and also because the most part of the device which will be in contact with the biological environment is this ink, cell culture assays were performed in order to analyze the cytotoxicity of this ink. To carry these culture assays, two different types of cells were used. The main objective of these assays is to study if Polyimide ink is toxic or if it inhibits cell growth.

The images of each sample of PI beneath Caco-2 cells are shown in Table 9. During the test, it was observed that the cells growth above the ink is slower compared with the cells growth above the Petri dish; however, after few days, cells are totally confluent on the ink. From the images, it is observed that, at 72 hours of test, cells growth is progressive as the surface of squares increases, but after 288 hours it is not possible see a significant difference between the samples. At 288 hours, cell confluence with presence of vacuoles (elements of differentiation) was observed. Therefore, from these results one might conclude that cells adhere on the ink; also, cell differentiation occurs and, finally, the polyimide ink is not toxic to the Caco-2 cells until 6.7 mg (weight of biggest square of PI): cellular density of 1.38×10^4 cells/cm².

The images of each sample of PI beneath PC-12 cells are shown in Table 10. As observed to the Caco-2 cells, during the test, was observed that the cells growth on the ink is slower compared with the cells growth on the Petri dish. From the images, it is observed that after 96 hours it seems to exist an inhibition of cells growth when the squares surface is increased; however, there is no indication of cell death (beyond the normal expected); at a certain point the cells growth stabilizes. Therefore, from the images, it can be concluded that the cells adhere on the ink and the polyimide ink seems inhibit cells growth, but does not show characteristic toxic to the PC-12 cells until 5.5mg (weight of biggest square of PI): cellular density of 3.38×10^4 cells/cm².

Table 9: Images of the Caco-2 cells growth on printed polyimide after 3 and 12 days of cells culture.

	After 72 hours of culture	After 288 hours of culture
Square 1		
Square 2		
Square 3		

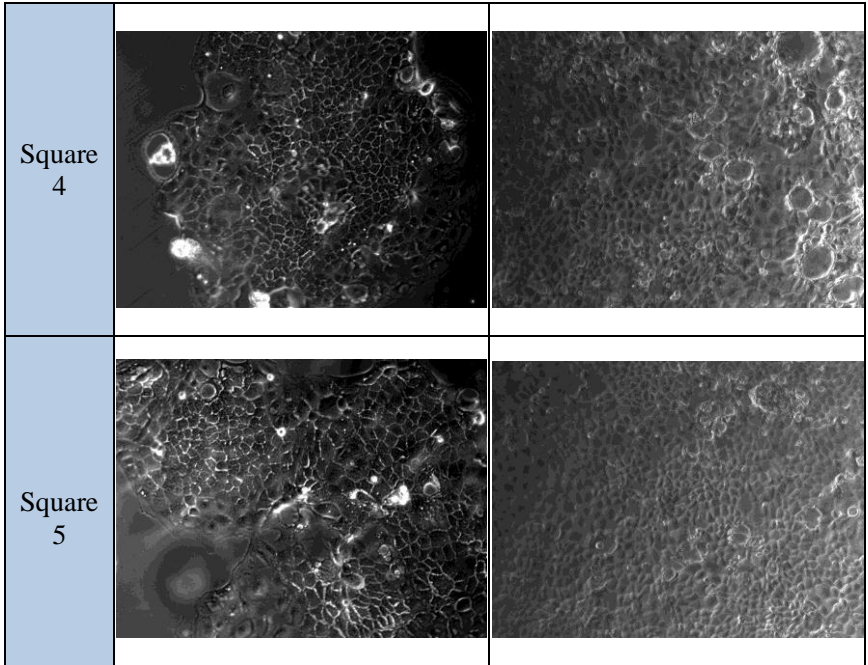
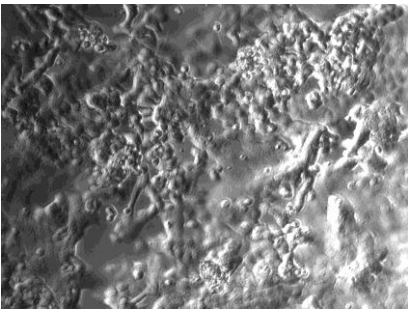
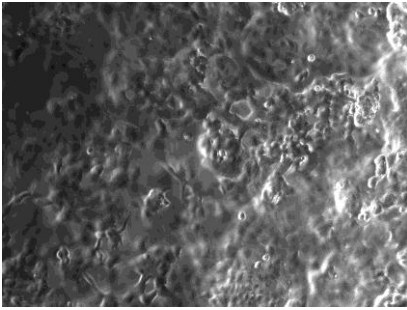
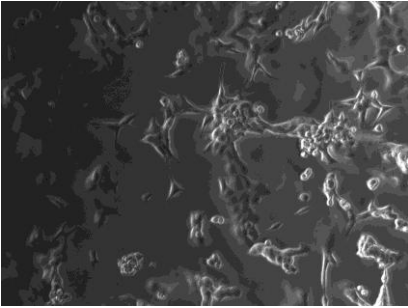
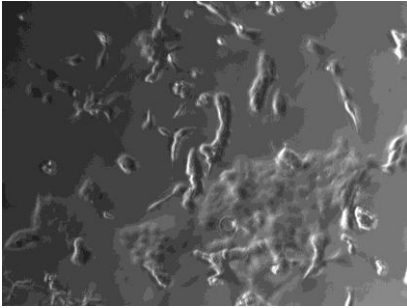
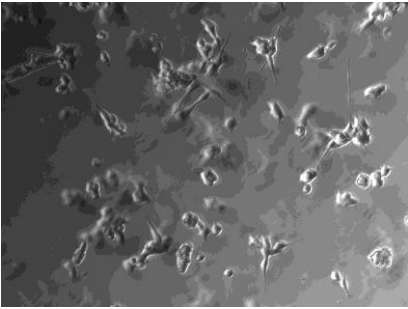
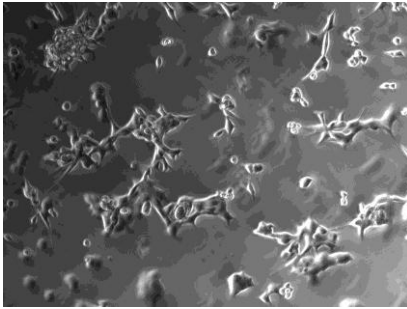


Table 10: Images of the PC-12 cells growth on printed polyimide after 4 days of cells culture.

	
PC-12 growth on Petri dish	PC-12 growth on Square 1
	
PC-12 growth on Square 2	PC-12 growth on Square 3
	
PC-12 growth on Square 4	PC-12 growth on Square 5

4.10 MTS ASSAY

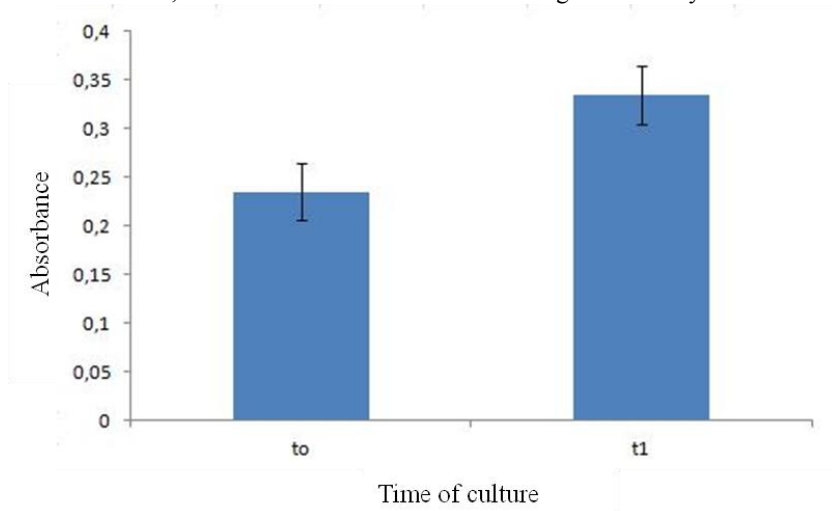
MTS colorimetric assay was used for quantitative assessment of cell viability as a function of time of culture. Figure 53 shows the results obtained by this experimental method for 24 h of culture.

In MTS assay, mitochondrial activity was evaluated at the initial time ($t = 0$) and after 1 day of culture ($t = 1$) as shown in Figure 53. The MTS assay quantifies, by concentration measuring, the soluble formazan resulting from a reduction reaction of tetrazolium salt (MTS) through mitochondria of viable cells. Quantification of formazan product is performed by spectrophotometry (absorbance at 490 nm) and is directly proportional to the number of living cells in culture.

Figure 53 shows the absorbance as a function of culture time of B16F10 cells grown on top of device's surface (polyimide ink and PEDOT:PSS ink).

The behavioral profile was characterized by an initial phase of cell proliferation in the first 24 h. In this period there were no indications of cell death induction, but a significant increase in the number of cells.

Figure 53: Quantitative analysis of B16F10 cell viability, cultivated on top of surface's device, as a function of time of culture through MTS assay.



4.11 LIVE/DEAD ASSAY FOR CELL VIABILITY

Live/Dead assay is a method that has been used to qualitative and quantitative assays of cell death. Living cells are distinguished from dead cells by calcein AM, which is retained within live cells producing an intense and uniform green fluorescent color while the ethidium homodimer infiltrates the cells with damaged plasma membrane.

Live/Dead results show, in agreement with MTS results, that there is no indication of cell death, both on top of polyimide ink (Figures 54 and 55) as on top of PEDOT:PSS ink (Figure 56).

Figure 54: Qualitative image of cell culture upon Polyimide ink through Live/Dead assay.

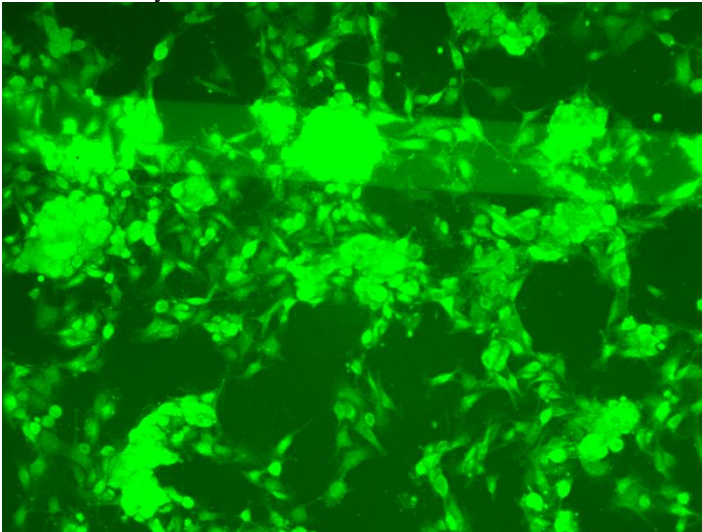
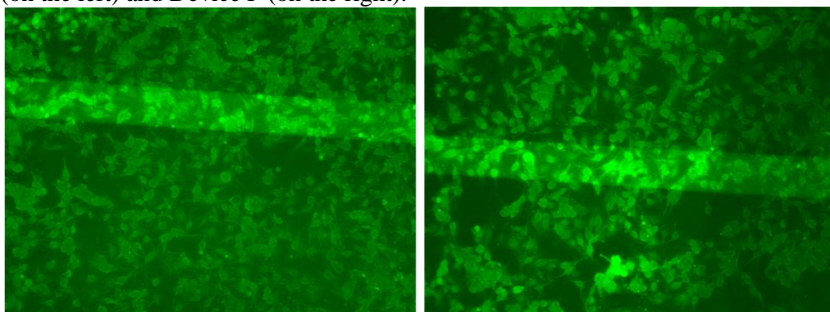
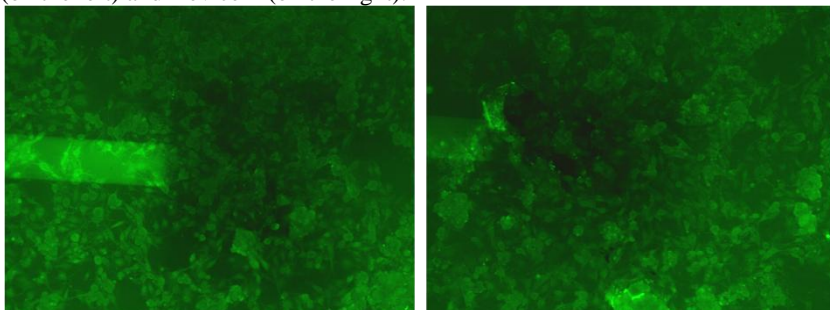


Figure 55: Live/Dead images of cells culture upon polyimide ink at Device S (on the left) and Device P (on the right).



Therefore, from the MTS results and from images of Live/Dead assay, it can be concluded that the cells adhere on the inks and both polyimide and PEDOT:PSS inks do not present toxic characteristic to the cells growth.

Figure 56: Live/Dead images of cells culture upon PEDOT:PSS ink at Device S (on the left) and Device P (on the right).



5. CONCLUSIONS

✓ Fully flexible organic electrodes can be fabricated by means of a simple and low cost technique.

✓ By their transparent nature, the use of parylene C as substrate and the polyimide as protective layer enabled the electrodes to be translucent.

✓ Parylene C used as substrate allowed the device to be easily removed from the original surface, which can be transferred to a new substrate with an excellent conformation, even upon irregular forms.

✓ Both silver nanoparticle and PEDOT:PSS, as well Polyimide inks were successfully deposited via an inkjet printing method through the adjustment of main printing parameters.

✓ Oxygen plasma treatment on PaC's surface is not critical but better results (as better values of electrical conductivity for conductive inks, for example) were achieved after its use.

✓ The use of oxygen plasma treatment on PaC improved the printability of PEDOT:PSS ink by changing PaC's hydrophobic nature to hydrophilic nature, resulting in a smoother and uniform surface and better resolution.

✓ Printing three layers of polyimide ink results in a thicker protective layer, which ensures that the electrodes are isolated from the external environment.

✓ The optimization of annealing conditions (time and temperature) allowed achieving satisfactory values of electrical conductivity both for PEDOT:PSS and silver inks, without degrading PaC.

✓ Cell adhesion assays performed with PC-12 (96 h of culture), Caco-2 (288 h of culture) and B16F10 (24 h of culture) demonstrated that the cells adhered on top of the inks and a cell differentiation occurs, which indicates Polyimide and PEDOT:PSS inks do not show toxic characteristics to the cells.

In summary, results show that inexpensive and biocompatible devices can be obtained using inkjetted organic inks and fabricated by direct writing without any particular pre-patterning or self-alignment techniques.

BIBLIOGRAPHY

ABIDIAN, M. R.; COREY, J. M.; KIPKE, D. R.; MARTIN, D. C., **Conducting-polymer nanotubes improve electrical properties, mechanical adhesion, neural attachment, and neurite outgrowth of neural electrodes.** *Small* 2010;6(3):421-9.

ABIDIAN, M. R.; KIM, D. H.; MARTIN, D. C., **Conducting polymer nanotubes for controlled drug release.** *Adv Mater* 2006;18:405-9.

ABIDIAN, M. R.; MARTIN, D. C., **Experimental and theoretical characterization of implantable neural microelectrodes modified with conducting polymer nanotubes.** *Biomaterials* 2008;29:1273-83.

ASPLUND, M.; VON HOLST, H.; INGANÄS, O., **Composite biomolecule/PEDOT materials for neural electrodes.** *Biointerphases* 2008;3:83-93.

ASPLUND, M.; NYBERG, T.; INGANÄS, O., **Electroactive polymers for neural interfaces.** *Polym. Chem.*, 2010;1:1374-1391.

BARRET, M., **Impression par jet de matière de transistors organiques sur support souple.** Ph.D Thesis, Ecole Nationale Supérieure des Mines de Saint-Etienne, Gardanne, France, 2007.

BARTOLO, D.; BOUDAUD, A.; NARCY, G.; BONN, D.; **Dynamics of non-Newtonian droplets.** *Phys Rev Lett.* 2007;26:99(17):174502.

BERGGREN, M.; RICHTER-DAHLFORS, A., **Organic bioelectronics.** *Adv Mater* 2007;19(20):3201-13.

BLAU, A.; MURR, A.; WOLFF, S.; SERNAGOR, E.; MEDINI, P.; IURILLI, G.; ZIEGLER, C.; BENFENATI, F., **Flexible, all-polymer microelectrode arrays for the capture of cardiac and neuronal signals.** *Biomaterials* 32;2011:1778-1786.

BOLIN, M. H.; SVENNERSTEN, K.; WANG, X.; et al., **Nano-fiber scaffold electrodes based on PEDOT for cell stimulation.** *Sensors Actuators B* 2009;142:451-456.

BROCHU, P.; PEI, Q., **Advances in dielectric elastomers for actuators and artificial muscles.** *Macromol Rapid Commun* 2010;31(1):10-36.

BYSTRENOVA, E.; JELITAI, M.; TONAZZINI, I.; LAZAR, A. N.; HUTH, M.; STOLIAR, P. ; et al., **Neural networks grown on organic semiconductors.** *Adv Funct Mater* 2008;18 (12):1751-6.

CHANG, T. Y.; YADAV, V. G.; LEO, S. D.; MOHEDAS, A.; RAJALINGAM, B.; CHEN, C-L.; SELVARASAH, S.; DOKMECI, M. R.; KHADEMHOSEINI, A., **Cell and Protein Compatibility of Parylene-C Surfaces.** *Langmuir*, 2007;23(23):11718–11725.

CHEN, P. J.; SHIH, C. Y.; TAI, Y. C. **Design, fabrication and characterization of monolithic embedded parylene microchannels in silicon substrate.** *Lab Chip* 2006;6(6):803-810.

CHEN, Y. Y.; LAI, H. Y.; LIN, S. H.; CHO, C. W.; CHAO, W. H.; LIAO, C. H.; TSANG, S.; CHEN, Y. F.; LIN, S. Y., **Design and fabrication of a polyimide-based microelectrode array: Application in neural recording and repeatable electrolytic lesion in rat brain.** *Journal of Neuroscience Methods* 182 (2009) 6–16.

CHIOLERIO, A.; MACCIONI, G.; MARTINO, P.; COTTO, M.; PANDOLFI, P.; Rivolo, P.; Ferrero S.; Scaltrito L., **Inkjet printing and low power laser annealing of silver nanoparticle traces for the realization of low resistivity lines for flexible electronics.** *Microelectronic Engineering* 2011;88;8,2481–2483.

CHOI, M-C; KIM, Y; HA, C- S., **Polymers for flexible displays: from material selection to device applications.** *Prog Polym Sci* 2008;33(6):581-630.

COFFEY, R. J., **Deep brain stimulation devices: a brief technical history and review.** *Artif Organs*, 2009;33(3):208-20.

COLLAZOS-CASTRO, J. E.; POLO, J. L.; HERNÁNDEZ-LABRADO, G. R.; PADIAL-CAÑETE, V.; GARCÍA-RAMA, C., **Bioelectrochemical control of neural cell development on conducting polymers.** *Biomaterials* 2010;31: 9244-9255.

CUI, X. T.; ZHOU, D. D.; **Poly (3,4-Ethylenedioxythiophene) for Chronic Neural Stimulation.** Systems and Rehabilitation Engineering 2007;15:4: 502 – 508.

CUI, X.; LEE, V. A. ; RAPHAEL, Y. ; WILER, J. A. ; HETKE, J. F.; ANDERSON, D. J.; et al., **Surface modification of neural recording electrodes with conducting polymer/biomolecule blends.** J Biomed Mater Res 2001;56: 261–72.

CUI, X.; MARTIN, D. C., **Electrochemical deposition and characterization of poly(3,4- ethylenedioxythiophene) on neural microelectrode arrays.** Sensors Actuators B, 2003;89:92-102.

CURTIS, A. B., **Fundamentals of cardiac pacing.** 1st ed. Jones Bartlett Publishers; 2009; 245p.

DE GANS, B. J.; DUINEVELD, P. C.; SCHUBERT, U. S., **Inkjet Printing of Polymers: State of the Art and Future Developments.** Adv. Mater. 2004; 16(3):203–213.

DE GANS, B. J.; SCHUBERT, U. S.; **Inkjet printing of well-defined polymer dots and arrays.** Langmuir, 2004;20(18):7789-93.

DEEGAN, R. D. O.; BAKAJIN, T. F.; DUPONT, G.; HUBER, S. R. N.; WITTEN. T. A., **Capillary flow as the cause of ring stains from dried liquid drops.** Nature (London) 1997;389:827–829.

DEEGAN, R. D., **Pattern formation in drying drops.** Phys Rev E Stat Phys Plasmas Fluids Relat Interdiscip Topics. 2000;61(1):475-85.

DEMIREL, M. C.; SO, E.; RITTY, T. M.; NAIDU, S. H.; LAKHTAKIA, A., **Fibroblast cell attachment and growth on nanoengineered sculptured thin films.** J. Biomed. Mater. Res., Part B 2007; 81(1):219-223.

DENNEULIN, A.; BLAYO, A.; NEUMAN, C.; BRAS, J., **Infra-red assisted sintering of inkjet printed silver tracks on paper substrates.** J Nanopart Res 2011;13(9):3815–3823.

DONOGHUE, J. P., **Bridging the brain to the world: a perspective on neural interface systems.** Neuron 2008;60(3):511-21.

ESKIN, S. G.; ARMENIADES, C. D.; LIE, J. T.; TREVINO, L.; KENNEDY, J. H., **Growth of cultured calf aortic smooth muscle cells on cardiovascular prosthetic materials.** J. Biomed. Mater. Res. 1976;10 (1):113-122.

FORREST, S. R., **The path to ubiquitous and low-cost organic electronic appliances on plastic.** Nature 2004;428(6986):911-8.

FOWKES, F. M., **Attractive forces at interfaces.** Industrial and Engineering Chemistry. 1964;56:40-52.

GARCIA, T.; BITTENCOURT, E.; JOVA, Z., **Estudo do efeito do plasma de argônio, oxigênio e misturas na limpeza da superfície do alumínio por análise goniométrica.** Revista Ciência e Tecnologia, 2010;13(22/23):63-69.

GEORGE, P. M.; LYCKMAN, A. W. ; LAVAN, D. A. ; HEGDE, A. ; LEUNG, Y. ; AVASARE, R. ; et al., **Fabrication and biocompatibility of polypyrrole implants suitable for neural prosthetics.** Biomaterials 2005;26(17):3511-9.

GHASEMI-MOBARAKEH, L.; PRABHAKARAN, M. P.; MORSHED, M.; NASR-ESFAHANI, M. H.; RAMAKRISHNA, S., **Electrical stimulation of nerve cells using conductive nanofibrous scaffolds for nerve tissue engineering.** Tissue Eng Part A 2009;15 (11):3605-19.

GREEN, R. A.; LOVELL, N. H.; POOLE-WARREN, L. A., **Cell attachment functionality of bioactive conducting polymers for neural interfaces.** Biomaterials 2009;30: 3637–3644.

GREEN, R. A.; LOVELL, N. H.; WALLACE, G. G.; et al., **Conducting polymers for neural interfaces: challenges in developing an effective long-term implant.** Biomaterial 2008;29: 3393–3399.

GUANGCHUN, L.; PICKUP, P. G., **Ion transport in poly(3,4-ethylenedioxythiophene)- poly(styrene-4-sulfonate) composites.** Phys. Chem. Chem. Phys. 2000;2:1255-60.

GUIMARD, N. K.; GOMEZ, N.; SCHMIDT, C. E., **Conducting polymers in biomedical engineering**. Prog Polym Sci 2007;32(8-9):876-921.

HANSEN, F. K., **The Measurement of Surface Energy of Polymers by Means of Contact Angles of Liquids on Solid Surfaces - A short overview of frequently used methods**. University of Oslo, 2004.

HELGESEN, M; SØNDERGAARD, R; KREBS, F. C, **Advanced materials and processes for polymer solar cell devices**. J Mater Chem 2010;20(1):36-60.

HILL, E. K.; WATSON, R. L.; DUNSTAN, D. E.; **Rheofluorescence technique for the study of dilute MEH-PPV solutions in Couette flow**. J Fluoresc. 2005 May;15(3):255-66.

IGUCHI, N.; KASANUKI, H.; MATSUDA, N.; SHODA, M.; ONISHI, S.; HOSODA S., **Contact Sensitivity to Polychloroparaxyline Coated Cardiac Pacemakers**. Pacing Clinic. Electrophysiol., 1997;20(2 Pt 1): 372-373.

ISAKSSON, J; KJALL, P; NILSSON, D.; ROBINSON, N. D.; BERGGREN, M.; RICHTER-DAHLFORS, A., **Electronic control of Ca²⁺ signalling in neuronal cells using an organic electronic ion pump**. Nat Mater 2007;6(9):673-9.

JAKIMOVSKI, P.; RIEDEL, T.; HADDA, A.; BEIGL, M., **Design of a printed organic RFID circuit with an integrated sensor for smart labels**. Systems, Signals and Devices (SSD). 2012, 9th International Multi-Conference, 2012:1 – 6.

JINNO, S.; MOELLER, H. C.; CHEN, C. L.; RAJALINGAM, B.; CHUNG, B. G.; DOKMECI, M. R.; KHADEMHOSEINI, A., **Microfabricated multilayer parylene-C stencils for the generation of patterned dynamic co-cultures**. J Biomed Mater Res A. 2008;86(1):278-88.

KAPUR, D.; MUNDY, J. L., **Wu's method and its application to perspective viewing**. Artificial Intelligence, 1988;37(1-3):15-36.

KIM, D.; JEONG, S.; LEE, S., PARK, B. K.; MOON, J.; **Organic thin film transistor using silver electrodes by the ink-jet printing technology.** *Thin Solid Films* 2007;515:7692–7696.

KIM, D-H.; VIVENTI, J.; AMSDEN, J. J.; XIAO, J.; VIGELAND, L.; KIM, Y-S.; BLANCO, J. A.; PANILAITIS, B.; FRECHETTE, E. S.; CONTRERAS, D.; KAPLAN, D. L.; OMENETTO, F. G.; HUANG, Y.; HWANG, K-C.; ZAKIN, M. R.; LITT, B.; ROGERS, J. A., **Dissolvable films of silk fibroin for ultrathin conformal bio-integrated electronics.** *Nature Materials* 2010;9:511–517.

KIM, D-H.; RICHARDSON-BURNS, S.; POVLIICH, L. ; ABIDIAN, M. R.; SPANNINGA, S. ; HENDRICKS, J. ; MARTIN, D. C. , **Indwelling Neural Implants: Strategies for Contending with the In-Vivo Environment** , (Ed: W. M. Reichert), CRC Press, Taylor Francis, Boca Raton, FL 2008 , 271p.

LAI, J.; SUNDERLAND, B.; XUE, J.; YAN, S.; ZHAO, W.; FOLKARD, M.; MICHAEL, B. D.; WANG, Y., **Study on hydrophilicity of polymer surfaces improved by plasma treatment.** *Applied Surface Science*, 2006, Volume 252, Issue 10, 3375-3379.

LE, H. P., **Progress and Trends in Ink-jet Printing Technology.** *Journal of Imaging Science and Technology* 1998, vol. 42, number 1, 49-62.

LEE, C-L.; CHANG, K-C.; SYU, C-M., **Silver nanoplates as inkjet ink particles for metallization at a low baking temperature of 100°C.** *Colloids and Surfaces A: Physicochem. Eng. Aspects* 2011;381:85–91.

LIM, J. A.; LEE, W. H.; LEE, H. S.; LEE, J. H.; PARK, Y. D.; CHO, K., **Self-Organization of Ink-jet-Printed Triisopropylsilylethynyl Pentacene via Evaporation-Induced Flows in a Drying Droplet.** *Adv. Funct. Mater.* 2008;18:229.

LIN, Y.; WALLACE, G. G.; **Factors influencing electrochemical release of 2,6-anthraquinone disulphonic acid from polypyrrole.** *Journal of Controlled Release*, 1994;30(2):137–142.

LIU, Y-F.; HWANG, W-S.; PAI, Y-F.; TSAI, M-H., **Low temperature fabricated conductive lines on flexible substrate by inkjet printing.** *Microelectronics Reliability*, 2012;52:2:391–397.

LIU, Z.; SU, Y.; VARAHRAMYAN, K., **Inkjet-printed silver conductors using silver nitrate ink and their electrical contacts with conducting polymers.** *Thin Solid Films*, 2005;478(1-2):275-279.

LIU, Z.; SU, Y.; VARAHRAMYAN, K., **Inkjet-printed silver conductors using silver nitrate ink and their electrical contacts with conducting polymers.** *Thin Solid Films*, 2005, 478, 275–279.

LOEB, G. E.; WALKER, A. E.; UEMATSU, S.; KONIGSMARK, B. W., **Histological reaction to various conductive and dielectric films chronically implanted in the subdural space.** *J. Biomed. Mater. Res.* 1977;11 (2): 195-210.

LUDWIG, K. A.; URAM, J. D.; YANG, J.; MARTIN, D. C; KIPKE, D. R., **Chronic neural recordings using silicon microelectrode arrays electrochemically deposited with a poly(3,4-ethylenedioxythiophene) (PEDOT) film.** *J Neural Eng* 2006;3: 59–70.

LUO, S.; ALI, E. M.; TANSIL, N. C., **Poly(3,4-ethylenedioxythiophene) (PEDOT) nanobiointerfaces: thin, ultrasmooth, and functionalized PEDOT Films with *in vitro* and *in vivo* biocompatibility.** *Langmuir* 2008 24: 8071–8077.

LYFORD, P. A.; SHALLCROSS, D. C.; GRIESER, F.; PRATT, H. R., **The Marangoni effect and enhanced oil recovery Part 2. Interfacial tension and drop instability.** *The Canadian Journal of Chemical Engineering*, 1998. Vol. 76, p. 175-182.

MAGDASSI, S., **The Chemistry of Inkjet Inks.** World Scientific Pub. 2010; Chapter 1;345p.

MALHOTRA, B. D.; CHAUBEY, A.; SINGH S. P., **Prospects of conducting polymers in biosensors.** *Anal Chim Acta* 2006;578(1):59-74.

MALLIARAS, G.G.; FRIEND, R.H., **An organic electronics primer.** *Physics Today*, 2005;58: 53–58.

MANNERBRO, R.; RANLÖF, M.; ROBINSON, N.; FORCHHEIMER, R., **Inkjet printed electrochemical organic electronics**. Synthetic Metals 2008;158: 556–560.

MARGALIT, E.; MAIA, M.; WEILAND, J. D.; GREENBERG, R. J.; FUJII, G. Y.; TORRES, G.; et al., **Retinal prosthesis for the blind**. Surv Ophthalmol 2002;47(4):335-56.

MEIER, H.; LÖFFELMANN, U.; MAGER, D.; SMITH, P. J.; KORVINK, J. G., **Inkjet printed, conductive, 25 µm wide silver tracks on unstructured polyimide**. Phys. Status Solidi A, 2009, 1-5.

MOLINA-LUNA, K.; BUITRAGO, M. M.; HERTLER, B.; SCHUBRING, M.; HAISS, F.; NISCH, W.; et al., **Cortical stimulation mapping using epidurally implanted thin-film microelectrode arrays**. J Neurosci Methods 2007;161(1):118-25.

MÜLLER, D.; RAMBO, C. R.; RECOUVREUX, D. O. S.; PORTO, L. M.; BARRA, G. M. O., **Chemical in situ polymerization of polypyrrole on bacterial cellulose nanofibers**. Synthetic Metals, 2011; 161:106-111.

MÜLLER, D.; MANDELLI, J. S.; MARINS, J. A.; SOARES, B. G.; PORTO, L. M.; RAMBO, C. R.; BARRA, G. M. O., **Electrically conducting nanocomposites: preparation and properties of polyaniline (PAni)-coated bacterial cellulose nanofibers (BC)**. Cellulose (London), 2012;19(5):1645-1654.

NAVARRO, X.; KRUEGER, T. B.; LAGO, N.; MICERA, S.; STIEGLITZ, T.; DARIO, P., **A critical review of interfaces with the peripheral nervous system for the control of neuroprostheses and hybrid bionic systems**. J Peripher Nerv Syst 2005;10 (3):229-58.

NDREU A., **Electrospun nanofibrous scaffolds for tissue engineering**. Ph.D Thesis, Graduate School of Natural and Applied Sciences of Middle East Technical University, Ankara, Turkey, 2007.

NILSSON, D., **An Organic Electrochemical Transistor for Printed Sensors and Logic**. Dissertation No. 921, Linköpings Universitet, Norrköping, 2005.

NOORDEGRAAF, J.; **Conformal Coating Using Parylene Polymers.** Med. Device Technol., 1997;8(1):14-20.

NYBERG, T.; SHIMADA, A.; TORIMITSU, K., **Ion conducting polymer microelectrodes for interfacing with neural networks.** J. Neurosci. Meth. 2007;160:16-25.

PERAMO, A.; URBANCHEK, M. G.; SPANNINGA, S. A.; et al., **In situ polymerization of a conductive polymer in acellular muscle tissue constructs.** Tissue Eng A 2008;14: 423–432.

ORGANIC ELECTRONICS ASSOCIATION, **OE-A Roadmap for Organic and Printed Electronics**, 4th ed., Frankfurt, 2011.

PERELAER J.; SMITH, P. J.; HENDRIKS, C. E.; VAN DEN BERG, A. M. J.; SCHUBERT, U. S.; **The preferential deposition of silica micro-particles at the boundary of inkjet printed droplets.** Soft Matter, 2008;4:1072-1078.

PETERS, M. S.; SCHROETER, A. L.; HALE, H. M. V.; BROADBENT, J. C.; **Pacemaker contact sensitivity.** Contact Dermatitis. 1984;11:214–218.

PICKUP, P. G., **Electrochemistry of electronically conducting polymer films.** Modern Aspects of Electrochemistry, 2002;33:549-597.

Polyimide Ink – Chisso, available from www.chisso.co.jp/english, accessed Saturday, August 20, 2011 at 20h00.

POOLE-WARREN, L.; LOVELL, N.; BAEK, S.; GREEN, R., **Development of bioactive conducting polymers for neural interfaces.** Expert Rev Med Devices 2010;7 (1):35-49.

RICHARDSON-BURNS, S. M.; HENDRICKS, J. L.; FOSTER, B.; POVLIICH, L. K.; KIM, D-H.; MARTIN, D. C., **Polymerization of the conducting polymer poly(3,4-ethylenedioxythiophene) (PEDOT) around living neural cells.** Biomaterials 2007;28:1539–52.

RODGER D. C.; FONG A. J.; LI W.; AMERI H.; AHUJA A. K.; GUTIERREZ C.; LAVROV I.; ZHONG H.; MENON P. R.; MENG E.; BURDICK J. W.; ROY R. R.; EDGERTON R. V.; WEILAND J. D.;

HUMAYUN M. S.; TAI Y-C., **Flexible parylene-based multielectrode array technology for high-density neural stimulation and recording.** Sensors and Actuators B: Chemical, 2008;132(2):449–460.

ROGERS, J. A.; SOMEYA, T.; HUANG, Y., **Materials and mechanics for stretchable electronics.** Science, 2010;327(5973):1603-7.

RUBEHN, B.; BOSMAN, C.; OOSTENVELD, R.; FRIES, P.; STIEGLITZ, T., **A MEMS-based flexible multichannel ECoG-electrode array.** J Neural Eng 2009;6(3):036003.

SCHMIDT, E. M.; MCINTOSH, J. S.; BAK, M. J., **Long-term implants of parylene-C coated microelectrodes.** Med. Biol. Eng. Comput. 1988;26 (1):96- 101.

SHEFFLER, L. R.; CHAE, J., **Neuromuscular electrical stimulation in neurorehabilitation.** Muscle Nerve 2007;35(5):562-90.

SIMON, D. T.; KURUP, S.; LARSSON, K. C.; HORI, R.; TYBRANDT, K.; GOINY, M., **Organic electronics for precise delivery of neurotransmitters to modulate mammalian sensory function.** Nat. Mater. 2009;8:742-6.

SINGH, M.; HAVERINEN, H. M.; DHAGAT, P.; JABBOUR, G. E., **Inkjet Printing – Process and Its Applications.** Adv. Mater. 2009, 21, 1-13.

SOLTMAN, D.; SUBRAMANIAN, V., **Inkjet-printed line morphologies and temperature control of the coffee ring effect.** Langmuir, 2008, 24;2224-2231.

SOLTMAN, D.; SUBRAMANIAN, V., **Inkjet-printed line morphologies and temperature control of the coffee ring effect.** Langmuir, 2008, 24, 2224-2231.

Specialty Coating Systems – Parylene Applications, available from www.scscoatings.com, accessed Saturday, August 20, 2011 at 22h00.

Specialty Coating Systems – Parylene Specifications, available from www.scscoatings.com, accessed Saturday, August 20, 2011 at 20h30.

STIEGLITZ, T., **Neural prostheses in clinical practice: biomedical microsystems in neurological rehabilitation.** Acta Neurochir Suppl 2007;97(1):411-8.

STIEGLITZ, T.; RUBEHN, B.; HENLE, C.; KISBAN, S.; HERWIK, S.; RUTHER, P.; et al., **Braincomputerinterfaces: an overview of the hardware to record neural signals from the cortex.** In: Verhaagen, J.; Hol, E. M.; Huitenga, I.; Wijnholds, J.; Bergen, A. B.; Boer, G. J.; et al., editors. Prog brain res. Elsevier; 2009:297-315.

SUBRAMANIAN, V.; FRECHET, J.M.J.; CHANG, P.C.; HUANG, D.C.; LEE, J.B.; MOLESA, S.E.; MURPHY, A.R.; REDINGER, D.R.; VOLKMAN, S.K., **Progress Toward Development of All-Printed RFID Tags: Materials, Processes, and Devices.** Proceedings of the IEEE, 2005;7:1330-1338.

TEKIN, E.; DE GANS, B.; SCHUBERT, U. S., **Ink-jet printing of polymers – from single dots to thin film libraries.** J. Mater. Chem., 2004, 14, 2627 – 2632.

TEKIN, E.; SMITH, P. J.; HOEPPENER, S.; VAN DEN BERG, A. M. J.; SUSHA A. S.; ROGACH A. L.; FELDMANN J.; SCHUBERT U. S., **Inkjet Printing of Luminescent CdTe Nanocrystal-Polymer Composites.** Adv. Funct. Mater. 2007;(17):23–28.

TOOKER, A.; MENG, E.; ERICKSON, J.; TAI, Y. C.; PINE, J. **Biocompatible parylene neurocages. Developing a robust method for live neural network studies.** Eng. Med. Biol. Mag. 2005;24(6):30-33.

VENKATRAMAN, S.; HENDRICKS, J.; KING, Z. A.; SERENO, A. J.; RICHARDSON-BURNS, S.; MARTIN, D.; CARMENA J. M., **In Vitro and In Vivo Evaluation of PEDOT Microelectrodes for Neural Stimulation and Recording.** Neural Systems and Rehabilitation Engineering, 2011; 19:3: 307 – 316.

WALLACE, G. G.; MOULTON, S. E.; CLARK, G. M., **Electrode-Cellular Interface.** Science 2009;324(5924):185-186.

WALLACE, G.; **Nanostructured Electrodes: New Bionic Interfaces.** IFMBE Proceedings, 2007;14.

WANG, X.; SHAPIRO, B.; SMELA, E., **Visualizing ion currents in conjugated polymers.** Adv. Mater. 2004;16:1605-9.

WEI, L.; LAKHTAKIA, A.; ROOPNARIANE, A. P.; RITTY, T. M.; **Human fibroblast attachment on fibrous parylene-C thin-film substrates.** Materials Science and Engineering: C, 2010;30(8):1252–1259.

WEISENBERG, B. A.; MOORADIAN, D. L., **Hemocompatibility of materials used in microelectromechanical systems: platelet adhesion and morphology *in vitro*.** J. Biomed. Mater. Res. 2002;60 (2): 283-291.

WEN Y, LIU Y. **Recent progress in n-channel organic thin-film transistors.** Adv Mater 2010;22(12):1331e45.

WILK, S. J.; RICHARDSON-BURNS, S. M.; HENDRICKS, J. L.; MARTIN, D. C.; OTTO, K. J., **Poly(3,4-ethylenedioxythiophene) as a micro-neural interface material for electrostimulation.** Frontiers in neuroengineering. 2009; 2:7.

WILSON, B. S.; DORMAN, M. F., **Interfacing sensors with the nervous system: Lessons from the development and success of the cochlear implant.** Sensors J, 2008;8(1):131-47.

WOODWARD, R. P., **Surface Tension Measurements Using the Drop Shape Method.** Available from First Ten Angstroms, USA. www.firsttenangstroms.com/pdfdocs/STPaper.pdf, accessed Monday, August 22, 2011 at 10h00. (R.P. Woodward, FTA200 Measurement Capabilities, 2007 (<http://www.firsttenangstroms.com/pdfdocs/mea.pdf>).

WRIGHT, D.; RAJALINGAM, B.; KARP, J.; SELVARASAH, S.; LING, Y.; YEH, J.; LANGER, R.; DOKMECI, M. R.; KHADEMHOSEINI, A., **Reusable, reversibly sealable parylene membranes for cell and protein patterning.** J. BIOMED. MATER. RES 2008;85A(2):530-538.

WRIGHT, D.; RAJALINGAM, B.; SELVARASAH, S.; DOKMECI, M. R.; KHADEMHOSEINI, A., **Generation of static and dynamic**

patterned co-cultures using microfabricated parylene-C stencils. *Lab Chip*, 2007;7(10):1272-9.

XIAO, Y. H.; CUI, X. Y.; HANCOCK, J. M.; BOUGUETTAYA, M., REYNOLDS, J. R.; MARTIN, D. C., **Electrochemical polymerization of poly(hydroxymethylated-3,4-ethylenedioxythiophene) (PEDOT-MeOH) on multichannel neural probes.** *Sensors Actuators B* 2004;99:437-43.

XIE, X. Z.; RIETH, L.; TATHIREDDY, P.; SOLZBACHER, F., **Long-term in-vivo Investigation of Parylene-C as Encapsulation Material for Neural Interfaces.** *Procedia Engineering*, 2011;25:483-486.

XUE, F.; LIU, Z.; SU, Y.; VARAHRAMYAN, K., **Inkjet printed silver source/drain electrodes for low-cost polymer thin film transistors.** *Microelectronic Engineering* 83 (2006) 298-302.

YAMATO, H.; OHWA, M.; WERNET, W., **Stability of polypyrrole and poly(3,4-ethylenedioxythiophene) for biosensor application.** *J. Electroanal. Chem.* 1995;397:163-70.

YANG, J.; KIM, D-H., HENDRICKS, J. L.; LEACH, M.; NORTHEY, R.; MARTIN D. C., **Ordered surfactant-templated poly(3,4-ethylenedioxythiophene) (PEDOT) conducting polymer on microfabricated neural probes.** *Acta Biomater* 2005; 1:125-36.

YANG, N.; ZOSKI, C. G., **Polymer films on electrodes: investigation of ion transport at poly(3,4-ethylenedioxythiophene) films by scanning electrochemical microscopy.** *Langmuir* 2006;22:10338-47.

YANG, S. Y.; KIM, B. N.; ZAKHIDOV, A. A.; TAYLOR, P. G.; LEE, J. K.; OBER, C. K.; LINDAU, M.; MALLIARAS, G. G., **Detection of Transmitter Release from Single Living Cells Using Conducting Polymer Microelectrodes.** *Adv. Mater.* 2011;23:1-5.

YOSHIOKA, Y.; JABBOUR, G. E.; **Desktop inkjet printer as a tool to print conducting polymers.** *Synthetic Metals* 2006;156:779-783.

ZHANG, C.; THOMPSON, M. E.; MARKLAND, F. S.; SWENSON, S., **Chemical surface modification of parylene C for enhanced**

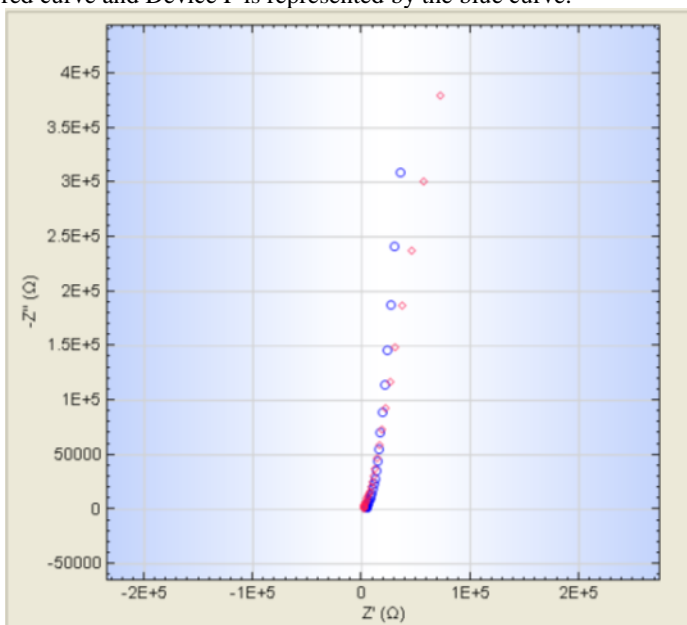
protein immobilization and cell proliferation. *Acta Biomaterialia*, 2011;7(10):3746–3756.

APPENDIX A - ELECTROCHEMICAL IMPEDANCE SPECTROSCOPY

EIS was performed for the samples printed in both ways (silver printed first – Device S and PEDOT:PSS printed first, Device P). Printed PEDOT films exhibits intrinsic redox activity, which favors to the low impedance (Cui X. T. et al., 2007).

The impedance plots (Nyquist) comparing both devices are shown in Figure 57.

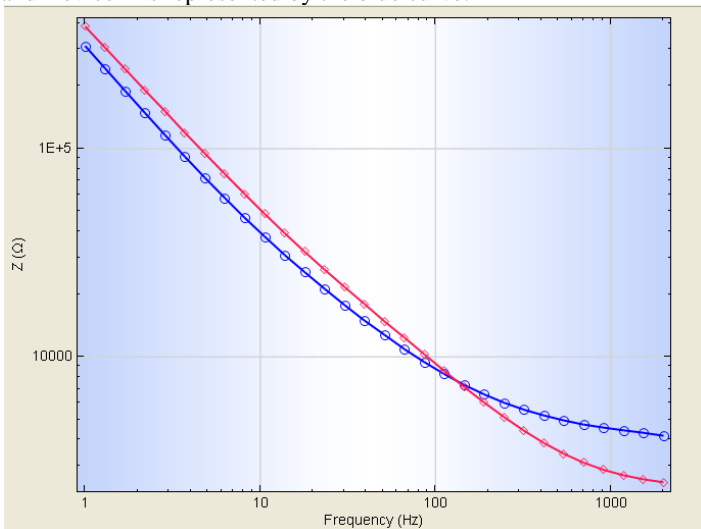
Figure 57: Nyquist plot comparing both devices. Device S is represented by the red curve and Device P is represented by the blue curve.



From the Figure 57, it can be seen that there is no significant difference between the curves, and that there is only a weak dispersion between the values at low frequencies. These curves are consistent with results found in the literature. A 90° capacitive line predominates in the impedance plots and extends down to very low. There is only a feeble deviation from the capacitive line at high frequencies, denoting quick charge transfer at the metal/polymer and polymer/solution interfaces, even as

fast charge transport in the polymer bulk frequencies (Bobacka J. et al., 2000). From the Bode plot, it is observed that Device P presents a slight higher impedance than Device S at high frequencies. The Bode plot for these devices is shown in Figure 58.

Figure 58: Bode plot for both devices. Device S is represented by the red curve and Device P is represented by the blue curve.



To verify if the devices are stable in the course of time, three measurements were performed at the same contact pad for each device. Each measurement was performed with a difference of 10 minutes. The devices showed a good stability for this time of measurement. The Nyquist and Bode plots for both devices are shown in Figure 59.

Likewise, the impedance values for right lines and left lines in the same device were measured for both devices. For Device S, this measurement was performed to lines of the same width and the results were very close (Figure 60). For Device P, measurements were performed to lines of different widths and the results show that the impedance values are higher to the line of bigger width (Figure 61).

Low impedance results in a more efficient interface for constant current stimulation and in higher signal-to-noise ratios for refined electrophysiological recordings.

Figure 59: Nyquist (on the left) and Bode plot (on the right) showing the stability of (a) Device P and (b) Device S.

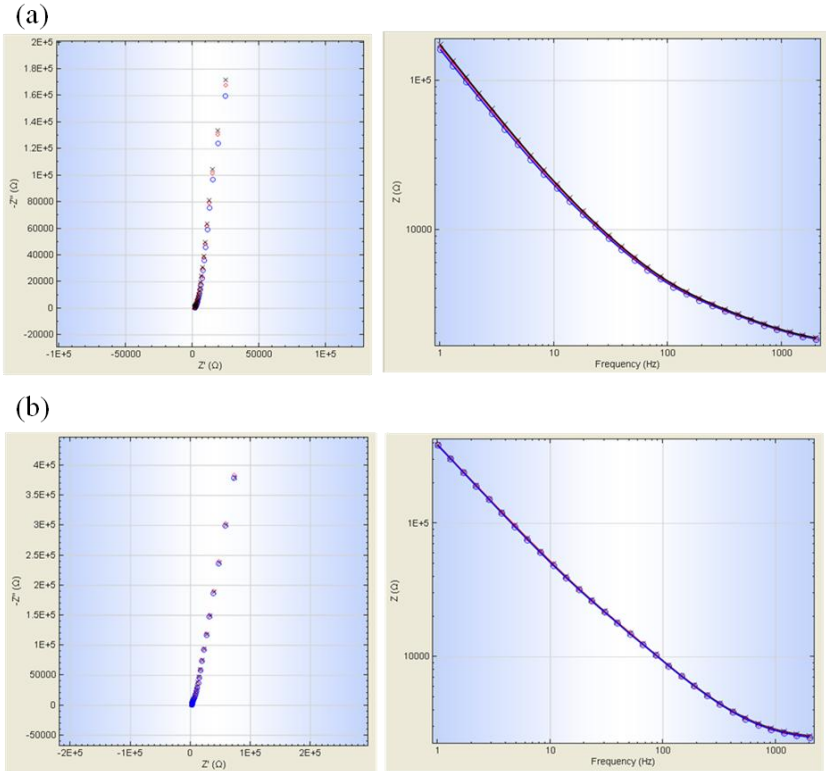


Figure 60: Nyquist (on the left) and Bode plot (on the right) for Device P. Right line is represented by the blue curve and left line is represented by the red line.

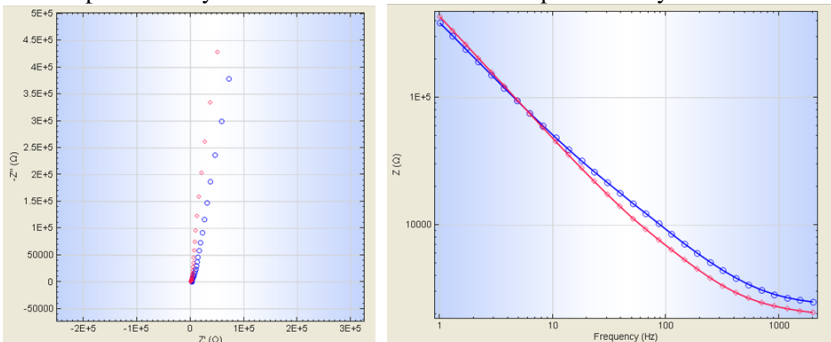
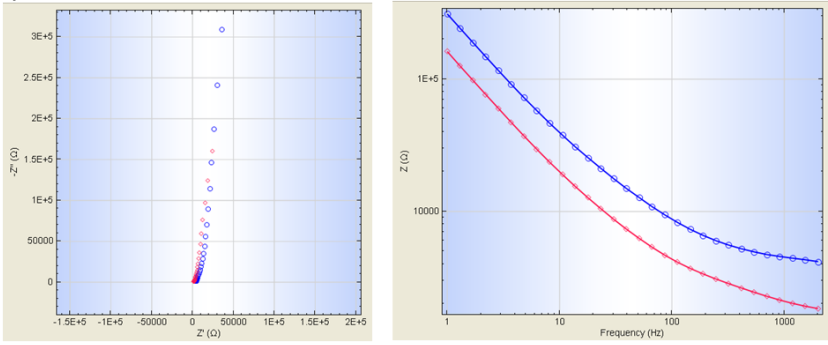
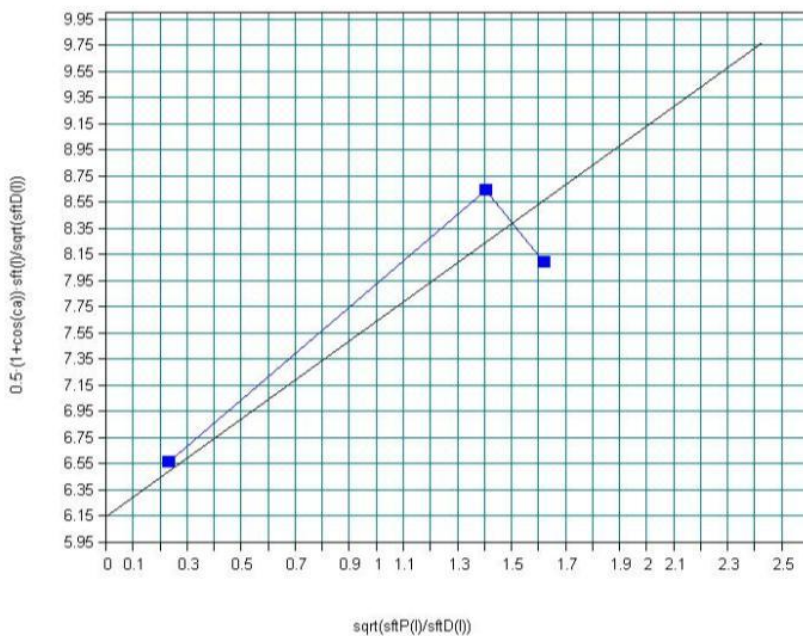


Figure 61: Nyquist (on the left) and Bode plot (on the right) for Device S. Right line (bigger width) is represented by the blue curve and left line is represented by the red line.



APPENDIX B - GRAPHIC OF WU'S METHOD

Figure 62: Graphic of surface energy obtained from the Wu's method, measured with the goniometer.



APPENDIX C - EXAMPLES OF ORGANIC FLEXIBLE DEVICES

Some examples of organic and printed electronics products are shown in Figures 63 and 64. (Source: OE-A Roadmap for Organic and Printed Electronics)

Figure 63: Transponder chip and printed RFID tag.

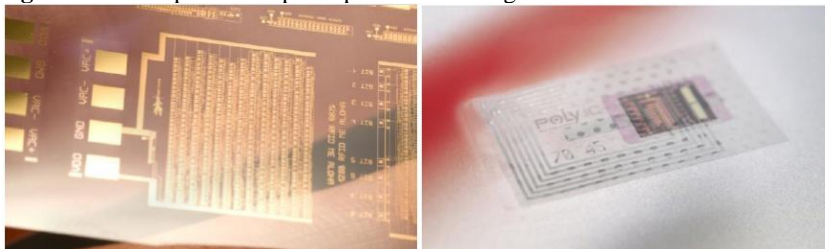


Figure 64: Printed RFID as electronic product code and printed sensor for measuring electrical activity of the heart (ECG).

